UNIVERSITÀ
DEGLI STUDI
DI PALERMO

Dottorato di Ricerca in Fisica - XXX Ciclo

DEVELOPMENT OF A NEW SATURATED VAPOUR-ANODE, SATURATED VAPOUR-CATHODE AMTEC-LIKE DEVICE

Dr. Eng. Gianluca Tumminelli

PhD Coordinator:
Prof. Massimo Palma

Tutor:
Prof. Marco Barbera

Blank page

UNIVERSITÀ DEGLI STUDI DI PALERMO

Table of contents

Blank page

PREFACE

It is back in the Nineties when the developed Countries have taken awareness about the impossibility to maintain the energy consumptions of the last decades. "Energy efficiency" represents the ratio between the amount of energy consumed in useful products or services with respect to total energy input. Greater energy efficiency and energy savings can be achieved either by various complex technologies, components and systems, or by a more conscious and responsible behaviour of final users. Then, economic and environmental motivations moved towards the direction of environment protection.

The energetic efficiency can be easily expressed with three concepts:

- savings on energetic expenses for families;
- better comfort;
- help to environment.

To make a safer, more competitive, more sustainable, low energetic consumption-economy, our Country has already fixed a target of savings to 2016 equal to 9,6% with respect to the average annual consumption of the period 2001-2006, equivalent to 10,8 Mtoe (*Million Tonnes of Oil Equivalent*), which corresponds to about **4 billion Euros** (*calculated assuming a crude oil cost of 75$ per barrel and a Dollar-Euro change of 1,25*). If measures for the improvement of the energetic efficiency are properly implemented, such a goal is actually achievable. Economic advantages for consumers, once realized the improving interventions, are immediately visible from savings in bills, furthermore, thanks also to national and regional incentive measures, the payback of the investment occurs in the short-medium period.

Heavy interventions have already been programmed in all fields of our society:

- in the domestic sector, a heavy recourse to more efficient technologies could permit to get reduction in consumptions up to 12% even within year 2020, about 4 Metp less than current trend, equal to about 1,4 billion Euros (*calculated assuming a crude oil cost of 75$ per barrel and a Dollar-Euro change of 1,25*);

- in the commercial sector, the diffusion of better performing air conditioning systems, boilers and electrical devices, capable to grant significant reduction in consumptions in the short-medium period: about 2 Metp with respect to current trend, over 10% of sector consumption (according to PAEE 2007 the estimate of reduction in 2016 is 2 Metp);
- in the transport sector, the use of more performing vehicles represents the main option for the reduction of consumption in the medium period (2020 onwards). As in the long period an opportunity for reduction of consumptions is represented by the decrease in the demand of movement with private means (about 15% less than current trend), the main technological option in the short-medium period is represented by the energetic efficiency. Sector consumptions may reduce, in fact, of 12% in 2020 with respect to the reference projection (about 5,7 Metp, in accordance to the estimation made in the draft of the "Piano straordinario per l'efficienza e il risparmio energetico", March 2010);
- in the technological and industrial sector, the reduction of consumptions is about 2% in 2020 with respect to current trend. The slight reduction in the medium period, proof of some rigidity of the sector, follows instead, in the long period, a more significant reduction, equal to 16% in 2050.

The International Energy Agency (IEA) recommends to prefer energetic efficiency as a strategy for carbon dioxide emissions reduction, because such solution has the best chances of success, at lower costs.

"The best strategy to reduce CO_2 emissions, from now to 2050, is to improve the energetic efficiency: there are several ways to do that. In the short period, this must be our highest priority" IEA, Energy.

In practice, it is not always so easy to make these advantages concrete. Governments, companies and single citizens can make their own, but it is necessary a coordination for these actions. Main obstacles to investments in energetic efficiency are: insufficient competences, lacking of resources and limited capitals.

The present research project belongs to the general technology development field aimed at maximizing the conversion of the solar energy into electrical energy and heat, in

such a way to reach global efficiency far greater than the traditional photovoltaic technology efficiency, which is about 16%.

One of the technologies capable to convert efficiently and directly the thermal energy or the solar energy into electrical energy is the Alkali Metal ThermoElectric Converter (AMTEC) [1, 2]. Despite such device has a high theoretical efficiency, close to the Carnot cycle efficiency, its application at industrial scale has been so far limited by low durability, low power output/weight ratio and high cost.

The present work of thesis is about the modelling, development and electrical characterization of a new AMTEC-like not-rechargeable prototypal device, which could be used for the industrial production of a second generation of electrochemical/membrane-based cells for the high efficiency production of electrical energy.

The present work is divided into seven chapters. In the first one, I present the state of the art of the devices for the direct conversion of thermal energy at high temperature (e.g. from solar energy concentration) into electrical energy. A detailed description of the AMTEC cell is given in the second chapter. In chapter III the selection of new materials is proposed for the design of a second generation AMTEC-like device. Chapter IV presents a simple test apparatus set-up to investigate novel materials. In Chapter V I present currently developed AMTEC cell models and describe novel modelling based on a statistical-thermodynamics approach, for the prediction of the generated voltage, current and power extractable by a simplified cell, as well as the full polarization curve (voltage vs current characteristic).

Chapter VI describes experimental campaigns carried out in order to assess the validity of the mathematical model developed and to demonstrate the capability of the device of using a new working fluid and a new electrolyte. Preliminary tests have been carried out with hydrogen as working fluid, useful to check and solve criticalities occurred in the first developed device.

The realization of a second modified version of the device, capable to operate with zinc, as well as a modified version of the whole experimental apparatus, is described in Chapter VII in view of performing a new test campaign for future development.

The results of the present research have been included in two submitted papers and one on-going patent request, which can be summarised as follows:

Paper 1: Tumminelli et al., "A thermodynamic-statistical model of the electrical characteristics of a 2nd generation AMTEC-type cell for the renewable heat-to-electrical energy direct conversion", submitted to AIP – Journal of Renewable and Sustainable Energy.

Paper 2: Tumminelli et al., "Towards an AMTEC-like device based on non-alkali metal for efficient, safe and reliable direct conversion of thermal to electric power", accepted by AEIT International 2018 Annual conference, Bari 3-5 October 2018.

Patent request: Tumminelli et al., "Dispositivo per la conversione di energia, sistema di conversione di energia e relativo procedimento di conversione di energia", deposited on 2018, July 31st with number 102018000007710.

CHAPTER I

INTRODUCTION

1.1 Thermo-electric Conversion

The latest technological frontier for the production of electric energy from photovoltaic and the recovery of thermal energy are bi-functional photovoltaic panels. It is a system that, taking advantage of the solar light and heat through bi-functional photovoltaic panels, is capable to increase the efficiency of photovoltaic panels for the production of the electrical current (cooling down the panels themselves), on one hand, and also to simultaneously recover thermal energy (heat) to supply a heat pump air conditioning system, adopted for winter heating, or summer air conditioning, as well as for the production of hot water.

The heat recovery is made by means of an insulated aluminium enclosure which is installed just below the PV panel. The box, having the same shape of the panel, contains a copper coil which, being in contact with the bottom surface of PV cells, cools down the panel. The cooling occurs by direct expansion through circulation of a cooling liquid. Such a liquid, taking heat away from the panel, recovers heat and transfer it to a system which is capable to use it for heating or conditioning.

The disadvantages of such a system are:

- Huge amounts of silicon used;
- Excessive cost;
- The heated water does not reach high temperatures;
- Payback time too long.

In particular, considering the cost, such a technology needs incentives for photovoltaic, the so-called “Conto Energia”. Considering the current perspectives, the so-called “V Conto Energia” will have a very short lifetime, so the economical revenue of such plants will be based exclusively on grid parity cash flow, which in facts limit today their diffusion on a large scale.

As an example, an attempt to improve the efficiency of solar energy conversion is the use of concentration systems (which act in the way of reducing entropy) coupled to systems that directly transform highly concentrated radiant energy into electricity (photovoltaic effect), or systems that directly convert high temperature thermal energy into electrical energy. This work focuses on the latter one.

The main systems for the direct conversion of thermal energy at high temperature into electricity, that can be matched to a solar energy concentrator (SEC) are:

1) Alkali Thermocouple Converter (**AMTEC**: *Alkali Metal Thermal Electric Converter*),
2) Seebeck Thermocouple Converter (**TEG**: *ThermoElectric Generator*);
3) Stirling engines.

In the following, the operating principle, the main technical features, and the advantages/disadvantages of the above mentioned devices, are presented. A more detailed analysis of the AMTEC cell is provided in the next Chapter.

1.2 The AMTEC cell

The **AMTEC** electrochemical device is capable of statically converting the thermal energy into electricity. For the conversion process, this system employs an alkali metal such as sodium or potassium. In AMTEC cycles, a solid electrolyte (e.g. β-alumina) is used as the basis for carrying electrical charges. On both sides of the electrolyte there are two electrodes firmly connected to it and they are in turn electrically connected via an external circuit. In the circuit, an electric load is connected in series.

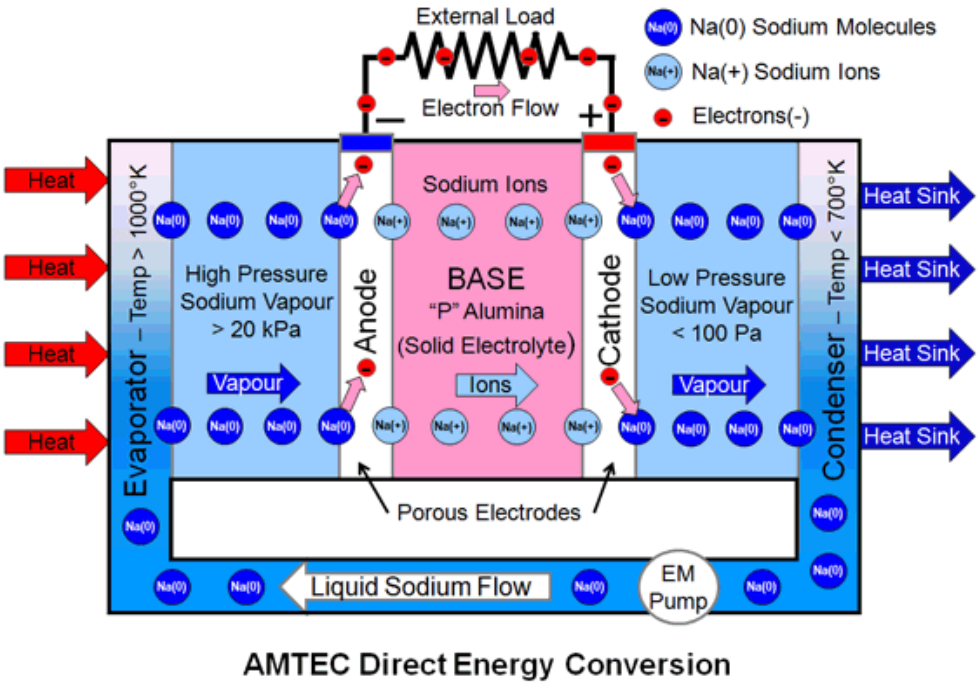

Figure 1. Schematics of an AMTEC system operation principle [3].

For the conversion process, this system employs an alkali metal such as sodium, lithium or potassium as working fluid, and a solid electrolyte (e.g. β-alumina) as the basis for carrying electrical positive charges [1, 4, 5, 6, 7]. On both sides of the electrolyte, two electrodes firmly connected to it are in turn connected electrically to an external circuit where an electric load is applied.

Alkali metal atoms ionise at the interface between the electrode and the electrolyte (oxidation). The positive charges can cross the electrolyte, while free electrons can only migrate from the anode to the cathode through the external load, if present, and then recombine with the cations passed through the membrane to form again the neutral metal atom (reduction).

Such a process is driven by the higher pressure at the anode side and is made possible by the non-permeability of the solid electrolyte to neutral atoms and free electrons. This means that the alkali vapour atoms must ionise to expand from the high pressure side to the low pressure side of the Beta-Alumina Solid Electrolyte (BASE),

generating free alkali cations onto the solid electrolyte and free electrons at the electrode (see figure 1).

As long as the external electric circuit is open, alkali cations, driven by the pressure difference, can pass through the BASE and accumulate on the opposite surface (lower pressure side), while free electrons, unable to pass through the electrolyte, accumulate on the anode (higher pressure side).

This charge separation process continues until electrostatic repulsion balances the differential pressure. When closing the external circuit on an electric load, it is possible to exploit the electric potential so generated: electrons start to flow through the load, produce electric work and return to the cathode where they are recombined with the alkali metal cations.

During the recombination process occurring in the gaseous state at lower temperature, neutral alkali metal atoms move towards the condenser, where they return to the liquid state and are pumped back into the higher temperature region. In this way, a continuous current is obtained.

Two main types of AMTEC cycles exists, the so-called liquid-anode and the vapour-anode cycles, depending on the phase of the alkali metal in contact with the anode [1, 8, 9, 10].

The metal used as working fluid also determines the operating temperatures, which typically range between 900 K and 1300 K at the hot source (anode), and between 400 K and 700 K at the cold source (cathode).

The main advantages of AMTECs are: no moving parts, small size, no material flows outside the cell enclosure, relatively low operating temperatures suitable for their coupling with thermal waste from other processes, high theoretical energy conversion efficiency. On the other hand, some important disadvantages exist, such as: thermal degradation of BASE due to high operating temperatures resulting in a low durability (-25% power output in 500 hours, -50% power output in 18,000 hours) [11, 12], safety issues due to the use of potentially dangerous alkali metals (sodium, lithium), quite low power output per unit

weight (16 W/kg) with respect to other thermal-to-electric energy direct converters [13, 14, 15], high maintenance and production costs [16].

In order to overcome some of the mentioned limitations so far encountered by the AMTEC cells, I investigated a new type of AMTEC type cell operating with a working fluid different than an alkali metal, a solid electrolyte constituted by proper conditioned ion conductive membrane, and an operating mode which does not require the use of a pump for fluid recirculation.

1.3 The TEG cell

A TEG thermal converter transforms the thermal energy into electricity through the Seebeck effect. This thermoelectric effect occurs when, two different metal conductors in a circuit, are kept at different temperatures. Such temperature difference generates a voltage difference resulting in a current through the junction. This effect is more pronounced in semiconductors.

In a system using this effect, there are: a heat source, a **TEG module**, a heat sink, and an applied load.

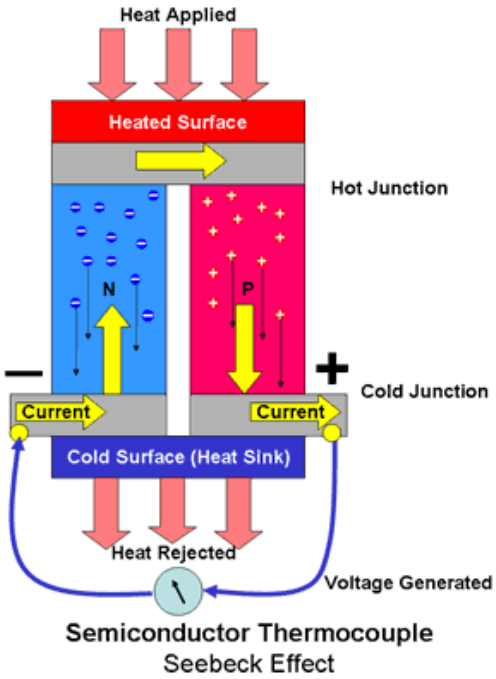

Figure 2. Schematics of a TEG system operation principle [17].

The TEG module is placed in the central part of the thermo-converter and consists of a semiconductor pellet array doped with both positive and negative charge carriers. N/p junctions are configured to be electrically connected in series, but at the same time thermally in parallel.

This is possible by using a metallic ceramic substrate that wraps the pellets and the circuits that connect them to form a single layer. The layer, called *Functionally Graded Material* (FGM), allows thermal stress relaxation on TEG cells that are particularly fragile and simultaneously promotes heat flow.

The efficiency of these systems depends essentially on the nature of semiconductor pairs and the operating temperature of the two surfaces. Generally, the temperature difference inside the thermoelectric module must be between 200 and 300 K. The efficiency of theoretical energy conversion achieved by the **TEG** is 10% but currently the HZ-20 modules of the Hi-Z Technology consisting of semiconductors with bismuth and tellurium have yields of about 5%, with a temperature range of 520-300 K. The theoretical

yield of exergetic conversion is 21%. The real yield of exergetic conversion of the HZ-20 commercial form is 11%.

The advantages of TEG thermal converters are:

1) No moving parts;
2) High power output per unit of weight: HZ-20 = 160 W/Kg, theoretical = 300 W/Kg;
3) Stability in performance characteristics (voltage-current). Business models are guaranteed to operate longer than 10 years;
4) High availability in the components market as well as extreme simplicity of construction that allows production costs to be reduced (4.400 €/kW);
5) Temperature values of the hot and cold walls low, therefore able to be used in highly degraded thermal waste

As far as the disadvantages of TEG Thermo-converters are concerned, the major limit is, however, the energy conversion efficiency which is in practice of the order of 5%.

1.4 The Stirling Engine

The Stirling engine belongs to the family of closed-loop combustion engines. As an evolving fluid, it uses air or nitrogen in most cases, but in new versions where performance is optimized, helium or hydrogen can be used. The ideal thermodynamic cycle, carried out by the evolving fluid, is the Stirling cycle. In the operation of the Stirling system, there is the movement of the pistons following expansion and compression of the gas passing alternately from a warm to a cold environment. This obviously has to be passed through a heat regenerator.

The high temperature source is actually the hot exchanger. This, being released from the car, can be of any kind. The cold exchanger or low temperature source is usually a cross-flow tube blower exchanger that uses water as a coolant. Depending on the positions taken by the plungers, four phases are identified:

1) Transfer of the hot fluid from the vertical cylinder (high temperature) to the horizontal cylinder (low temperature) with the crossover of the regenerator;
2) Compression of cold gas with a work L_c.
3) The gas compression in the horizontal cylinder expands the gas into the vertical cylinder which at the same time undergoes an expansion due to the temperature rise due to the regenerator and the hot surface. This expansion produces the work L_e.
4) The work L_e, through the shaft to which both pistons are connected, causes an expansion to the cold cylinder that recalls the hot gas contained in the vertical cylinder and restarts the cycle.

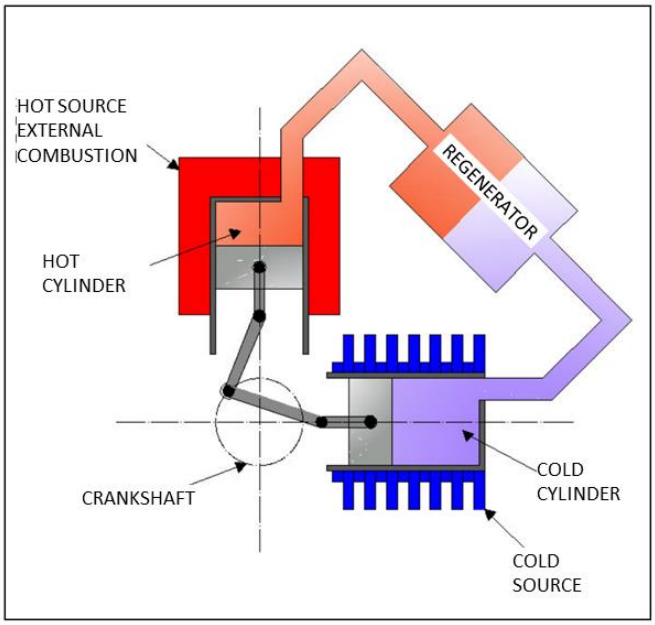

Figure 3. Schematics of a Stirling Engine system operation principle [16]**.**

It is clear that the work done is greater than compression work and frustration losses. Stirling's energy performance is closely related to its thermodynamic configuration. It has the same maximum theoretical thermal yield of a Carnot cycle but in the latest versions it is in the order of 33%. Considering the mechanical yields and the alternator of 0.82 and 0.92, respectively, the system has an electrical output of about 25%. For innovative prototypes, the efficiency of thermal conversion can reach a maximum of about 57%, which, considering the mechanical performance and the alternator, results in an electrical performance of the system of about 43%.

The advantages of *Stirling* engines are:

1) High efficiency of conversion of thermal and electrical energy;

2) Possibility to operate with a wide temperature range of the hot spring;

3) Thanks to external combustion, the number of maintenance and oil changes is also considerably reduced.

4) High power per unit of weight (can also reach 170 W/kg);

5) The cost of the Stirling engines is not high and varies from 1500 €/kW for large size plants (50 ÷ 200 kW) up to 3500 € / kW for small power plants.

As far as its disadvantages are concerned, substantially the largest limit is the high starting time due to the considerable thermal inertia of the system itself.

Table 1 compares the main characteristics of the three thermoelectric power generation technologies described above, with in addition the GaAs photovoltaic cell [16].

Table 1. Comparison between the main thermoelectric power generation technologies. Taken and adapted from [16]**.**

		AMTEC	*TEG*	*STIRLING*	*GaAs*
Energetic Efficiency [%]	*Theor*	**40**	**10**	**43**	**35**
	Real	**19**	**5**	**25**	**27**
Maximum temperature [K]		**1.000-1.300**	**300-800**	**1.000**	**350**
Cold source temperature [K]		**400-700**	**200-500**	**300**	**300**
Duration [hours]		**170**	**90.000**	**60.000**	**40.000**
Cost [€/kWh]		**10.000**	**4.000**	**1.500-3.500**	**500-750**
Mechanical moving parts		**NO**	**NO**	**YES**	**NO**
Potentially hazardous substances		**YES**	**NO**	**NO**	**NO**
Maintenance costs		**HIGH**	**VERY LOW**	**LOW**	**VERY LOW**
ORC system compatibility		**HIGH**	**LOW**	**VERY LOW**	**VERY LOW**
Power/Weight ratio [W/kg]		**16**	**160**	**170**	**200**

As it can be seen, all the technologies described above have their own pros and cons, and AMTECs seem so far less developed than others, but one of the most promising.

CHAPTER II

THE AMTEC CELL

2.1 Basic Principles of Operation

The AMTEC technology appears as a very promising technology for the direct conversion of the energy collected by a solar concentrator into electrical energy considering that its operating temperature range allows the usage of the thermal "*waste*" energy for a second conversion into electrical energy through Organic Rankine Cycle (**ORC)** systems with a mark increase of the global system performance (SEC + AMTEC + ORC).

For this reason, I decided to focus the Ph.D. research project on the AMTEC cell, trying to remove some of the known limitations, pointed out in table 1, and to try to obtain a device with reduced cost of industrial production, increased cell life time, increased power per unit of weight and with low maintenance costs and risks for human health and for the environment.

The research project is supported by the company Qohelet Solar Italia, which offered financial co-funding and by INAF-OAPA which offered scientific and technical advices.

In order to better understand the scientific and technological goals of the proposed research project, it is advantageous to focus on each single basic component of the AMTEC cell that can individually determine significant performance variations.

First of all, it is necessary to make a distinction that, while keeping the operating principle unchanged, divides AMTEC systems into two categories: forced recirculation systems or natural recirculation systems. The substantial difference lies in the liquid alkali metal circulation from the low-temperature zone to the high-temperature zone: it uses a pumping system in the former and uses gravity in the latter.

It is clear that moving a high temperature fluid requires exquisite technology, but it is also true that this entails advantages in the heat transmission and power generation phenomena that result in an increased system performance.

Ultimately, this aspect needs to be properly evaluated in the present project.

2.2 Liquid-Anode and Vapour-Anode Cycles

There are two types of AMTEC cycles respectively called liquid-anode cycle and vapour-anode cycle. Figure 4a shows the liquid-anode cycle.

The electrolyte, on the one hand, is in contact with a porous electrode in turn immersed in a sodium gas phase while the other side is in contact with the sodium metal in the liquid state that acts as an electrode itself.

When the electrodes are electrically connected through an external circuit, sodium (but the same can be said of any other metal and especially alkali metals) ionises to the interface between β-alumina and the anode.

The cations pass through β-alumina, while electrons that cannot pass it (being a protonic membrane, conducting positive ions and waterproof to the passage of negative charges) are forced to flow from the anode to the cathode, through the outer circuit recombining in this way with the cations, neutralizing them with cathode formation of neutral sodium atoms.

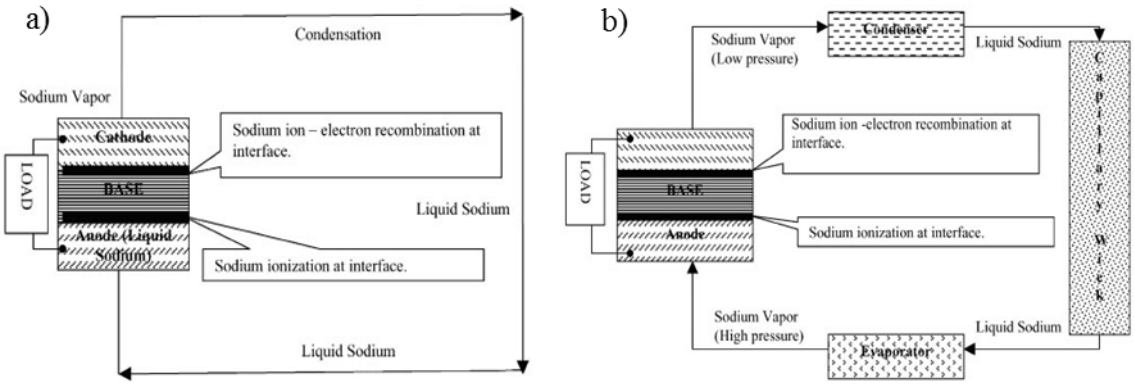

Figure 4. AMTEC liquid-anode cycle (a); AMTEC vapour-anode cycle (b) [12].

The gaseous sodium is then condensed, in a suitable condenser, collected and conveyed through a demister and then sent to the hot semi-cell that hosts the liquid anode through a recirculating system. Figure 4b shows the vapour-anode cycle.

In this case, both sides of β-alumina are in contact with sodium or any other alkali

metal in the vapour state.

In the cell element core that hosts the anode is high temperature steam and high pressure, while in the other semi-cell cell that houses the cathode there is steam at low temperature and low pressure.

An anode electrode is placed on the side of β-alumina in contact with the high pressure sodium vapour, while the cathode electrode is placed on the other side of β-alumina in contact with the sodium vapour at lower temperature and pressure.

Sodium vapour subject to higher pressure tend to expand, however, β-alumina is a protonic membrane impermeable to the passage of both negative and neutral atoms and conducting positive ions.

For sodium, the only way to expand to balance the two different pressure semi-cells Gibbs's chemical potential, is by ionising its neutral atoms, producing free alkali cations and electrons. The β-alumina, allowing the passage of alkali cations, thus facilitates the expansion of the metal from a higher pressure to a lower one.

Sodium cations are gradually accumulating on the semi-cell of the low-pressure side (that is, cathode), while the electrons remain stationary on the semi-cell of the high-pressure side (that is, anode). This creates a difference in potential balance that prevents the further flow of cations from one half to the other.

By electrical contacting the two electrodes through an external load, the electrons driven by the potential difference, will produce a current and consequently an electrical work on the external load.

At the cathode, the electrons recombine with the cations, neutralizing them, and thus allow a new stream of cations from the high-pressure semi-cell to the low-pressure one.

Obviously, if the pressure difference between the two environments is not maintained, after a certain time, they will find themselves in equilibrium or under isobaric conditions and the potential difference to the electrodes would gradually decrease.

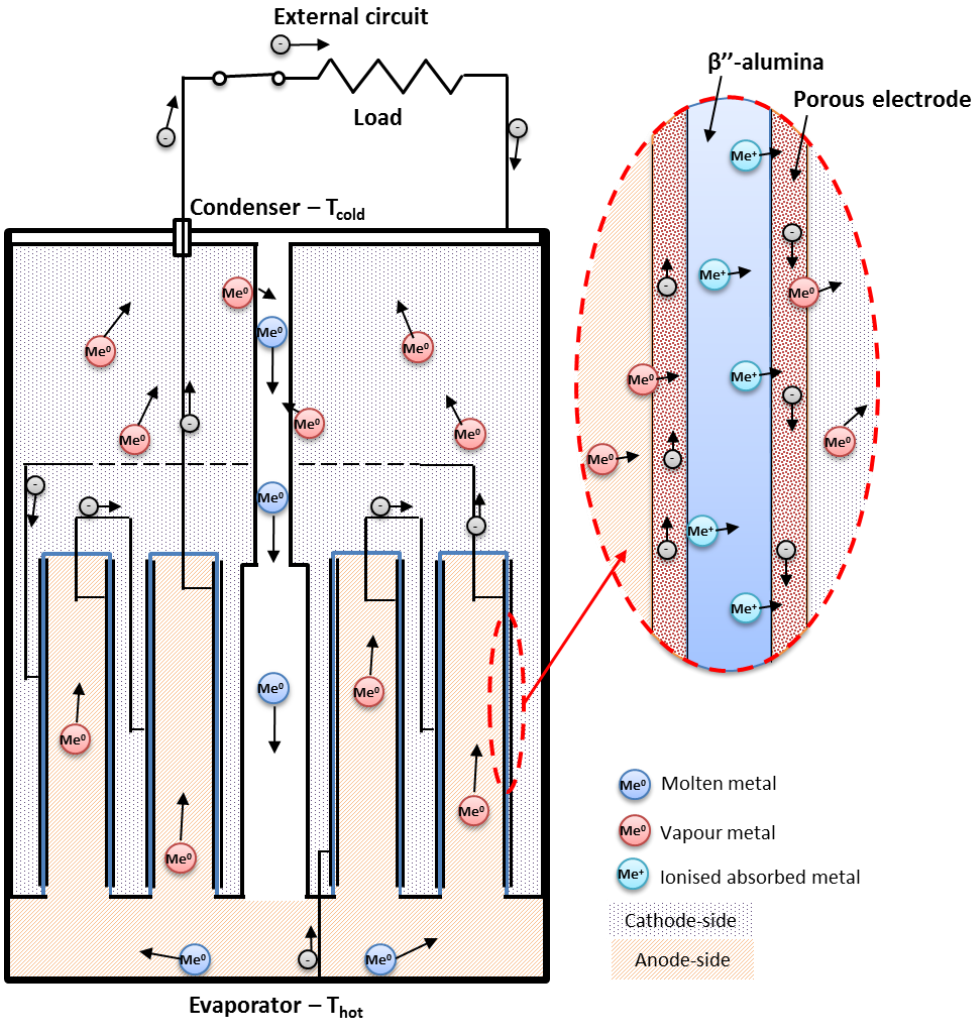

Figure 5. Schematic drawing of a multitube vapour anode/vapour cathode AMTEC device used for space applications. The main components of the cell and operation principle are shown.

2.3 Thermodynamic cycle of the fluid

After the examination of the components that form the AMTEC cell and their function, one can better understand the physics of the transformation involved and the thermodynamic cycle performed by the working fluid crossing the various components of the cell.

It should be noted that each thermodynamic transformation represented on the state diagram (P-V or T-S) between two consecutive points, is realized by a specific part or component of the cell (e.g. evaporation, lamination, condensation).

The following one is for example the thermodynamic cycle performed by sodium in an AMTEC cell with forced circulation:

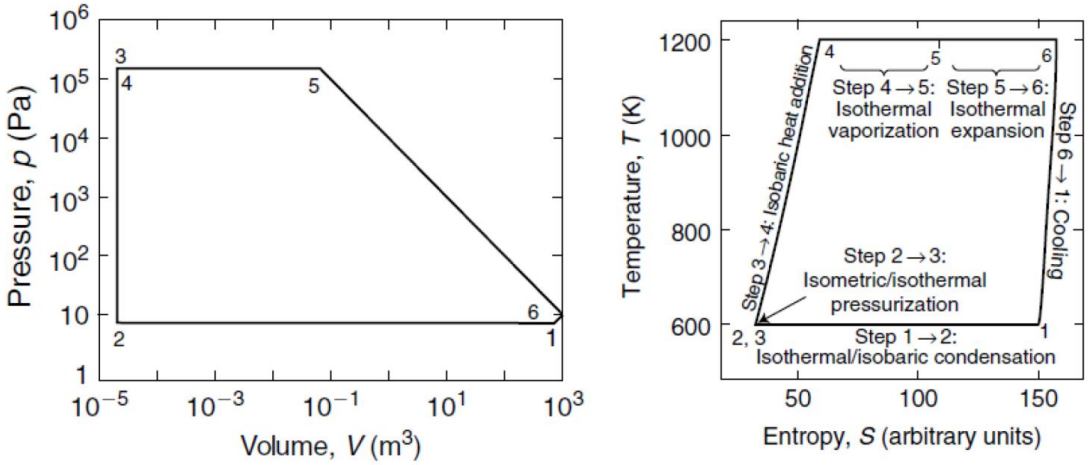

Figure 6. Thermodynamic cycle occurring in an AMTEC system. Taken and adapted from [18]**.**

1 → 2 Isothermal and isobaric condensation (condenser). This transformation takes place in the "condenser" component where through a heat exchanger, the heat extraction takes place by the heat transfer fluid and an isothermal phase passage occurs at the boiling temperature between sodium liquid sodium vapour;

2 → 3 Isothermal liquid sodium pressurization (high pressure zone). This transformation takes place by means of a pump that cuts work to the liquid (work in the case of natural circulation is done by the force of gravity);

3 → 4 Isobaric heat absorption. This transformation takes place in the "evaporator" component where thermal energy is shed on sodium which at this stage is heated up to the boiling temperature at the pressure set by the pump;

4 → 5 Isothermal and isobaric evaporation (BASE electrolyte). This transformation takes place in the "BASE electrolyte" component that allows the passage of sodium cation;

5 → 6 Isothermal expansion up to initial pressure (low pressure zone). This transformation takes place in the "Cathode" component that hosts the electrons and where the sodium cation is neutralized;

6 → 1 Quasi-isentropic cooling of vaporized sodium with the beginning of a new cycle (cavity between electrolyte and condenser). This transformation occurs in the cavity between the electrolyte and the condenser. The sodium vapours cool to the boiling temperature at the initial pressure.

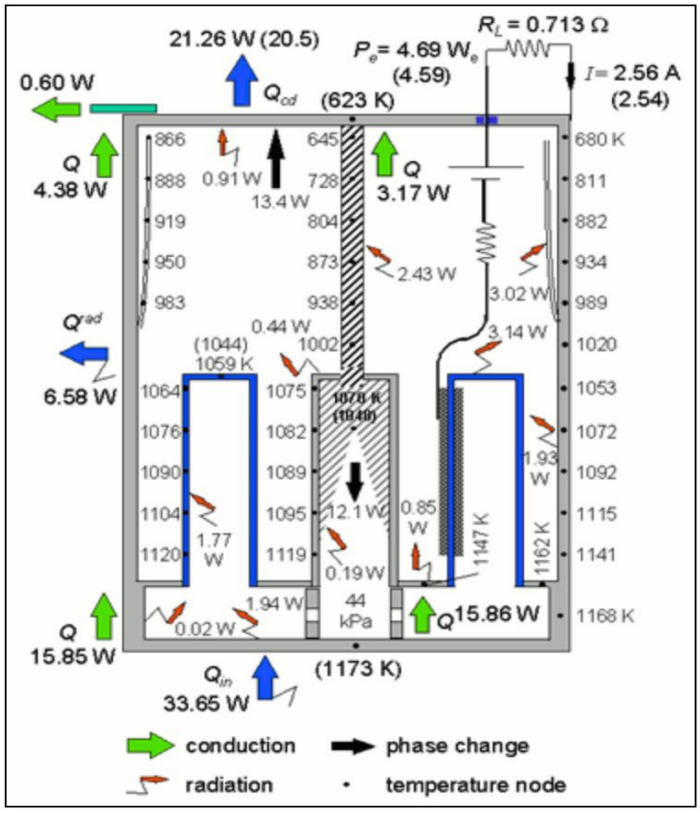

Figure 7. Schematics of the operating cycle of the AMTEC cell [19].

2.4 Cell assembly

Below is a brief list of components of a cell with natural recycle:

1. The **electric circuit** consisting of an internal and an external circuit. This, as is easily perceived, guides the current flow to the external load. Inside, there are the terminals of the individual electrolytes (31) needed to determine the internal parallel series configuration and the internal electric conductor (33) that collects the resulting flow leading to the outside. On the outside, there is the terminal (35) which is the component made of conductive material that guides the flow of electrons to the external load, which is closed with the wall which is in electric contact with the alkali ionic metal;

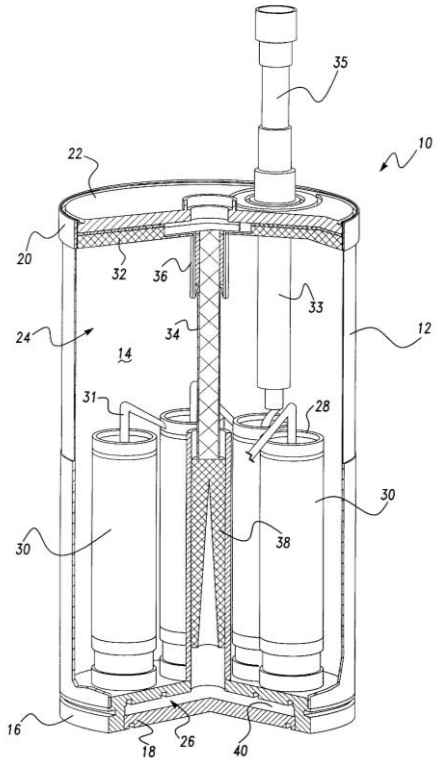

Figure 8. Schematic drawing of an AMTEC cell with indication of main items (see text for details) [20]**.**

2. **Base electrolyte** (30) is the heart of the AMTEC cell. In the most popular models it is solid and tubular. The material used in most cases is β-alumina. This ceramic material has the chemical-physical property of allowing the passage of positive ions and at the same time preventing the electrons from acting as an electrical insulator;
3. The **outer casing** including the lower cover (18) and the top cover (20) is the part in contact with the outside. This, on the one hand hosts the Hot Point (16) and the Cold Point (22) on the other. In the project phases, it is important to bear in mind that this part of the cell is continually subjected to thermal stress at high temperatures. In the most popular models, the cell wall is made of stainless steel to lower heat losses due to the reflection of this material;
4. The component required to change the state to alkali metal is **the evaporator** (38). This component is in contact with the hot wall made of material with high absorption power and low reflection of solar radiation in order to optimize the conversion efficiency solar radiation-thermal energy.
5. On the opposite side of the hot wall, there is **the condenser** (32). This component is in contact with the cold wall, lowering the gas-vapour temperature of the working fluid, condensing it and conveying it into the main artery bringing the fluid back to the evaporator; the working temperature of this component is determined by several parameters that can take advantage of different technological solutions for heat dissipation and/or maintaining stable working temperature values.
6. As anticipated, the **return artery** (34) is the channel leading the condensed metal back to the evaporator; in this part of the cell, the circulator is introduced in the case of forced recirculation;
7. Very important for the good functioning of the cell, the **high pressure zone** (26) is located near the hot spot where, by contact with the high temperature wall, the liquefied metal vaporizes to move near the base and restart the ionisation process. The design of this component or part of it must take into account high temperatures and high pressures;

8. Another very important component is the electrode. In most popular models, electrodes are manufactured in Molybdenum (Mo), titanium nitride and rhodium-tungsten alloys. The cathode is installed in the base for chemical deposition of vapours or sputtering, while the anode is applied to the base by the Weber process and then coated with the molybdenum to prevent electrical leakage inside it. Its function is to drive the load current. Finally, the thermal shields have the function of limiting the parasitic heat loss by irradiation.
9. The heat extraction system is a heat exchanger placed in contact with the condenser and capable of maintaining the cold wall of the condenser at a constant temperature through the circulation of a fluid (typically diathermic or steam oil according to the temperature of the condenser work of the ORC group and the AMTEC cell).

Figure 9. A particular configuration of an AMTEC converter with housing (left) removed [21]**.**

In the next sections, I discuss the role of the working fluid and the electrolyte on the performances of the AMTEC cell to identify possible alternative solutions with respect to those currently adopted in already tested devices. I will then describe a simplified, not-

rechargeable AMTEC-like cell, designed and built to support the experimental campaign on new working fluids and new electrolytes and present preliminary results of the experimental campaign.

2.5 Cell Materials

As seen in Chapter I, the AMTEC is an electrochemical device able to statically (i.e. without movement of mechanical parts but through a simple thermodynamic cycle carried out by a working fluid) and directly convert heat into electrical energy. To date, alkali metal fluids (lithium, sodium or potassium, and finally caesium) have been tested for the conversion process.

To date, the most used working fluid, according to the wide available literature, is sodium because of its excellent chemical and physical properties, which offer the best compromise between low ionisation energy (495 kJ/mol), low temperature of vaporization and reduced atomic dimensions.

As far as the electrolyte is concerned, the most used and discussed in literature today is the BASE (Beta Alumina Solid Electrolyte), initially used in the Sodium Sulphur Battery.

The sodium-β-alumina appears as a crystalline phase with highly variable composition containing aluminium oxide, Al_2O_3, and sodium oxide, Na_2O or Na_2O_5, in a nominal ratio of 5:1, and a small amount of metal oxide, usually lithium or magnesium, which stabilizes the β-crystalline structure. β-alumina is insulating compared to the electron transport and it is thermodynamically stable and chemically inert in contact with both sodium and low pressure sodium vapours. The two sides of β-alumina are electrically connected to two electrodes.

Sodium (but also any other metal and especially alkali metals), ionises to the interface between β-alumina and the anode (electrochemical oxidation). Cations pass through beta-alumina while electrons, failing to pass through, are forced to flow from the anode to the cathode through the external electric circuit and recombine with the cations,

neutralizing them with formation of neutral sodium atoms at cathode-side (electrochemical reduction).

If a sodium recycle system is present, the electrochemical cell never runs out and continues to produce current indefinitely.

However, sodium leads to technological problems, the most important of which is the decrease in the electrical power produced and consequently the degradation of electrochemical performance of the cell with time, a phenomenon caused by the degradation of the BASE electrolyte.

This prevents the use of such devices in all applications requiring long operation periods, unless both restoration and maintenance work is carried out frequently.

Several factors may cause electrolyte degradation and they are essentially related to a combined action of:

a) high working temperatures (1000 K),
b) chemical aggressiveness of sodium vapour which causes changes in the crystalline lattice of the electrolyte and chemical contamination.

Modification of the lattice due to the high operating temperature occurs as sodium leakage from the electrolyte structure, formation of fused dendrites in the electrolyte and formation of cracks or modifications in the microstructure. The fused sodium dendrites, once originated, can propagate in the electrolyte, possibly even for its entire thickness, causing a short-circuit of the cell especially if the electrolyte pores are too large. Electrons may find an alternative, easier (i.e. “less resistive”) path from the anode/electrolyte interface directly to the electrolyte/cathode interface, together with the working fluid cations. This results in a bypass of the external electric circuit and then in an electrical power loss, due to the reduction of current density (current per unit surface area of cell electrolyte) flowing through the external load. In other words, the propagation of sodium, from the high pressure to the low pressure side, occurs without ionisation at the anode/electrolyte interface.

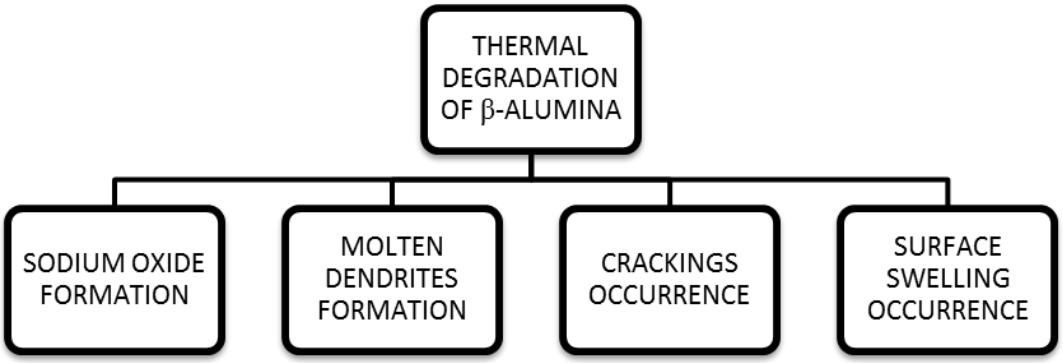

Figure 10. Possible mechanisms of thermal degradation of β-alumina.

The products of reactions between the sodium vapours and the material which the cell is built of (e.g. stainless steel but also special steels) can also enter the structure of the crystalline lattice of the electrolyte and settle on the edges of the grain or even replace some Na^+ ions in the structure itself (chemical contamination by reticular substitution) or simply deposit on the surface of the electrolyte and block the pore action by physically inhibiting the passage of sodium cations. All of these phenomena cause the reduction of the current density, hence increasing the resistance of the electrolyte to ionic transport.

The missed ionisation due to thermal effects or chemical aggressiveness of sodium results in a decrease in the number of electrons per surface area (current density) that flow through the external circuit and, consequently, a reduction in the power output, which is equal to the product between the cell voltage and the current circulating in the external electrical circuit.

CHAPTER III

TOWARDS A SECOND GENERATION AMTEC-LIKE CELL

3.1 Introduction

The presented results on currently developed AMTEC cells have shown that in order to make such type of thermoelectric converter of real interest for industrial applications, it is necessary to identify technological and design solutions able to improve the performance of such electrochemical devices in terms of stabilizing the cell power over time.

Recently, in the Technical Physics Laboratories of the University of Perugia, experiments have been carried out concerning the use of new materials for the realization of solid electrolyte and the adoption of caesium in replacement of traditional alkali metals (lithium, sodium or potassium) [1].

Among the main advantages offered, for example, by the use of caesium as a working fluid compared to lithium, there could be both lower ionisation energy and lower fusion temperatures, which would synergistically determine the opportunity to build AMTEC devices able to work at considerably lower temperatures than those currently available.

In the following paragraphs, we analyse the main components of the AMETEC cell and try to identify possible improvements that could bring to a second generation AMETEC-like cell.

3.2 The Working Fluid

Figure 11 illustrates the flow path of the alkali metal inside the AMTEC cell. Essentially, evaporating in the high temperature zone and condensing into the low pressure one, a continuous process is regenerated thanks to the thermal energy transferred from the outside.

The amount of flow is significantly linked to the available thermal energy, which means that any thermal oscillation of the heat source will inevitably affect the amount of charge available.

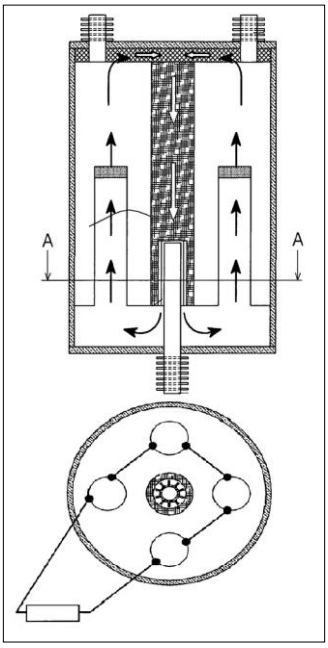

Figure 11. Simplified front sectional view and top view of an AMTEC cell, with indication of the flow path of the working fluid. Taken and adapted from [22]**.**

It is clear that working fluid and electrolyte are in turn chemically related one to the other, because the BASE must have in its lattice the same atoms as the working fluid to allow ionic conduction.

The main parameters to be considered in order to choose the working fluid are:

(1) **The melting point**. The working fluid melting temperature shall not be too high to avoid technological problems and to ensure compatibility with a SEC device, neither too low to work with high performance in both the AMTEC device (hot wall temperature/cold wall temperature ratio) and in the ORC group.

(2) **The boiling temperature**. The working fluid shall have a low boiling temperature to avoid high technological problems and to ensure compatibility with a SEC device. The boiling temperature, however, shall not be too low to work with high performance in both the AMTEC device (ratio hot wall temperature/ cold wall temperature) and in the ORC group.

(3) **Low electronegativity** and (4) **low ionisation energy**. If one wants to operate with a working fluid capable of crossing a mechanically stable solid electrolyte membrane (typically a β”-alumina), it will have to easily ionise in the form of cations and consequently have a low electronegativity and a low ionisation energy.

(5) **Atomic radius dimensions**. The working fluid must be a chemical element capable of moving or rather “spreading” easily into the electrolyte porosity. Therefore, it must have an atomic dimension including the electronic cloud not too large and in any case compatible with the porosity of the crystalline lattice of the electrolyte.

(6) **Material hazardousness**. Work fluid must be a material that is not classified as dangerous for human health and environment to minimize the risk of accidents and to lower the disposal costs of the device after the useful life of the device.

(7) **Material cost.** Working fluid must be a cheap material to optimize the cost of industrial production of the cell.

One of the activities of preliminary studies and research is, as previously stated, the choice of the new working fluid. In principle, this fluid could be chosen from the elements of the entire periodic table in light of the seven requirements listed above. In order to have a limited number of eligible candidates for the AMTEC cell’s “craft” workflow, one will need to identify selection criteria based on the above-mentioned seven requirements that exclude unsuitable elements and allow focusing on research activities within a limited number of possible candidates. In the following table, which lists the items in the periodic table, the non-eligible items will be highlighted in red.

As first exclusion parameter, the present research has been limited to metal elements, i.e. all non-metals and semi-metals have been excluded as potential working fluids. Moreover, only elements which can ionise to monovalent or divalent stable cations have been taken into account, i.e. those **belonging to groups IA (alkali metals), IIA (alkali-hearth metals), IB and IIB (transitional metals), and IIIA and IVA**, as it is known that higher valence cations unlikely diffuse through solid electrolytes [23, 24].

The third exclusion criterion used for material selection has been the melting point temperature. This value ensures the liquid state of the working fluid component in the cold side of the cell. In compliance with the heat cascade system one intends to implement, in order to ensure adequate thermal exchange, the melting temperature shall be lower than the maximum outlet temperature of the heat exchange medium used. For example, if the selected thermal fluid is a diathermic oil, this value can be ca. 430°C, which is equal to the maximum allowable wall temperature for a common diathermic oil (Therminol VP1).

Higher melting temperatures can be achieved e.g. by using overheated steam (500-600 °C) as heat transfer fluid, but in this case some the technological disadvantages occur, such as high pressure equipment. Other carriers, such as molten salts can operate at higher temperatures as well, at pressures lower than steam, but with solidification problems when the system is inactive.

For the purposes of the present work, the maximum melting point temperature was set to 430 °C.

Then, the fourth discriminant parameter has been the boiling point. This value is related to:

1) the temperature reached with the solar conversion system;
2) the temperature of the thermal waste one intends to realize;
3) the physical state the element must have during operation (typically liquid and vapour);

In particular, the boiling point of the element chosen as the "working fluid", shall ensure that the physic state of the material is liquid at the operating temperature and pressure of the cold-side. Such a temperature shall also be compatible with the maximum wall temperature allowable for the thermal fluid of the cooling system, which in turn should hopefully be high enough to meet the minimum temperature requirement of a third conversion system (e.g. Organic Rankine Cycle) possibly coupled to the device.

The element chosen as working fluid shall vaporise at the temperature and pressure of the hot wall and undergo ionisation. Last, but not least, the maximum boiling

temperature should be lower than the melting temperature of the solid electrolyte and cell enclosure materials themselves. As an example, in order to exploit a heat sink by coupling to an ORC system, a suitable boiling temperature range for the working fluid material is 280 ÷ 1350 °C[1]. Anyway, for the purposes of the present work, elements boiling in the interval 25 °C up to 2,500 °C have been included among potential solutions.

The fifth and sixth parameters used as discriminant are the electronegativity and the first ionisation energy, which are related to the ease of extraction of an electron from the atom. In fact, if one would carry a process of cationic transport through the electrolyte (negative ion transport electrolytes are not mechanically stable at typical operating temperatures) one should select elements having a quite low first ionisation energy (say, lower than 1,200 kJ/mol). This means to exclude non-metals, the whole semiconductors family, and also some metals with high values of first ionisation energy. Moreover, I've also imposed an upper limit to the Pauling electronegativity (say < 2.50).

Finally, regarding environmental and economic motivations, I decided to select not hazardous and not toxic elements, in order to comply with a "green energy" policy, and not too expensive metals (say < 2,500 $/kg) in order to be economically competitive with respect to other devices.

[1] Actually, the upper temperature limit leads to technological issues concerning the maximum temperature reachable with a SEC system, forcing to operate under vacuum even inside the hot zone of the cell.

Table 2. List of chemical elements examined depending on melting point, boiling point, electronegativity, energy of first ionisation, atomic radius and cost, for the application as working fluid in the AMTEC-like simplified device developed in the present work.

NAME	FAMILY	ATOMIC SYMBOL	GROUP	MELTING POINT [°C]	BOILING POINT [°C]	PHYSICAL STATE	ELECTRONEGATIVITY	ENERGY OF FIRST IONISATION [kJ/mol]	COST [$/100g]
Helium	NON METAL	He	VIIIA	-272,2	-268,9	g	N/A	2372	5,2
Neon	NON METAL	Ne	VIIIA	-248	-248,7	g	N/A	2081	33
Argon	NON METAL	Ar	VIIIA	-189,2	-185,7	g	N/A	1521	0,5
Krypton	NON METAL	Kr	VIIIA	-157	-152	g	3,00	1351	33
Xenon	NON METAL	Xe	VIIIA	-111,8	-107,1	g	2,60	1170	120
Radon	NON METAL	Rn	VIIIA	-71	-61,8	g	N/A	1037	N/A
Oganesson	NON METAL	Uuo	VIIIA	N/A	N/A	N/A	N/A	N/A	N/A
Fluorine	NON METAL	F	VIIA	-219,8	-188,1	g	3,98	1681	190
Chlorine	NON METAL	Cl	VIIA	-101	-34,6	g	3,16	1251	0,15
Bromine	NON METAL	Br	VIIA	-7,2	58,8	l	2,96	1140	4,9
Iodine	NON METAL	I	VIIA	113,5	184	s	2,66	1008	8,3
Astatine	NON METAL	At	VIIA	302	337	s	2,20	917	N/A
Tennessine	NON METAL	Uus	VIIA	N/A	N/A	N/A	N/A	N/A	N/A
Hydrogen	NON METAL	H	IA	-259,1	-252,9	g	2,20	1312	12
Carbon	NON METAL	C	IVA	3367	4827	s	2,55	1086	2,4
Nitrogen	NON METAL	N	VA	-209,9	-195,8	g	3,04	1402	0,4
Oxygen	NON METAL	O	VIA	-218,4	-183	g	3,44	1314	0,3
Phosphorous	NON METAL	P	VA	44,1	280	s	2,19	1012	4
Sulphur	NON METAL	S	VIA	112,8	444,7	s	2,58	1000	24
Selenium	NON METAL	Se	VIA	217	685	s	2,55	941	14
Boron	SEMIMETAL	B	IIIA	2079	2550	s	2,04	801	250
Silicon	SEMIMETAL	Si	IVA	1410	2355	s	1,90	787	5,4
Germanium	SEMIMETAL	Ge	IVA	947,4	2830	s	2,01	762	360
Arsenic	SEMIMETAL	As	VA	817	617	s	2,18	947	320

NAME	FAMILY	ATOMIC SYMBOL	GROUP	MELTING POINT [°C]	BOILING POINT [°C]	PHYSICAL STATE	ELECTRONEGATIVITY	ENERGY OF FIRST IONISATION [kJ/mol]	COST [$/100g]
Antimony	SEMIMETAL	Sb	VA	631	1950	s	2,05	834	4,5
Tellurium	SEMIMETAL	Te	VIA	449,5	989,8	s	2,10	869	24
Polonium	SEMIMETAL	Po	VIA	254	962	s	2,00	812	N/A
Aluminium	METAL	Al	IIIA	660	2467	s	1,61	578	1,8
Gallium	METAL	Ga	IIIA	29,8	2403	s	1,81	579	220
Indium	METAL	In	IIIA	156,6	2080	s	1,78	558	120
Tin	METAL	Sn	IIIA	232	2270	s	1,96	709	8
Thallium	METAL	Tl	IIIA	303	1457	s	1,62	589	48
Lead	METAL	Pb	IVA	327,5	1740	s	2,33	716	1,5
Bismuth	METAL	Bi	VA	271	1560	s	2,02	703	11
Nihonium	METAL	Uut	IIIA	N/A	N/A	N/A	N/A	N/A	N/A
Flerovium	METAL	Fl	IVA	N/A	N/A	N/A	N/A	N/A	N/A
Moscovium	METAL	Uup	VA	N/A	N/A	N/A	N/A	N/A	N/A
Livermorium	METAL	Lv	VIA	N/A	N/A	N/A	N/A	N/A	N/A
Scandium	METAL	Sc	IIIB	1541	2832	s	1,36	633	1400
Titanium	METAL	Ti	IVB	1660	3287	s	1,54	659	6,1
Vanadium	METAL	V	VB	1890	3380	s	1,63	651	220
Chromium	METAL	Cr	VIB	1857	2672	s	1,66	653	10
Manganese	METAL	Mn	VIIB	1244	1962	s	1,55	717	1,7
Iron	METAL	Fe	VIIIB	1535	2750	s	1,83	762	6,7
Cobalt	METAL	Co	VIIIB	1495	2870	s	1,88	760	21
Nickel	METAL	Ni	VIIIB	1453	2730	s	1,91	737	7,7
Copper	METAL	Cu	IB	1083	2567	s	1,90	745	2,7
Zinc	METAL	Zn	IIB	419,6	906	s	1,65	906	3,7
Yttrium	METAL	Y	IIIB	1523	3337	s	1,22	600	220
Zirconium	METAL	Zr	IVB	1852	4377	s	1,33	640	16
Niobium	METAL	Nb	VB	2468	4742	s	1,60	652	18
Molybdenum	METAL	Mo	VIB	2617	4612	s	2,16	684	11

NAME	FAMILY	ATOMIC SYMBOL	GROUP	MELTING POINT [°C]	BOILING POINT [°C]	PHYSICAL STATE	ELECTRONEGATIVITY	ENERGY OF FIRST IONISATION [kJ/mol]	COST [$/100g]
Technetium	METAL	Tc	VIIB	2172	4877	s	1,90	702	N/A
Ruthenium	METAL	Ru	VIIIB	2310	3900	s	2,20	710	1400
Rhodium	METAL	Rh	VIIIB	1966	3727	s	2,28	720	13000
Palladium	METAL	Pd	VIIIB	1554	3140	s	2,20	804	15
Silver	METAL	Ag	IB	962	2212	s	1,93	731	120
Cadmium	METAL	Cd	IIB	320,9	765	s	1,69	868	6
Hafnium	METAL	Hf	IVB	2227	4600	s	1,30	659	120
Tantalum	METAL	Ta	VB	2996	5425	s	1,50	761	120
Tungsten	METAL	W	VIB	3410	5660	s	2,36	770	11
Rhenium	METAL	Re	VIIB	3180	5600	s	1,90	760	540
Osmium	METAL	Os	VIIIB	3045	5030	s	2,20	839	7700
Iridium	METAL	Ir	VIIIB	2410	4130	s	2,20	878	4200
Platinum	METAL	Pt	VIIIB	1772	3827	s	2,28	868	4700
Gold	METAL	Au	IB	1064	3080	s	2,54	890	4400
Mercury	METAL	Hg	IIB	-38,9	357	l	2,00	1007	5
Rutherfordium	METAL	Rf	IVB	N/A	N/A	N/A	N/A	N/A	N/A
Hafnium	METAL	Db	VB	N/A	N/A	N/A	N/A	N/A	N/A
Seaborgium	METAL	Sg	VIB	N/A	N/A	N/A	N/A	N/A	N/A
Bohrium	METAL	Bh	VIIB	N/A	N/A	N/A	N/A	N/A	N/A
Hassium	METAL	Hs	VIIIB	N/A	N/A	N/A	N/A	N/A	N/A
Meitnerium	METAL	Mt	VIIIB	N/A	N/A	N/A	N/A	N/A	N/A
Darmstadtium	METAL	Ds	VIIIB	N/A	N/A	N/A	N/A	N/A	N/A
Roentgentium	METAL	Rg	IB	N/A	N/A	N/A	N/A	N/A	N/A
Copernicium	METAL	Cn	IIB	N/A	N/A	N/A	N/A	N/A	N/A
Actinium	METAL	Ac	Actin.	1050	3200	s	1,10	499	N/A
Thorium	METAL	Th	Actin.	1750	4790	s	1,30	587	N/A
Protactinium	METAL	Pa	Actin.	1570	4000	s	1,50	568	N/A
Uranium	METAL	U	Actin.	1132	3818	s	1,38	598	N/A

NAME	FAMILY	ATOMIC SYMBOL	GROUP	MELTING POINT [°C]	BOILING POINT [°C]	PHYSICAL STATE	ELECTRONEGATIVITY	ENERGY OF FIRST IONISATION [kJ/mol]	COST [$/100g]
Neptunium	METAL	Np	Actin.	640	3900	s	1,36	605	N/A
Plutonium	METAL	Pu	Actin.	641	3232	s	1,28	585	N/A
Americium	METAL	Am	Actin.	994	2607	s	1,30	578	N/A
Curium	METAL	Cm	Actin.	1340	N/A	s	1,30	581	N/A
Berkelium	METAL	Bk	Actin.	986	N/A	s	1,30	601	N/A
Californium	METAL	Cf	Actin.	N/A	N/A	N/A	1,30	608	N/A
Einstenium	METAL	Es	Actin.	N/A	N/A	N/A	1,30	619	N/A
Fermium	METAL	Fm	Actin.	N/A	N/A	N/A	1,30	627	N/A
Mendelevium	METAL	Md	Actin.	N/A	N/A	N/A	1,30	635	N/A
Nobelium	METAL	No	Actin.	N/A	N/A	N/A	1,30	642	N/A
Lawrencium	METAL	Lr	Actin.	N/A	N/A	N/A	N/A	N/A	N/A
Lanthanum	METAL	La	Lanth.	920	3454	s	1,10	538	64
Cerium	METAL	Ce	Lanth.	798	3257	s	1,12	534	57
Praseodymium	METAL	Pr	Lanth.	931	3017	s	1,13	527	170
Neodymium	METAL	Nd	Lanth.	1016	3127	s	1,14	533	110
Promethium	METAL	Pm	Lanth.	1042	3000	s	N/A	535	N/A
Samarium	METAL	Sm	Lanth.	1074	1794	s	1,17	545	130
Europium	METAL	Eu	Lanth.	822	1529	s	N/A	547	3600
Gadolinium	METAL	Gd	Lanth.	1313	3273	s	1,20	593	191
Terbium	METAL	Tb	Lanth.	1365	3230	s	N/A	569	1800
Dysprosium	METAL	Dy	Lanth.	1412	2567	s	1,22	573	210
Holmium	METAL	Ho	Lanth.	1474	2700	s	1,23	581	740
Erbium	METAL	Er	Lanth.	1529	2868	s	1,24	589	270
Thulium	METAL	Tm	Lanth.	1545	1950	s	1,25	597	4100
Ytterbium	METAL	Yb	Lanth.	819	1196	s	N/A	603	530
Lutetium	METAL	Lu	Lanth.	1663	3402	s	1,27	524	6900
Beryllium	METAL	Be	IIA	1278	2970	s	1,57	899	530
Magnesium	METAL	Mg	IIA	649	1090	s	1,31	738	3,7

NAME	FAMILY	ATOMIC SYMBOL	GROUP	MELTING POINT [°C]	BOILING POINT [°C]	PHYSICAL STATE	ELECTRONEGATIVITY	ENERGY OF FIRST IONISATION [kJ/mol]	COST [$/100g]
Calcium	METAL	Ca	IIA	839	1484	s	1,00	590	11
Strontium	METAL	Sr	IIA	769	1384	s	0,95	549	100
Barium	METAL	Ba	IIA	725	1640	s	0,89	503	55
Radium	METAL	Ra	IIA	700	1140	s	0,90	509	N/A
Lithium	METAL	Li	IA	180,5	1342	s	0,98	520	27
Sodium	METAL	Na	IA	97,8	883	s	0,93	496	7
Potassium	METAL	K	IA	63,25	760	s	0,82	419	85
Rubidium	METAL	Rb	IA	38,9	686	s	0,82	403	1200
Caesium	METAL	Cs	IA	28,4	669	s	0,79	376	1100
Francium	METAL	Fr	IA	27	677	s	0,70	380	N/A

If one considers also production costs, hazardousness of the material (first requirement: not radioactive), restrained toxicity for both human and environment in order to reduce the costs of disposal and the risks in case of accident/explosion/fire etc. of the system, the potential candidates could be those reported in Table 3: Gallium, Indium, Tin, Thallium, Lead, Zinc, Cadmium, Mercury, Lithium, Sodium and Potassium.

Table 3. List of selected chemical elements suitable for the application as working fluid in the AMTEC-like simplified device developed in the present work.

NAME	FAMILY	ATOMIC SYMBOL	GROUP	MELTING POINT [°C]	BOILING POINT [°C]	PHYSICAL STATE AT T=20°C	ELECTRONEGATIVITY	ENERGY OF FIRST IONISATION [kJ/mol]	COST [$/100g]
Gallium	METAL	Ga	IIIA	29,8	2403	s	1,81	579	220
Indium	METAL	In	IIIA	156,6	2080	s	1,78	558	120
Tin	METAL	Sn	IIIA	232	2270	s	1,96	709	8
Thallium	METAL	Tl	IIIA	303	1457	s	1,62	589	48
Lead	METAL	Pb	IVA	327,5	1740	s	2,33	716	1,5
Zinc	METAL	Zn	IIB	419,6	906	s	1,65	906	3,7
Cadmium	METAL	Cd	IIB	320,9	765	s	1,69	868	6
Mercury	METAL	Hg	IIB	-38,9	357	l	2,00	1007	5
Lithium	METAL	Li	IA	180,5	1342	s	0,98	520	27
Sodium	METAL	Na	IA	97,8	883	s	0,93	496	7
Potassium	METAL	K	IA	63,25	760	s	0,82	419	85

The research project was first oriented to the selection of suitable metals, among those listed above, that could be the new working fluid(s) for the AMTEC-like device to be developed. The main goals are: reduction of risks for health and environment and optimisation of industrial manufacturing, maintenance and disposal costs at the end of life of the device.

3.3 The Solid Electrolyte

Ceramic membranes belong to the special category of separating means that are widely used in various industries, from the pharmaceutical one to water purification and desalination processes, from the oil & gas industry to the electrochemical one.

The main function of a membrane (in general) is to act as a separating barrier, i.e. to physically segregate two environments where different operating conditions may also occur, for example a different pressure, a different temperature, a different concentration, or a different electrical potential, depending on the process occurred (gas separation, pervaporation, reverse osmosis, nanofiltration, ultrafiltration, microfiltration, dialysis, electrodialysis).

The main feature of ceramic membranes is the material they contain: in fact, the use of inorganic materials, so-called "ceramics", such as Al_2O_3, TiO_2, ZrO_2, SiO_2, usually produced by clay baking processes, siliceous sands or alumina-silicates gives the membrane mainly chemical resistance against corrosive agents and thermal resistance for high temperature operation. The addition of certain additives also improves mechanical strength by providing an extremely versatile and easily available, low cost, stable and low maintenance service.

Among the most popular industrial applications are: filtration of cast metals or exhaust gas filters for diesel engines. The peculiarity of ceramic membranes is in fact the ability to operate at high temperatures, which makes them suitable for a large number of applications where polymer membranes cannot be used.

Usually the ceramic membranes are composite, i.e. realized by overlapping two or more layers of different materials, at least one of which serves as a real ceramic support, which gives mechanical strength and has a more or less porous structure, while a second layer, whose thickness is much smaller and whose structure is dense and compact, acts as a filter element.

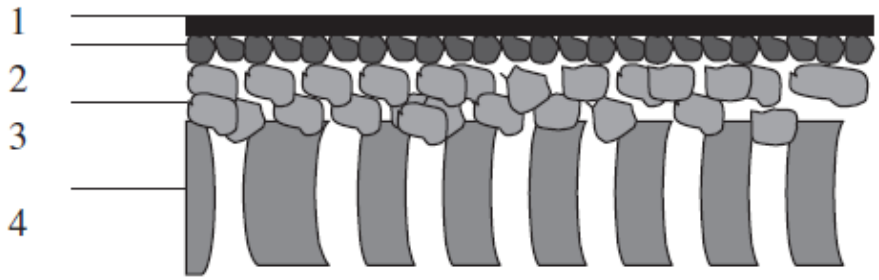

Figure 12. Schematic representation of an asymmetric composite membrane. (1) dense layer of modified separator (no porosity absent or <2nm); (2) separator layer (porosity 2-50 nm); (3) intermediate layers (pores 50-1000 nm); (4) Porous support (1-15 mm porosity). Adapted from [25]**.**

A particular subcategory of ceramic membranes is represented by the conductive ceramic membranes, which are used in the field of batteries, fuel cells and electrochemical reactors.

A material that gives positive ions electrical conductivity is beta-alumina, a dense and polycrystalline ceramic in which ionic species (such as sodium ions, potassium ions, lithium ions or other kind of ions) are transferred during the production process, which will form the "mobile ions" within the alumina matrix. Thus, they make membranes capable to be passed through by a species rather than others, provided in ionic form, so that for each ion that is absorbed into one side of the membrane and spreads therein, there is one that is desorbed on the opposite side. For example, if an ionic conductive oxygen membrane is immersed in a region where a chemical oxygen potential gradient exists, the oxygen ion will permeate through the membrane, from higher chemical potential points to smaller chemical potential points, while the neutrality of the charge will be kept by a proportional stream of electrons in the opposite direction.

The electrical conductivity of an ionic ceramic membrane is a very important parameter since the membrane itself can act as an internal short circuit conductor, so that such membranes may not require electrodes or external circuits.

This type of membrane is produced by the technique of electrophoretic deposition, which promotes the migration of colloidal particles or charged species into solution, under the action of an applied external electric field, towards an electrode with an opposite charge with respect to the particles, which will deposit on it creating a thin layer.

In particular, in a bathtub called "galvanic bath" there is a solution of a salt of the metal to be deposited and there are immersed two electrodes, one of which forms the object to be covered (cathode on which the reaction of electrochemistry occurs) and the other consists of an inert metal or of the same metal present in solution (anode on which the electrochemical oxidation reaction occurs). By applying a potential difference between the electrodes, the metal cations will migrate to the cathode while the solution anions migrate to the anode. At cathode, cations are reduced to the neutral state for the purchase of one or more electrons related to the electrode via the outer circuit and coming from the anode, on which they have been developed at the expense of the same metal constituting the latter, which will be consumed liberating ions in solution (so-called "sacrificial anode").

This production technology allows to finely modulate the thickness of the deposited layer according to needs and to limit defects in products such as air bubbles or gases that can lead to cracks and fractures.

The main parameters for the choice of the electrolyte are:

- The presence and mobility of the ion network of the selected working fluid element;
- The molecular structure at the cell working temperatures (hot wall temperature);
- The crystalline lattice;
- The duration of electrochemical activity and the decay of the electrolyte properties;
- Stability and mechanical properties.

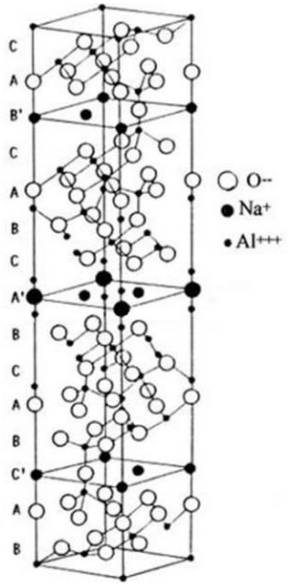

Figure 13. Disposition of oxygen, sodium and aluminium atoms in the crystalline lattice, in a sodium beta-alumina [26]**.**

The BASE electrolyte structure should be highly porous, electrically insulating and at the same time mechanically stable and resistant, acting also as a barrier to the passage of electrons and different components of the working fluid cations (typically Lewis bases). These features are typical of ceramic materials. The most commonly used component is β-alumina. This material has a crystalline structure and belongs to the ceramic family. The main features are: high ionic conduction (cation) and poor electron conductance. To allow the ionisation process, Al_2O_3 alumina base is doped with the metal chosen. This alters the chemical structure. In the crystalline lattice obviously there are atoms of the chosen working fluid element available for ion conduction.

In our case, identifying the eleven candidate elements as cell working fluid, using BASE as a β-alumina electrolyte, one could alternate the doping component in the eleven different configurations by obtaining: 1) Ga- β-alumina, 2) In-β-alumina, 3) Sn-β-alumina, 4) Tl-β-alumina, 5) Pb-β-alumina, 6) Zn-β-alumina, 7) Cd-β -alumina, 8) Hg-β-alumina, 9) Li-β-alumina, 10) Na-β-alumina, 11) K-β-alumina.

In the case of Sodium, $Na_2O_5Al_2O_3$ has a laminar structure in which each layer has a thickness of 1 nm between solid O^{2-} ions blocks where Al^{3+} ions occupy the octahedral and tetrahedron interstices. The Na^+ ion can then move freely on the perpendicular planes, resulting in an anisotropic structure. Ultimately, the ionic conduction level is closely linked to the molecular structure and any change in it, it directly influences the ionic strength and therefore the power produced. Below there is an example of how the structure can affect ionic conduction.

In this case, the β-alumina structure (hexagonal, a_0 = 0.559 nm, c_0 = 2.261 nm) and the structure of β"-alumina (rhombohedral, a_0 = 0.560 nm, c_0 = 3.395 nm) are compared. What can be noted is that the rhombohedral one can lead to an amount of Na^+ ions greater than 50% of the hexagonal structure. This is due to the configuration that take oxygen ions.

The result of the brief analysis clearly indicates that ion conduction occurs through the openings or interstices in the crystalline lattice of the electrolyte and hence any punctual defects thereof, caused by the absence of atoms in the working position and/or consequent or parallel lack of interstitial, results in a loss of electrochemical properties of the electrolyte and ultimately of cell power.

3.4 The Electrodes

Mass transport and fluid-solid interface kinetics in AMTEC systems strongly depends on electrode nature and porosity, as well as on temperature.

Generally, for several applications in electrochemical processes, the so-called **Dimensionally Stable Anodes** (DSA) are adopted.

Normally, electrodes (anodes and cathodes) are made of a base material, which is responsible of both mechanical stability and a uniform distribution of cell current. Titanium is characterized by both above mentioned features.

Many "insoluble" electrodes, that means they do not dissolve in solution by chemical aggression, in fact are made of titanium as base component. Occasionally, in some electrodes precise amount of Niobium (Nb), Tantalum (Ta) and Zirconium (Zr) are added.

Generally, electrodes are available in form of slab, maze, rod, wire, ribbon and can also be built for custom applications.

For some synthesis processes and/or some special applications, titanium electrodes can also have electrocatalytic selective activity higher than conventional nickel, lead, lead alloy, steel, graphite and magnetite electrodes.

Applications in which they are used include:

- Electrodialysis for waste water treatment, water conditioning and organic compounds synthesis;
- Cathodic protection of various structures such as off-shore platforms, ships, concrete reinforce bars;
- Humid electrodeposition of precious metals such as gold, rhodium, platinum, palladium and non-ferrous metals, such as chromium, nickel, copper, cobalt, tin and zinc;
- Production of chlorates, perchlorates, chlorine, caustic soda, ipochlorite etc.;
- Electrolytic production of chromic acid and hydrogen from water (water electrohydrolysis);
- Electrochemical polishing of electronic components;
- Galvanization of steel ribbons;
- Electrochemical recovery of metals;
- Electrophoresis.

Moreover, with titanium electrodes, the mud commonly present on conventional electrodes (e.g. in nickel, lead, steel or magnetite) does not appear when DSA are adopted.

The use of titanium electrodes often allows to save the cost for maintenance activities related to the removal of highly-toxic disposal-expensive metallic muds.

For this reason, most of the electrodes are titanium-based and allow to work with electrochemical devices where there is no accumulation of lead or other metallic heavy contaminants.

In this way, titanium electrodes are ecologically sustainable because they do not need the removal of electrochemical process hazardous muds. In addition, there is also an

energy saving of about 10-15% on electrolytic cells or an equal or greater production of energy in galvanic cells related to the lower cell over-potentials, the lower production costs, the higher corrosion resistance of electrodes: all these characteristics make titanium electrodes recommended for long duration performance.

In the following, a comparison of commercially available electrodes is reported:

- **PTA** Platinised Titanium Anode
- **PNA** Platinised Niobium Anode
- **PIA** Platinum and Iridium Anode
- **RUA** Ruthenium based Anode
- **IBA** Iridium based Anode
- **MMOA** Metal Mixed Oxide Anode
- **PDBA** Palladium based Anode

ELECTRODES		PTA	PNA	RUA	PIA	MMOA	IBA	PDBA
Electroplating	Precious Metals	➡		➤				
	Base metals	➡			◆	➤	➤	
Electrolytic Recovery	Precious Metals	➡	◆	➡	◆	➤		
	Base metals	➡	◆			➤		
Electro-Chemical Sensing		◆	◆		◆	➤		◆
Electro-Winning Refining of Metals		➤	◆			➤	◆	◆
Electro-Galvanizing					➡	➤		
Electro Tinning					◆	◆		
Electro Forming		➤			◆	◆	➤	
Regeneration Of Chromic acid		◆				◆		
Electro-Dialysis		➡	◆		◆	◆	◆	
Cathodic Protection		➡			➡	➤	➤	
Electrolytic production of	Chlorate		➡	➡				
	Chlorine		➤	➡	➤			
	Sodium hypo chlorate	➡	➡	➡	➤	◆		
	Hydrogen & Oxygen				◆		◆	
Electro synthesis Of Organic & Inorganic Compounds		◆			◆	◆	◆	➤

➡ Recommended ◆ Dependent on specific application ➤ Limited use

The electrochemical AMTEC-like cell designed and tested in the present research does not actually have electrodes deposited on the membrane surfaces. The role of the electrodes is provided by two stainless steel meshes which are electrically and mechanically connected with the two semi-cell flanges.

The lack of an electrode deposited on the membrane surface does not allow to drain significant current from the device, while such a device can be employed for experiments useful to measure open circuit cell voltage or very low currents in order to minimize over-potentials.

Experiments were initially conducted using hydrogen as working fluid, in order to verify the correspondence of theoretical data with experimental ones, at ambient temperature. Chemical hoods and laboratory equipment already in the availability of Istituto Nazionale di AstroFisica (INAP, Palermo) were used. The use of hydrogen also made it possible to check the correct operation and functionality of the device, i.e. the mechanical seal in pressure and/or vacuum, the mechanical seal and electrical insulation of the aluminium foil, and the electrical insulation of Macor spacers.

The use of a metal, even not alkali like zinc and even at high temperatures, in fact requires to operate under vacuum. This implies, in turn, the necessity to operate with perfect vacuum seals, because a possible contamination of the working environment due to lacking of external air would lead (at high temperature) to an immediate oxidation of the metal with consequent loss of efficiency and/or functionality of the device.

3.5 Material Procurement

Among the eleven potential elements pre-selected in Table 3, the safest and most readily available is zinc, so it was selected as first new working fluid to be tested. However, making this choice, I accepted pretty high melting and boiling points with respect to other pre-selected elements, giving priority to ease of handling and low cost.

As an electrolyte, instead, I chose to start the investigation with a simple porous β-alumina, doped with different metals (sodium, lithium, potassium, silver).

In order to start the experimental activities, 20 g of 99,999% pure metallic zinc 150 μm powder has been ordered from the following manufacturer:

Goodfellow Cambridge Ltd.
Ermine Business Park
Huntingdon PE29 6WR, England
Tel +44(0) 1480 424 800 Fax: +44(0) 1480 424 900
Email: info@goodfellow.com

Distributed in Italy by:

Prodotti Gianni S.r.l.
Via M.F. Quintilliano 30
Milano I-20138, Italia
Tel +39 02 5097 220 Fax +39 02 5097 276
Email: ricerca@prodottigianni.com

The following conductive ceramic membranes based on "functionalized" beta-alumina with different ionic species have been ordered:

n° 1 beta"-alumina sodium disc, mod. D20-1-LNZ, diameter 20mm, thickness 1mm

n° 6 beta"-alumina sodium discs, mod. D45-1.5-LNZ,diameter 45mm, thickness 1.5mm

n° 1 beta"-alumina potassium disc, mod. D20-1-LKZ, diameter 20mm, thickness 1mm

n° 1 beta"-alumina potassium disc, mod. D45-1.5-LKZ, diameter 45mm, thickness 1.5mm

n° 2 beta"-alumina lithium discs, mod. D20-1-LLZ, diameter 20mm, thickness 1mm

n° 2 beta"-alumina lithium discs, mod. D45-1.5-LLZ, diameter 45mm, thickness 1.5mm

n° 3 beta"-alumina silver discs, mod. D45-1.5-LAgZ, diameter 45mm, thickness 1.5mm

The ceramic membranes are manufactured and distributed by:

IONOTEC ltd.
14 Berkeley Court, Manor Park, Runcorn
Cheshire WA7 1TQ, England
Tel +44(0) 1928 579668 Fax +44(0) 1928 579627
E-Mail: contact@ionotec.com

The ceramic membranes supplier cannot provide membranes doped directly with zinc, because the production of such membranes would require several modifications on the manufacturing plant and would involve the presence of contaminations by by-products which would be very difficult to handle. Nevertheless, the supplier specified that the doping with any other metal would require a beta-alumina initially doped with one of the four above mentioned elements as starting substrate, and would rely on the substitution of the existing metals with the new metal inside the crystalline lattice.

The above-mentioned supplier declares, for the ordered membranes, the following chemical-physical properties (Table 4).

Table 4. Selected physical and electrical properties of BETA-aluminas membrane discs supplied by IONOTEC LTD.

Mobile ion	Na+	K+	Li+
Porosity (%)	1-2	2-3	1-2
Rupture strength (MPa)	250-350	200-300	
Weibull force factor	8-13	8-13	
Maximum pore size (μm)	5	8	
Maximum grain size (μm)	20	20	
Thermal expansion coefficient (x 10^{-6}) $°C^{-1}$			
0-500°C	7.2	7.45	
500-1000°C	8.6	8.5	
Resistivity (ohm m)			
25°C	6.0	12.5	190
100°C	0.6	2.5	14
200°C	0.1	0.4	1.6
300°C	0.042	0.18	0.58
400°C	0.026	0.091	0.33
500°C	0.023	0.059	0.23
600°C	0.020	0.040	0.18
Ionic conductivity $(ohm\ cm)^{-1}$			
25°C	0.002	0.0005	
200°C	0.092	0.021	
300°C	0.24	0.053	
400°C	0.38	0.10	

CHAPTER IV
DESIGN OF A SIMPLIFIED EXPERIMENTAL CELL

4.1 Work Plan

AMTEC devices, as described in chapter II, work in "closed loop" or through a "hydraulic circuit" in which the working fluid flows, and performing a closed thermodynamic cycle by using two different temperature surfaces (source and heat well respectively), allows the continuous regeneration (in theory indefinitely) of the pressure difference, and consequently of "chemical potential", the driving force of the process that determines the difference in electrical potential of the electrodes.

AMTEC devices cannot therefore be configured as simple "primary batteries" (i.e. non-rechargeable) that are subject to exhaustion or discharge. Like Molten Carbonate Fuel Cells (MCFCs) are "batteries", or rather, "electrochemical cells" capable of producing a constant electric current for a considerable lifetime, operating in a closed loop. Unlike MCFC cells, however, they exploit two galvanic semiconductors containing the same chemical species present but at different concentration.

From this point of view AMTEC cell is similar to a special "concentration cell-type rechargeable battery". For example, a primary (and therefore non-rechargeable) battery may be composed of two copper electrodes immersed in two solutions containing copper sulphate ($CuSO_4$) at a different concentration and separated by a porous septum or a salt bridge. The cathode compartment is composed of the semi-cell made of the metal immersed in the most concentrated solution, while the anode is made of the metal immersed in the most diluted solution.

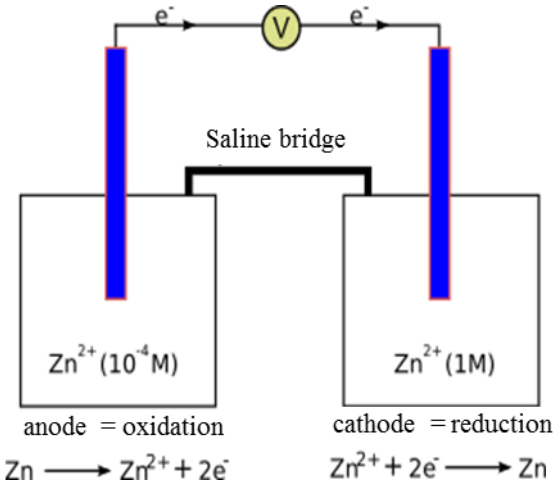

Figure 14. Scheme of a primary concentration cell with zinc salt solutions [27]**.**

The battery will discharge when the electrolyte concentrations in the two semiconductors become the same. For this reason, before realizing an AMTEC-like device I found appropriate to carry out experiments on working fluid and electrolyte in a first, simplified device with no hydraulic return circuit for the working fluid. In other words, experiments on working fluid and electrolyte can be carried out in a normal primary (and therefore non-rechargeable) stack of simpler construction, without thereby giving rise to the generic and validity of the results obtained, useful for the future construction of the AMTEC type device to be coupled with SEC.

On the basis of the above considerations, the device, hereinafter better illustrated, has been designed, and it will allow the experimental phase to be initiated on working fluid and electrolyte.

4.2 Mechanical Design

This designed electrochemical device, consists of two symmetric semi-cells which are electrically separated by a cationic membrane. For the purpose we used four standard Conflat DN40 flanges in AISI 316L stainless steel (Figure 15).

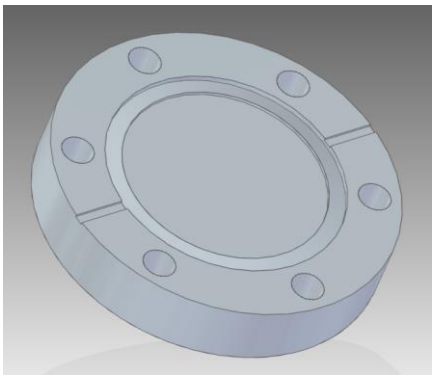

Figure 15. 3D rendering of the CONFLAT DN40 flange.

In particular, one flange is partially drilled with a diameter of 8.5 mm keeping a 1 mm thick layer untouched which is then perforated to make a grid with 1.2 mm diameter holes and 1.5 mm spacing (Figure 16). Such grid allows the alkali metal to get in contact with the β-alumina membrane and plays the role of the electrode.

Figure 16. 3D rendering of the worked flange.

The second DN40 flange is drilled through with a diameter of 6.6 mm. The two flanges separated by a copper gasket which provides vacuum sealing are then clamped together by use of 6 hexagonal head screws ISO standard M6 25 mm long (Figure 17).

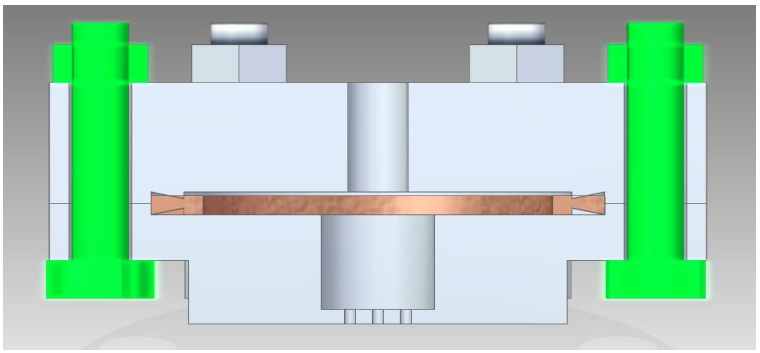

Figure 17. Side view of a semi-cell.

Through holes are drilled in both semi-cells at 30^{o} with respect to the native DN40 holes (Figure 18).

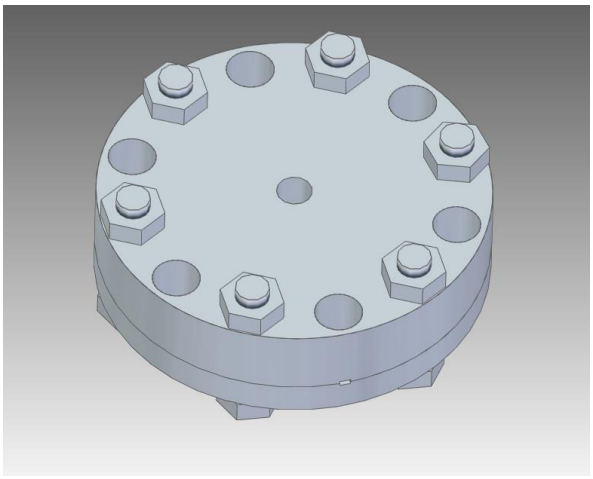

Figure 18. 3D rendering of a semi-cell.

The two symmetric semi-cells are clamped together, by use of 65 mm long ISO standard M4 hexagonal screws, with the β-alumina in between them isolating the two chambers operating at different pressures. Finally, 1/4" diameter steel tubes are TIG welded to the outer flanges, to connect the chambers to the outside gas system by means of Nupro SS-4H membrane valves (Figure 19).

Figure 19. Nupro SS-4H membrane valve.

Figure 20 shows a rendering of the two semi-cells assembled together to form the complete device.

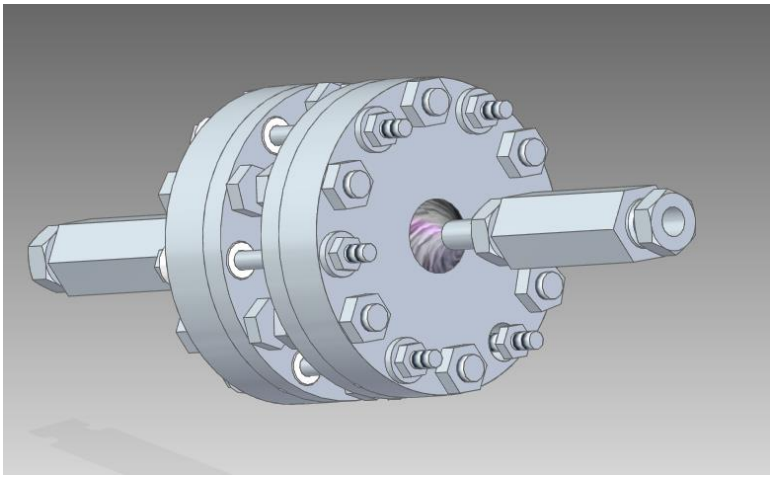

Figure 20. 3D rendering of the pair of experimental cells.

In the assembly phase, MACOR insulators (Figure 21) are inserted into the six 8.5 mm holes in order to ensure electrical insulation while simultaneously applying the right pressure on the base membrane.

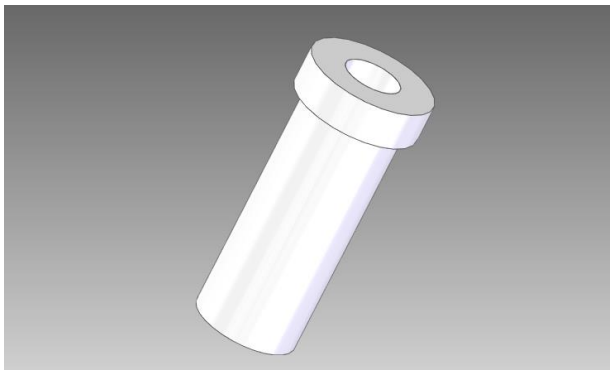

Figure 21. 3D rendering of the MACOR insulator used in the cells.

Figures 22 better describes the assembly phases through a 3D "exploded" device implemented at the INAF workshop.

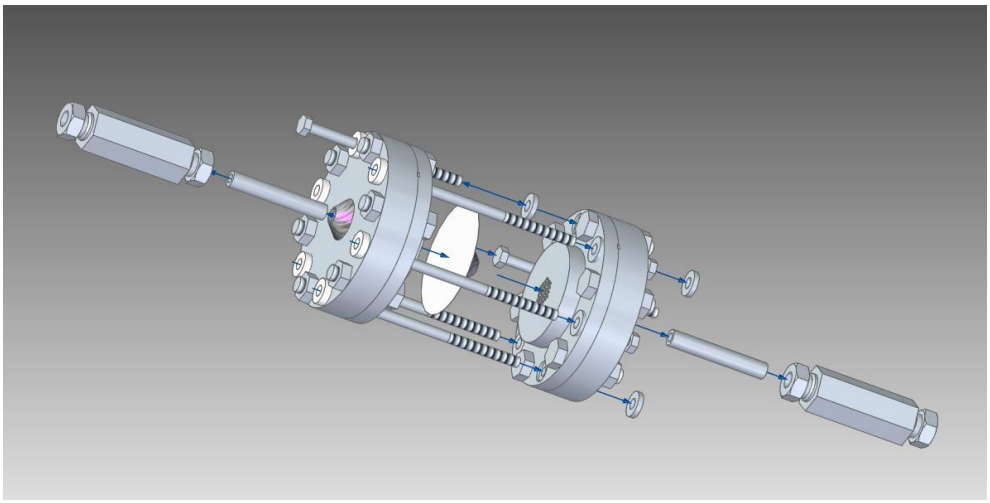

Figure 22. Exploded 3D view of the experimental system, with the focus on the bolts assembly.

Some pictures of device parts, taken during manufacturing and assembling, are reported in the following pages.

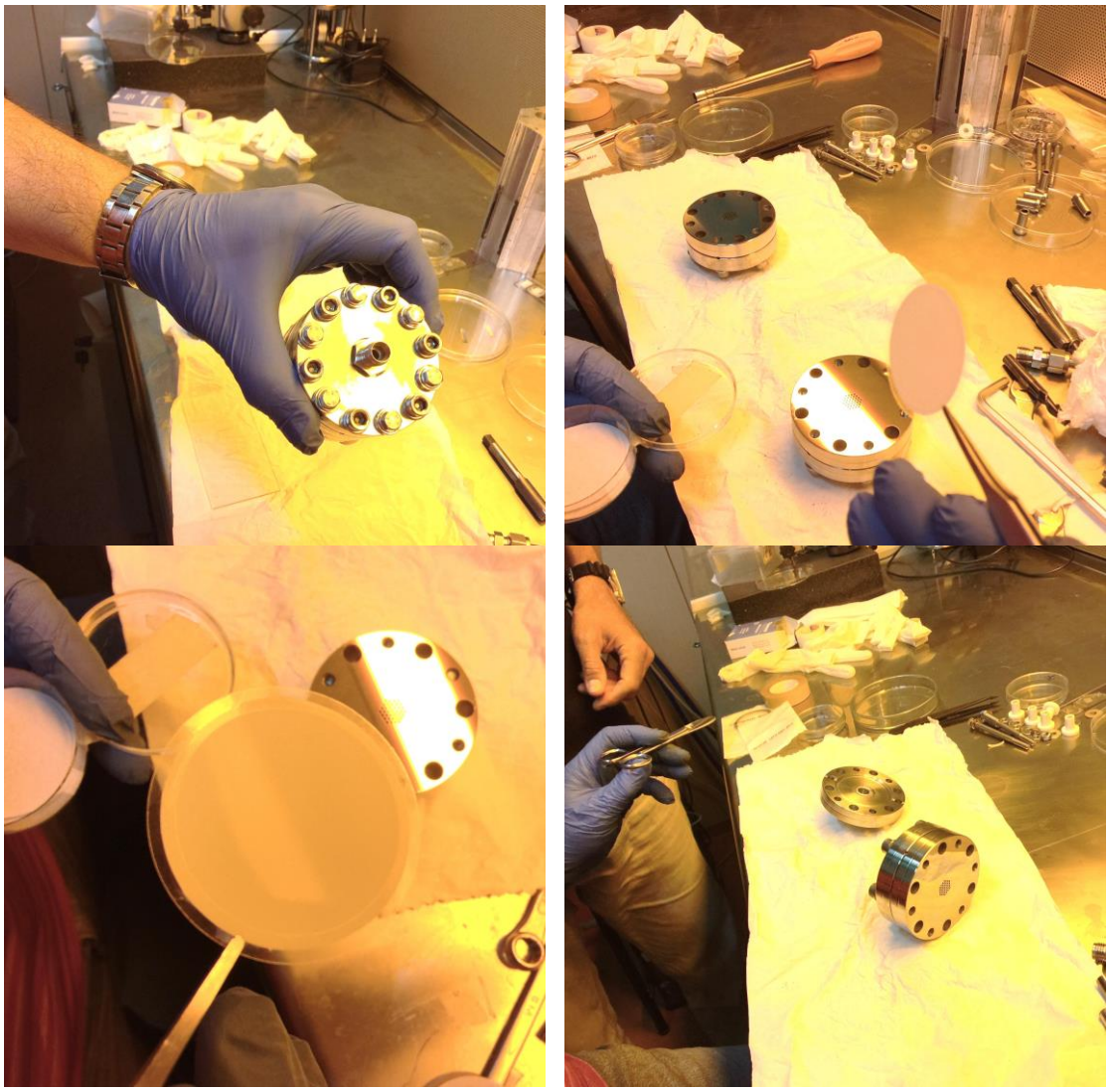

Figure 23. Selected parts of the cell, during manufacturing and assembly (1 of 2).

Figure 24. Selected parts of the cell, during manufacturing and assembly (2 of 2).

4.3 Design of the Experimental Test Apparatus

In order to carry out experiments on the working fluids and the doped BASE electrolyte membranes, the following experimental equipment was realized consisting of:

- No. 1 Turbomolecular vacuum pump
- No. 4 Nupro Valves
- No. 2 Druck PT x 1400 pressure gauges

- No. 2 Wika DI15 pressure readers
- No. 2 Boc EDWARDS type Pirani APG-M-NW16 pressure gauges
- No. 1 EDWARDS AGC pressure reader
- No. 1 2KW Oven model Carbolite HTCR6/28 with maximum temperature 600°C
- No. 1 Vacuum circuit

Figure 25 shows a schematic drawing and Figure 26 some pictures of the experimental apparatus set up for the preliminary tests performed using hydrogen as working fluid reported in the following pages.

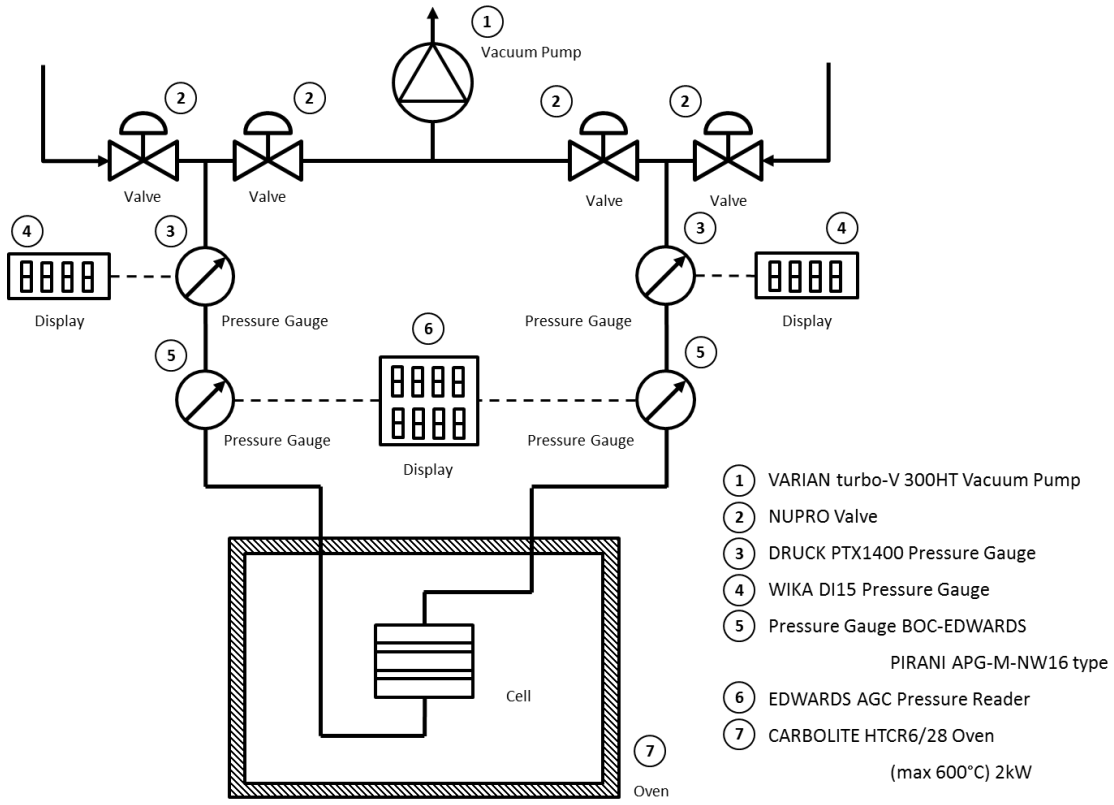

Figure 25. Schematic drawing of the experimental apparatus.

Figure 26. Selected parts of the experimental apparatus used for hydrogen tests (1 of 2).

Figure 27. Selected parts of the experimental apparatus used for hydrogen tests (2 of 2).

CHAPTER V

MODELLING OF THE DEVICE

5.1 General Principles of Electrochemistry

In order to proceed with the physical-mathematical modelling of the device, as designed, it is necessary to deeply analyse the electrical behaviour of a general electrochemical cell.

In electrochemistry, the expression "potential or cell voltage" identifies the difference in the electrical potential existing between the cathode and the anode of an electrochemical cell. This is true for any operating condition (close or open circuit); in the case of open circuit (i.e. without external load applied) you call it "Open Circuit Voltage" (OCV).

The cell potential can be calculated, if the potential of anode and cathode electrode are known, compared with the same potential of reference.

In order to measure the electrode potential of an unknown semiconductor, you use an electrochemical cell with three electrodes.

The cell voltage difference measured between the semiconductor with unknown potential and a reference electrode is an indirect measure of the electrode potential of the semiconductor itself.

The potential of the semiconductor is in this case measured to the heads of the working electrode and the reference electrode (while the auxiliary electrode has the only purpose of closing the electrical circuit).

The reference electrode has a well-established and stable electrode potential, which is independent of the current intensity that crosses the electrochemical cell in which it is inserted.

Among the most common reference electrodes, there are:

- The standard hydrogen electrode (E = 0,000 V);
- The calomel electrode;
- The copper-copper sulphate (II) electrode (E = -0,318 V);
- The palladium electrode-hydrogen;
- The Ag/AgCl electrode.

The electrode potential can be measured and also calculated on theoretical bases, if the potential reduction standards are known, by using the Nernst equation.

The standard reduction potential (abbreviated as E^0) of a conductor is the electrode potential of the element measured in a three-electrode cell with the standard hydrogen electrode as reference electrode (to which is conventionally assigned a potential $E^0 = 0.000$ V) measured at standard conditions or at a temperature of 298K, at a pressure of 100 kPa and at concentrations M (rigorously at unitary activity) of reagents and products of the oxide reduction reaction taking place in the semiconductor of which you measure the potential standard of reduction or the potential of standard electrode.

Consider the reduction reaction occurring in a semiconductor of the cell

$$Me_I{}^{z+} + ze^- \rightarrow Me_I \qquad (1)$$

where the oxidized species Me_I^{z+} present in the semiconductor acquires a number z of electrons reducing to Me_I.

The variation of Gibbs free energy for the above described reaction will be:

$$\Delta G = \Delta G^0 + RT \ln \frac{a_{Me_I}}{a_{Me_I{}^{z+}}} \qquad (2)$$

The free energy identifies by definition the useful work or, in the case of a semiconductor, the electrical work expressible as the product between the difference of potential and the electric charge, that is, by the number of electrons involved in the half-reaction per unit of mass expressed in moles:

$$\Delta G = -zF\Delta E \qquad (3)$$

where:

- ΔE is the measured potential of cell with three electrodes
- z is the number of electrons transferred in the semi-reaction

- F is the constant of Faraday, equal to 96485,309 C mol^{-1}.

Now, all the electrode potentials E, both in standard (E°) conditions and in any condition other than the standard ones, measured with a three-electrode cell, are always referred to the standard hydrogen electrode having the value E° = 0 by definition.

It follows therefore that in a cell with three electrodes:

$$\Delta E = E \tag{4}$$

and

$$\Delta E° = E° \tag{5}$$

that is the electrode potential (standard if one operates at a temperature of 298 K, at a pressure of 100 kPa and a unitary activity of reagents and products) coincides exactly with the difference in the measured voltage of the three electrodes cell.

Therefore, the above expression is reduced to:

$$\Delta G = -zFE \tag{6}$$

At this point, matching the expressions (2) and (4) one gets:

$$\Delta G^0 + RT\, ln \frac{a_{Me_I}}{a_{Me_I{}^{z+}}} = -zFE \tag{7}$$

and solving for the electrode potential:

$$E = -\frac{\Delta G^0}{zF} - \frac{RT}{zF} \ln \frac{a_{Me_I}}{a_{Me_I{}^{z+}}} \tag{8}$$

However, if the same reaction occurs under standard conditions, since the activities of the reduced species and oxidized species are equal to 1 by definition, (8) is reduced to:

$$E = -\frac{\Delta G^0}{zF} \tag{9}$$

But in this case $E = E°$ and therefore one can write also:

$$E^0 = -\frac{\Delta G^0}{zF} \tag{10}$$

Now, given that:

$$-\frac{RT}{zF} ln \frac{a_{Me}}{a_{Me^{z+}}} = \frac{RT}{zF} \ln \frac{a_{Me^{z+}}}{a_{Me}} \tag{11}$$

generalizing and setting as follows:

$$a_{Me^{z+}} = a_{ox}$$
$$a_{Me} = a_{red} \tag{12}$$

one finally gets:

$$E = E^0 + \frac{RT}{zF} \ln \frac{a_{ox}}{a_{red}} \tag{13}$$

which allows to theoretically calculate the electrode potential of a semiconductor being known the standard reduction potential of the species involved in the reaction occurring in the semiconductor.

In the case where multiple reduction reactions occur in the semiconductor, by generalizing, the final equation of Nernst is obtained, where the stoichiometric coefficients of reaction may also be non-unitary as in the half-reaction:

$$E = E^0 + \frac{RT}{zF} \ln \frac{\prod_i (a_{i,ox}^{\nu_{ox}})}{\prod_i (a_{i,red}^{\nu_{red}})} \quad (14)$$

where:

- E is the potential of the electrode or the potential of reduction in non-standard and generic conditions
- E^0 is the standard reduction potential
- R is the universal gas constant, equal to 8,314472 J K^{-1} mol^{-1} or 0,082057 L atm mol^{-1} K^{-1}
- T is the absolute temperature in K
- $a_{i,red}$ is the chemical activity of the i-th species in reduced form, that is on the right of arrow, in the semi-reaction of reduction
- $a_{i,ox}$ is the chemical activity of the i-th species in oxidised form, that is on the left of arrow, in the semi-reaction of reduction
- ν_{red} e ν_{ox} are their stoichiometric coefficients
- z is the number of electrons transferred in the semi-reaction
- F is the constant of Faraday, equal to 96485,309 C mol^{-1}.

The potential of any cell, experimentally measurable, can be theoretically calculated and approximated to the difference of the electrode potentials of the two cell semi-cells, in one of which the reduction reaction (1) occurs, and in the other one the oxidation reaction (15) of a second chemical species occurs in the form:

$$Me_{II} \rightarrow Me_{II}^{z+} + ze^- \quad (15)$$

therefore, the cell potential will be given by:

$$\Delta E = E_{(rxn.1)} + E_{(rxn.15)} = E_{cell} \tag{16}$$

The electrode potential of the second semiconductor is negative because the reaction is written in the direction going from the oxidized species to the reduced one. The cell potential E_{cell} can therefore be seen as the sum of two contributions: a contribution referring to the standard reduction potential E° and a contribution referring to the temperature and concentrations of the two species Me_I and Me_{II}, that oxidize and reduce in the two constituent semiconductors, as parts of the cell.

A special type of electrochemical cells is represented by the concentration cells.

In the concentration cells, the same oxidation rejection reaction takes place in the two semiconductors as the same chemical species are present but at different concentration (or rather, activity).

The two semiconductors have the same value as the standard electrode potential E° (being actually made up of the same chemical species), so the electrode potential depends only on the second contribution that appears in the Nernst equation, that is by $\frac{RT}{zF}\ln\frac{a_{Me_{ox}}}{a_{Me_{red}}}$.

The cell potential, in the hypothesis that both the anode and the cathode work at the same temperature T, is equal to the difference:

$$E_{cell} = \frac{RT}{zF}\ln\frac{a_{Me_{ox}}}{a_{Me_{red}}}\bigg|_{cathode} - \frac{RT}{zF}\ln\frac{a_{Me_{ox}}}{a_{Me_{red}}}\bigg|_{anode} \tag{17}$$

where:

$$a_{Me_{ox}} = a_{Me^{z+}}$$
$$a_{Me_{red}} = a_{Me} \tag{18}$$

5.2 Modelling of the Cell Voltage

Figure 28 depicts the main phases involved in the mechanism of voltage generation across an ionic ceramic membrane (BASE electrolyte).

Let's consider the system shown in the upper part of the mentioned figure, at $t=t_0$, initial time of the transient period. At this moment, two different pressures P_a and P_c are present in the two chambers of the device, with P_a greater than P_c. The ion ceramic membrane acts as an electric insulator between electrodes, which are the stainless steel self-same walls of the compartments.

Each time interval of the transitory of voltage generation can be easily divided into six sub-steps, as reported in Figure 28:

(a) the neutral atom or molecule of the working fluid approaches the membrane surface, moving from the bulk of the compartment;

(b) the neutral atom or molecule of the working fluid hits the membrane surface;

(c) it ionises at the interface, generating a free electron which is delocalized in the metallic electrode (anode) and a cation which moves through the membrane itself;

(d) the cation reaches the opposite side of the membrane;

(e) it "steals" a free electron from the valence level of the metallic bond and neutralizes, leaving an electron hole delocalized in the metallic electrode (cathode);

(f) the neutral atom or molecule leaves the membrane and moves towards the bulk. This results in an increased voltage difference between the two electrode, i.e. in the generation of an open circuit voltage which is growing during time, until equilibrium is reached ($t=t^*$). At equilibrium, the electrical driving force (voltage difference) equals the mechanical driving force (pressure difference or Gibbs potential): the latter would tend to make the molecules move from the anodic bulk towards the membrane surface, ionise at the membrane surface and pass through the membrane, while the former would tend to make cations move from the cathode-side towards the anode-side of the membrane. This finally means that

a "dynamic equilibrium" is reached: for each ionised atom or molecule which crosses the membrane, another cation moves in the opposite direction, driven by the electrical field, passing through the reverse steps (f) → (a).

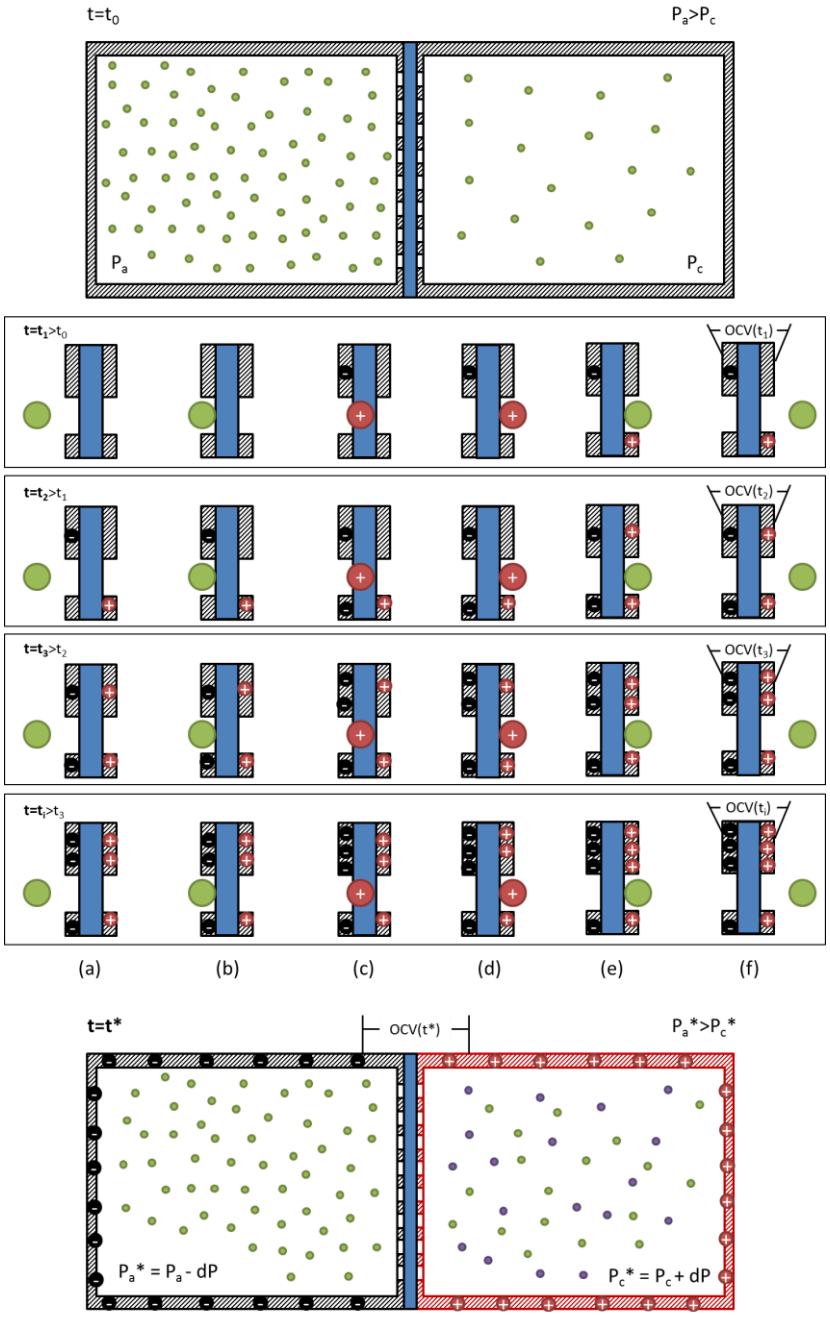

Figure 28. Mechanism of voltage generation across an ion ceramic membrane.

In order to describe phenomenologically what happens, in conditions of external open circuit, in the system as long as a (partial) pressure difference of the working fluid is maintained between the two sides of conductive ion membrane, it may be said that such pressure difference will promote the molecular diffusion of the ionised metal atoms (cations) from the higher-pressure compartment to the lower-pressure one. As charged particles, their motion can be seen for all purposes as electric current, which is difficult to measure experimentally but which is possible to estimate theoretically. The sum of all current contributions I_p due to single particles p results in a total current quite similar to that measurable during the transitory of charge of a capacitor in a RC circuit.

The fast motion of charges, at open circuit, results in a spatial segregation that polarizes the electrodes, generating the potential difference OCV. After the temporal transition, therefore, the internal charge current will cease to exist and the potential will stabilize at the value at open circuit, as calculated in the following. Under these conditions, the difference in electrical potential compensates Gibbs chemical potential difference due to the difference in pressure between the two semi-cells.

At equilibrium (t=t*), the summation of all internal current contributions will be equal to zero, or more precisely, for each particle that is ionised becoming a cation capable of cross the membrane (driven by the difference in chemical potential) there will be another cation that will cross in the opposite direction the membrane (driven by the difference in electrical potential). The total internal current will therefore be zero.

If one wanted to calculate the cell potential of the electrochemical device using the Nernst equation, as formulated above, he or she should know or measure the coefficients of activity of metallic cations and neutral atoms in the two semi-cells of the cell. An alternative formulation is therefore required to predict the cell potential with potentially direct measurements, which are easier to detect through laboratory instruments at our disposal.

The molar free energy of Gibbs G is defined as:

$$G = H - TS \tag{19}$$

In the electrochemical device designed, the infinitesimal variation of G in the total transformation bringing the metal from an initial concentration state of the reference state (e.g. standard temperature conditions of 298 K, pressure of 100 kPa and unitary activity of reagents and products) to another at set-up concentration is:

$$dG = dH - TdS - SdT \tag{20}$$

and recalling that $H = U + pV$, one gets:

$$dG = dU + d(pV) - TdS - SdT \tag{21}$$

From the first principle of thermodynamics $U = Q + W$ and replacing then:

$$dG = dW + dQ + d(pV) - TdS - SdT \tag{22}$$

Assuming that the temperature of the semi-cell keeps constant during the transformation ($dT = 0$) one can write for each semi-cell, that is for both anode and cathode:

$$dG = dW + dQ + d(pV) - TdS \tag{23}$$

If the transformation is reversible, since the vapours of the working fluid used can assimilate themselves to a perfect gas - given the high temperature and low pressure of the system (the vapour pressure of a metal is always a small fraction of the atmospheric pressure) - and assuming the oxidation reaction as reversible itself:

$$dQ_{rev} = TdS \tag{24}$$

$$dG = dW_{rev} + d(pV) \tag{25}$$

During the transient period, the total work can in turn be distinguished in work of expansion or of volume W_{exp} and extra work or useful work W_e. Provided that the volume is constant during the transitory (not-movable walls, $dW_{exp} = -pdV = 0$), the only work done is the electrical work necessary to move charges in order to create the electrical field, i.e. the electrical voltage OCV. Hence, $dW_e = zFdE$.

Taking into account the fact that $d(pV) = pdV + Vdp$:

$$dG = dW_e + Vdp = zFdE + Vdp \tag{26}$$

At equilibrium $dG = 0$, and so:

$$dE = -\frac{Vdp}{zF} \tag{27}$$

where *F* is the Faraday constant, *z* is the valence, *T* is the temperature. Assuming also that the perfect gas state equation is valid, the molar volume *V* will be equal to:

$$V = \frac{RT}{p} \tag{28}$$

Then:

$$dE = -\frac{Vdp}{zF} = -\frac{RT}{zF}\frac{dp}{p} \tag{29}$$

By integrating the previous expression at both anode and cathode, from the reference state to the final state in which the system is located (i.e. the anode at pressure p_a and the cathode at pressure p_c), one gets:

$$E_a = E_o - \frac{RT_a}{zF}\ln\frac{p_a}{p_o} \tag{30}$$

$$E_c = E_o - \frac{RT_c}{zF}\ln\frac{p_c}{p_o} \tag{31}$$

the open circuit voltage (OCV) will be equal to the voltage difference $E_{oc} = E_c - E_a$:

$$E_{oc} = E_o - \frac{RT_c}{zF}\ln\frac{p_c}{p_o} - \left(E_o - \frac{RT_a}{zF}\ln\frac{p_a}{p_o}\right) \cong \frac{RT_m}{zF}\ln\frac{p_a}{p_c} \tag{32}$$

where the membrane temperature has been introduced as average value between the temperatures into the anodic and cathodic compartments (for the sake of simplicity it can be approximated with the arithmetic mean without making a significant error, due to the very small thickness of the membrane compared to the characteristic dimension of the cell, Figure 29).

T. Cole in [13] adopts as temperature in (32) the highest value between the anode and the cathode temperatures, due to the fact that his device is a liquid-anode vapour-cathode AMTEC cell. In this case, in fact, the temperature of the BASE electrolyte can be identified with the anode-side temperature (higher pressure chamber), at steady state, as the molten metal (sodium) is in direct contact with the membrane, so it contributes to make the temperature uniform (since the heat transfer coefficient in saturated liquids is much higher than that in rarefied vapours [28]), whereas on the cathode-side (lower pressure chamber) vacuum conditions exist, as maintained by the condenser surface which works at lower temperature.

In the device described and modelled in the present work, instead, different conditions apply, as this is a vapour-anode / vapour-cathode AMTEC-like cell.

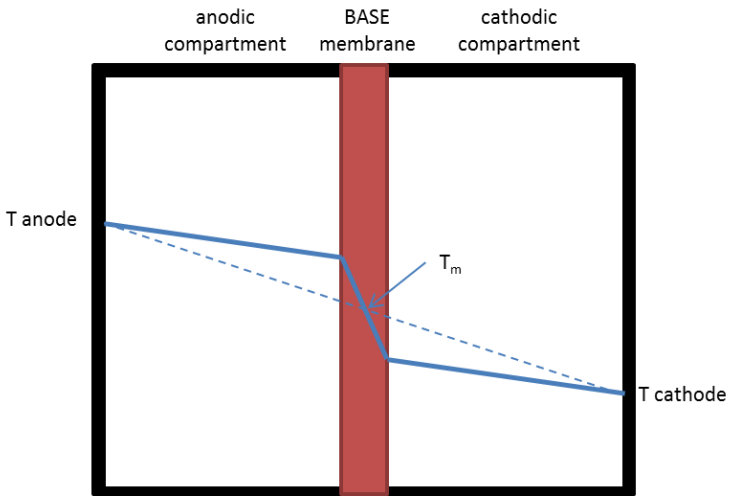

Figure 29. Qualitative temperature profiles in the simplified device, with indication of the average value Tm, to be used in Nernst's law.

By substituting in the previous expression, the temperature and working pressure values of our device, one can experimentally test the equivalence of the open circuit voltage value to the electrodes measured with the theoretically predicted value from (32).

One gets to the same conclusion if using a more rigorous electrochemical approach, like that reported on [29].

Let's consider the reaction:

$$\alpha_1 A_1 + \alpha_2 A_2 + \cdots = \beta_1 B_1 + \beta_2 B_2 + \cdots \tag{33}$$

during which z moles of electricity are exchanged. Such reaction is in equilibrium from the chemical point of view when it is not capable to make work in isothermal and isobaric condition, i.e.:

$$-W = \Delta U - T\Delta S + P\Delta V = 0 \tag{34}$$

(where U is the internal energy). To this equilibrium, the following condition can be associated, at temperature T and pressure P:

$$K_a = \frac{a_{B1}^{\beta 1} a_{B2}^{\beta 2} \dots}{a_{A1}^{\alpha 1} a_{A2}^{\alpha 2} \dots} \tag{35}$$

$$\Delta G^{\circ} = -RT \ln K_a \tag{36}$$

where a is the activity in equilibrium conditions.

If the system is not in equilibrium, the reaction tends to proceed towards equilibrium with capability of making work. It then results $W = -(\Delta U - T\Delta S + P\Delta V) > 0$.

If the reaction occurs in an electrochemical system, electrical forces will appear, so that they oppose the chemical forces for the determination of the equilibrium condition. Hence, an "electrochemical equilibrium" can exist in a system which is not in a purely chemical equilibrium. Such a particular electrochemical equilibrium, under the effect of external forces, can be described through the so-called **principle of virtual work**, which expresses the impossibility for a system in equilibrium to do or absorb work, when a displacement from equilibrium is imposed, even infinitesimal and compatible with boundary conditions. Such a displacement is called "virtual". In the case of an electrochemical system, the boundary condition is the impossibility of circulation of current between electrodes. The virtual displacement will be then the circulation of an infinitesimal current. More in general, one should consider as external forces even the pressure and the surface tension on the boundaries of the system.

Let's define the "reaction degree" λ_a of a reaction the ratio between the number of moles of a product which have been formed since the starting time and the stoichiometric coefficient of that product:

$$\lambda_a = \frac{n_{B1}}{\beta_1} = -\frac{n_{A1}}{\alpha_1} = \frac{q}{zF} \tag{37}$$

Let's indicate with ΔU, ΔH, ΔS, ΔV, ΔA the variations in internal energy, enthalpy,

entropy, volume and surface area of the system, respectively, corresponding to a unary reaction degree.

If the reaction occurs in an electrochemical system, the simultaneous circulation of z moles of electricity occurs. The virtual displacement considered above, corresponds to an infinitesimal reaction degree $d\lambda_a$. Infinitesimal variations in internal energy $\Delta U d\lambda_a$, enthalpy $\Delta H d\lambda_a$ and entropy $\Delta S d\lambda_a$will also occur, together with the circulation of the current $zFd\lambda_a$ and the variation in volume $\Delta V d\lambda_a$and in surface area $\Delta A\lambda_a$. If the electromotive force E exists between the electrodes of the regularly open electrochemical system, the following works can be associated (at constant T, P and surface tension):

Chemical work $$dW_{chem} = (\Delta U - T\Delta S)d\lambda_a \quad (38)$$

Volume work $$dW_{vol} = P\Delta V d\lambda_a \quad (39)$$

Electric work $$dW_{el} = zFE_{rev}d\lambda_a \quad (40)$$

Surface work $$dW_{sur} = \Gamma\Delta A d\lambda_a \quad (41)$$

In equilibrium conditions, the algebraic sum of the above mentioned works has to be equal to zero, i.e.:

$$dW_{chem} + dW_{vol} + dW_{el} + dW_{sur} = 0 \quad (42)$$

$$(\Delta U - T\Delta S)d\lambda_a + P\Delta V d\lambda_a + zFE_{rev}d\lambda_a + \Gamma\Delta A d\lambda_a = 0 \quad (43)$$

And then:

$$(\Delta U - T\Delta S) + P\Delta V + zFE_{rev} + \Gamma\Delta A = 0 \tag{44}$$

As the assumption of constant temperature and pressure is held and neglecting the surface tension term (which is significant only when the surface/volume ratio is high), one gets:

$$E_{rev} = \frac{(-\Delta U + T\Delta S - P\Delta V)}{zF} = -\frac{\Delta H - T\Delta S}{zF} = -\frac{\Delta G}{zF} \tag{45}$$

Just for the sake of completeness, deriving E_{rev} with respect to pressure (at constant T) and temperature (at constant P) it yields to:

$$\left.\frac{\partial E_{rev}}{\partial P}\right|_T = -\frac{\Delta V}{zF} \tag{46}$$

$$\left.\frac{\partial E_{rev}}{\partial T}\right|_P = \frac{\Delta S}{zF} \tag{47}$$

which represent the variation of the reversible electromotive force of an electrochemical system with pressure and temperature, respectively.

Recalling that the chemical potential μ_i of a component of the system is equal to the partial molar free energy G_i of the same component (by definition), one gets:

$$\mu_i = G_i = \left.\frac{\partial G}{\partial n_i}\right|_{T,P,n_j} \tag{48}$$

where *i* is the considered component and *j* indicates any other component different than *i*. Hence:

$$\Delta G = \sum \beta_i \mu_{B_i} - \sum \alpha_i \mu_{A_i} \tag{49}$$

From the expression of chemical potentials as function of current activities a':

$$\mu_i = \mu_i^\circ + RT \ln a'_i \tag{50}$$

$$\Delta G = \sum \beta_i \mu^\circ_{B_i} - \sum \alpha_i \mu^\circ_{A_i} + \sum RT \ln\left(a'_{B_i}\right)^{\beta_i} - \sum RT \ln\left(a'_{A_i}\right)^{\alpha_i} \tag{51}$$

And finally, recalling the correlation between ΔG and E_{rev} and lumping all constant terms μ° into $E°_{rev}$:

$$E_{rev} = E^\circ_{rev} + \frac{RT}{zF} \ln \frac{\left(a'_{A_1}\right)^{\alpha_1}\left(a'_{A_2}\right)^{\alpha_2} \ldots}{\left(a'_{B_1}\right)^{\beta_1}\left(a'_{B_2}\right)^{\beta_2} \ldots} \tag{52}$$

In condensed phase (solid or liquid), activity of the solute species tends to coincide with concentrations (unary activity coefficients) as concentration increases towards pure component.

If the electrochemical system also contains gaseous species (even in physical equilibrium with the corresponding species in condensed phase), the chemical potential for such components is a function of fugacity as follows:

$$\mu_i = \mu_i^\circ + RT \ln f'_i \tag{53}$$

Repeating the previous passages and separating the activity terms from the fugacity terms, one gets:

$$E_{rev} = E^{\circ}_{rev} + \frac{RT}{zF}\ln\frac{\left(a'_{A_1}\right)^{\alpha_1}\left(a'_{A_2}\right)^{\alpha_2}\ldots}{\left(a'_{B_1}\right)^{\beta_1}\left(a'_{B_2}\right)^{\beta_2}\ldots} + \frac{RT}{zF}\ln\frac{\left(f'_{A_1}\right)^{\alpha_1}\left(f'_{A_2}\right)^{\alpha_2}\ldots}{\left(f'_{B_1}\right)^{\beta_1}\left(f'_{B_2}\right)^{\beta_2}\ldots} \quad (54)$$

For example, working with sodium ($z = 1$) at a temperature of 1127 K (854°C), with a working fluid pressure at the anode of 80 kPa (sodium vapour pressure at 1127 K) and of 50 kPa at the cathode, then the expected open circuit voltage value of the device would be 0.69V.

It should be noted, however, that the open circuit voltage value does not depend on the metal chosen as working fluid, if not exclusively through the value of z that is the valence of the metal which is the same for all metals belonging to the same group (e.g. alkali metals $z = 1$, alkali earth metals $z = 2$, etc.).

By connecting the electrodes to an external load, it is possible to exploit the electric potential that is generated: the free electron generated at the anode will flow through the external load producing useful work and return to the cathode where they will join again to positive ions of the working fluid that have passed through the electrolyte as long as the equilibrium is reached, when it will obviously be $\Delta G = 0$ and $E_{oc} = 0$.

Figure 30 reports the values of the vapour pressure as a function of temperature for a selection of six elements suitable for being used as working fluids, among those pre-selected in Table 3.

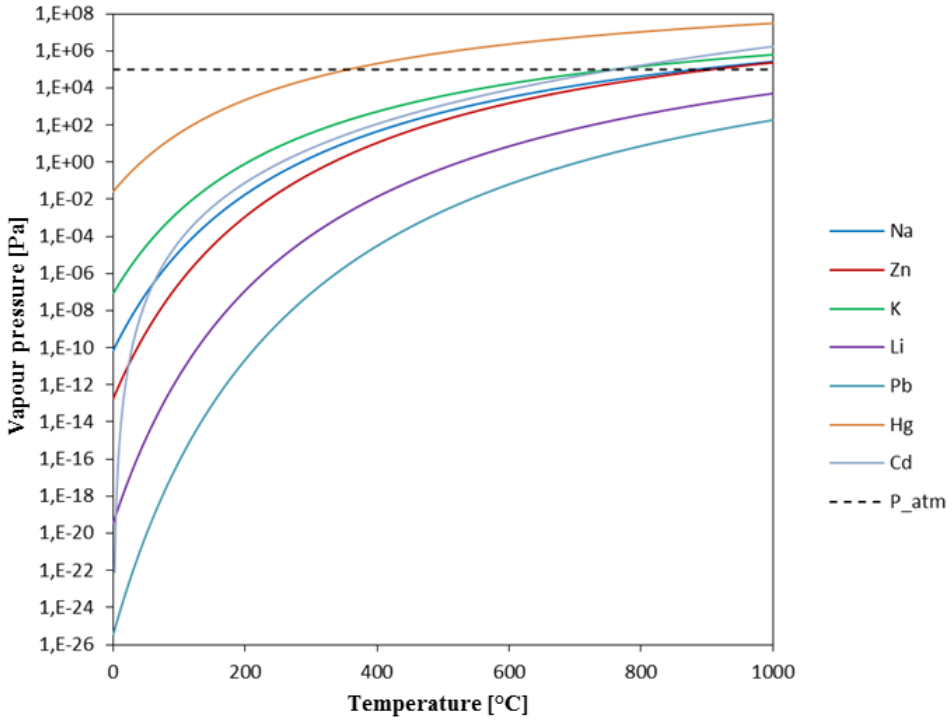

Figure 30. Vapour pressure predicted with data from NIST database [30] **for a selection of elements suitable for being used as working fluid, among those pre-selected in Table 3, as a function of temperature.**

From (32) shows the predicted values of open-circuit cell voltage E_{oc} when the anode-side pressure is equal to the vapour pressure of the metal at temperature T, and the cathode-side pressure is set as an example at 10^{-2} mbar.

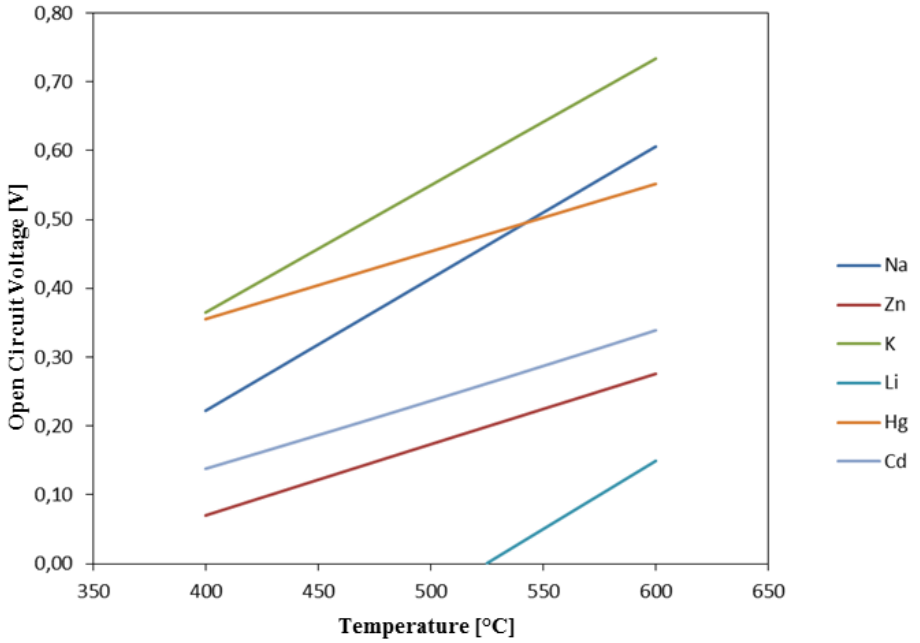

Figure 31. Theoretical calculated trends of the open circuit voltage as a function of the operating temperature for a selection of suitable working fluids (Na, Zn, K, Li, Hg, Cd) among those pre-selected in Table 3. Simulation conditions: anode-side pressure = vapour pressure of the metal at T; cathode-side pressure = 10^{-2} mbar (abs).

Let's now consider the galvanic chain:

$$- \boldsymbol{Fe} \mid \boldsymbol{Zn(P_2)} \mid \text{β-alumina} \mid \boldsymbol{Zn(P_1)} \mid \boldsymbol{Fe} +$$

being *Fe* the material of the electrode (stainless steel) and *β-alumina* is the electrolyte, with P_2 (anode) > P_1 (cathode), to which the following semi-reactions correspond:

positive terminal	$Zn^{2+} + 2e = Zn(P_1)$
negative terminal	$Zn(P_2) = Zn^{2+} + 2e$
global reaction (z=2)	$Zn(P_2) = Zn(P_1)$

Hence:

$$2FE = -\Delta G = \mu^{\circ}{}_{Zn} + RT\ln(P_2) - \mu^{\circ}{}_{Zn} - RT\ln(P_1) = RT\ln\frac{P_2}{P_1} \qquad (55)$$

The measurement of E allows to quantify the work of transport of the metal vapour (e.g. zinc) from pressure p_2 to pressure p_1. If one of the two pressures is known, the measurement of E allows to determine with great precision the unknown pressure. **The electrical work extractable from the device is equal to the mechanical work that can be retrieved by the expansion – through a turbine – of 1 mole of metal vapour from pressure p_2 to pressure p_1. In reversible and isothermal conditions the system absorbs from the environment an amount of heat which is exactly equal to the mechanical work done, as the internal energy of metal vapour (assumed as ideal gas) does not depend on the pressure and remains constant in an isothermal expansion process.** In the case of a voltage generator, the temperature coefficient indicates the variation of entropy due to the passage of the gas from pressure p_2 to pressure p_1 and it results as follows:

$$2F\frac{dE}{dT} = \Delta S = R\ln\frac{P_2}{P_1} \qquad (56)$$

so that the generator absorbs the amount of the heat $Q_{rev} = T\Delta S$ which equals the electrical work done by the cell. This is a limiting case in which the electrical work is done exclusively to the entropic contribution, without the intervention of the potential energy of chemical bonds. For further details on the derivation of the all the above listed equations please refer to [29].

Even when using infinitely large resistances, the measured cell voltage value will necessarily be a closed-circuit voltage value and hence lower than the theoretical open circuit voltage, and because of both the internal resistance of the concentration cell (which

results in a voltage drop) and the overvoltage phenomena to the electrodes.

The cell potential E_{cell} results from the sum of the following contributions:

$$E_{cell} = E_{cell,unload} + \eta_{el} + \eta_{\Omega} \quad (57)$$

where:

- $E_{cell\ unload}$ is the potential of the open-circuit cell
- η_{el} is the electrode over-potential;
- η_{Ω} is the ohmic drop.

Generally, in electrochemistry, the term "over-potential" identifies the difference between the electrode potential at the present operating conditions (when a certain current circulates) and the electrode potential at equilibrium (i.e. in the absence of Circulation of current, in open circuit). In formulae:

$$\eta = E_{cell,measured} - E_{cell,unload} \quad (58)$$

In this particular case:

$$\eta_{tot} = E_{cell,measured} - E_{oc} \quad (59)$$

where:

- $E_{cell.measured}$ is the experimentally measured potential of the cell (function of the current density *i* circulating in the cell, so it is a function of time);
- E_{oc} is the theoretical potential of the open circuit cell, that is the value of the potential calculated by (32);
- η_{tot} is the total over-potential of cell.

The over-potential is by definition:

- positive ($\eta > 0$) for the electrolytic cells that absorb the work required to cause the oxide reduction reaction (they act as users);
- zero ($\eta = 0$) for electrochemical cells at equilibrium, that is open circuit;
- negative ($\eta < 0$) for galvanic cells, that is for electrochemical cells that produce useful work or electrical work (they act as generators).

Over-potential is a measure of the voltaic efficiency of an electrochemical cell: in particular, in an electrolytic cell (which transforms electricity into chemical energy), the increase in over-potential causes the increase of electricity to be supplied to the cell; while in one Galvanic cell (which transforms chemical energy into electrical energy) as the over-potential increases, the amount of electrical energy that is delivered from the cell, decreases; in both cases the over-potential acts as a dissipation, generating heat.

The over-potential is related to the thermal power dissipated because of the Joule effect from the electrochemical cell through the relation:

$$\eta = \frac{\dot{Q}_J}{e} \tag{60}$$

where:

- Q_J is the thermal energy dissipated by the over-potential;
- e is the elementary charge.

The total over-potential can then be divided into the following contributions:

- *Ohmic drop:* the drop of potential caused by the electrical resistance of homogeneous phases (electrodes and electrolyte bulk);
- *Anodic over-potential:* non-ohmic over-potential localized in the semi-cell where oxidation occurs (anodic area);

- *Cathodic over-potential:* non-ohmic over-potential localized in the semi-cell where the reduction occurs (cathodic area).

The total over-potential of the electrode, due to the difference in electrode potential net of the ohmic drop, is related to the over-potential (anodic and cathodic) contributions, from the relation:

$$\eta_{el} = \eta_{an} - \eta_{cat} \tag{61}$$

where:

- η_{an} is the anodic over-potential;
- η_{cat} is the cathodic over-potential.

From a physical point of view, over-potential is essentially due to two phenomena:

- Concentration Polarization phenomena at interface (η_{conc}) that determine a difference in metal cation concentration between the area close to the surface of the electrode, the area between the electrode and the bulk beta and the area near the interface between working fluid and β-alumina itself;
- Charge transfer phenomena (η_{ct}, Charge Transfer), connected to the current transfer.

Occasionally, ohmic drops are also referred to as over-potential, with the expression "over-potential by ohmic polarization" η_{Ω}.

$$\eta = \eta_{conc} + \eta_{ct} \tag{62}$$

The polarization in an electrochemical system thus results in a potential variation, which is precisely the polarization over-potential.

Also, the over-potential by concentration polarization can also be determined theoretically from the Nernst equation:

$$\eta_{conc} = \frac{k_B T}{ze} ln \left[\frac{a_{Me_{ox}} / a_{Me_{red}} \Big|_s}{a_{Me_{ox}} / a_{Me_{red}} \Big|_b} \right] = \frac{RT}{zF} ln \left[\frac{a_{Me_{ox}} / a_{Me_{red}} \Big|_s}{a_{Me_{ox}} / a_{Me_{red}} \Big|_b} \right] \quad (63)$$

where:

- subscripts "ox" and "red" refer to the oxidized species and the reduced species;
- subscripts "s" and "b" refer to the electrode surface and the bulk of the electrolyte;
- a_{Me} is the metal activity;
- k_B is the Boltzmann constant;
- R is the universal gas constant;
- T is the absolute temperature;
- z is the valence;
- e is the elementary charge;
- F is the Faraday constant.

The over-potential by charge transfer (also called activation overvoltage) can instead be obtained by the **Butler-Volmer equation**:

$$i = i_0 \left[\exp\left(\frac{\overleftarrow{\alpha} z e \eta}{k_B T} \right) - \exp\left(\frac{\vec{\alpha} z e \eta}{k_B T} \right) \right] \quad (64)$$

where:

- $\overleftarrow{\alpha}$ and $\vec{\alpha}$ are respectively the anode charge transfer coefficient and the cathode charge transfer coefficient (representing the fraction of total overcurrent distributed between anode and cathode, respectively);

- i is the current density (equal to the ratio between current intensity and charge transfer area);
- i_0 is the exchange current density.

In the particular case where high overvoltage values are present, the Butler-Volmer equation is reduced to the Tafel equation:

$$\eta_{ct} = \pm\left(\frac{k_B T}{\alpha e}\right)\ln\left(\frac{i}{i_0}\right) \tag{65}$$

where:

- a positive sign is considered for anodic semi-reaction, and α represents the symmetry coefficient of the anode barrier $\vec{\alpha}$;
- a negative sign is considered for cathodic semi-reaction, and α represents the symmetry coefficient of the cathode barrier $\vec{\alpha}$.

The over-potential by ohmic polarization, instead, results from Ohm's law:

$$\eta_{\Omega} = \Delta V = RI \tag{66}$$

where:

- R is the electrical resistance;
- I is the current intensity.

The electrochemical device designed should therefore allow us to conduct an experiment, through which one will be able to evaluate its performance both at full and empty loads when the circulating current changes (more precisely it is the power delivered by the cell depending on the external load applied) with the different working fluids and electrolyte chosen.

Such results can of course be influenced by any overvoltage phenomena.

In the tests that will be carried out with the six candidate elements, overvoltage values will be estimated from experimental measurements of current density, cell voltage, and open circuit cell voltage. A merely theoretical calculation of the over-potential would require a deep knowledge of the electrochemical interface kinetics, which can be further elaborated and described both qualitatively and quantitatively, through a model providing various charge transfer mechanisms such as absorption, tunnelling, diffusion and desorption, depending on the material chosen for the construction of the anode and cathode and its porosity.

5.3 State of the Art of AMTEC modelling

A detailed and complete review about the AMTEC is given by Wu et al. in [1] who reported about modelling works of Schock et al. [31, 32] and Hendrix et al. [33], on one hand, and Tournier et al. [8], on the other hand, who developed thermal, electrical and vapour flow models, for vapour anode and liquid anode AMTEC cells, respectively. More sophisticated models, either based on a parametric approach or on a number of sub-models for pressure losses, radiation/conduction heat transfer and electrochemical processes, have also been developed by Tournier et al. at the University of New Mexico's Institute for Space and Nuclear Power Studies [34, 35, 36, 37, 38].

For the purposes of the present work it is worth to mention T. Cole's modelling and experimental investigation of a liquid-anode/vapour-cathode AMTEC cell [13]. The proposed modelling is based on the Langmuir assumption that the molar flux $\vec{n}$ from a surface at temperature T into vacuum is linearly related to the vapour pressure P_v of the evaporating material and to the sticking coefficient α of the gas molecules onto the surface, according to Hertz-Knudsen equation [39]:

$$\vec{n} = \frac{\alpha P_v}{\sqrt{2\pi P_M RT}} \tag{67}$$

where P_M is the molecular weight and R is the perfect gas constant. The sticking coefficient α is defined as the ratio of the number of adsorbate atoms (or molecules) that adsorb, or "stick", to a surface over the total number of atoms that impinge upon that surface during the same period of time, the sticking coefficient is a function of surface temperature, surface coverage and structural details as well as the kinetic energy of the impinging particles [40].

This means that the electric current density i, in any load condition, is:

$$i = zF\vec{n} = \frac{zF\alpha P_v}{\sqrt{2\pi P_M RT}} \tag{68}$$

being F the Faraday constant and z the element valence. With reference to the system sketched in Figure 32, Cole considered that, assuming negligible pressure drop across the porous electrode ($P_3 = P_4$), when electric current flows, an "overpressure" exists on the cathode-side of the BASE, necessary to make the desorbing atoms or molecules move towards the bulk of the cathodic semi-element. Such overpressure must be directly proportional to the value of the circulating current density (a greater pressure difference is needed to drive higher currents), then:

$$P_4(i) = P_4\big|_{i=0} + \frac{\sqrt{2\pi P_M RT_2}}{zF\alpha} i \tag{69}$$

being P_4 the local pressure at the BASE surface in contact with the porous electrode, T_2 the temperature of the BASE and $P_4(i=0) = P_1(T_2/T_1)^{0.5}$ [41].

Substituting (3) in the Nernst's law $E_{oc}=RTz^{-1}F^{-1}\ln(P_2/P_4)$, where T is here the operating temperature of the BASE (which can be considered isothermal at T_2) and P_2 is the local pressure at the BASE surface in contact with the liquid metal (which can be considered uniform in the whole anodic compartment, as it refers to a liquid), and using Ohm's law

$$\Delta V = E_{oc} - i\rho \tag{70}$$

where ρ is the areal resistance of the BASE (which is a function of temperature), after some steps, one gets to:

$$\Delta V = \frac{RT_2}{zF}\ln\left[\frac{zF\alpha P_2}{\sqrt{2\pi P_M RT_2}}\right] - \frac{RT_2}{zF}\ln\left[\frac{zF\alpha P_1}{\sqrt{2\pi P_M RT_1}} + i\right] - i\rho \tag{71}$$

in which the term P_4 disappeared by substitution, and the quantity $\frac{zF\alpha P_1}{\sqrt{2\pi P_M RT_1}}$ accounts for the pressure P_4 at $i=0$ (open circuit condition).

Equation (5) is of the form

$$\Delta V = C_0 - C_1\ln[\delta + i] - i\rho \tag{72}$$

with:

$$C_0 = \frac{RT_2}{zF}\ln\left[\frac{zF\alpha P_2}{\sqrt{2\pi P_M T_2}}\right] \qquad C_1 = \frac{RT_2}{zF} \qquad \delta = \frac{zF\alpha P_1}{\sqrt{2\pi P_M RT_1}}$$

The theoretical polarisation curve of a liquid-anode/vapour-cathode AMTEC device, according to this modelling, is not rigorously linear as Ohm's law would suggest, especially at low current densities. In fact, the logarithmic term in *i* represents a kind of "capacitive" effect due to the "overpressure" needed to supply the circulating current in the rarefied gaseous medium. Such term is negligible at high current densities, whereas it becomes significant when current density approaches zero. Experimental measurements performed on such type of cells show good agreement with such modelling, although a

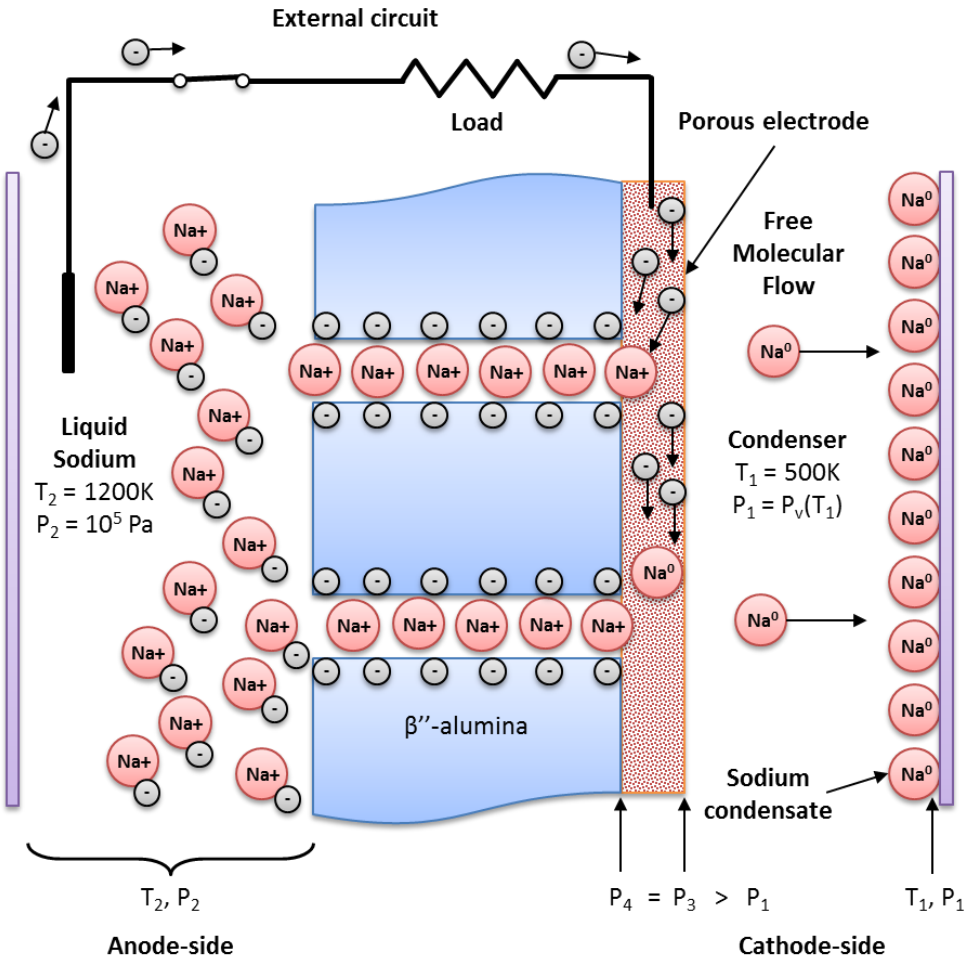

Figure 32. Microscopic processes occurring in the BASE and its interfaces, in a liquid anode-vapour cathode AMTEC cell (adapted from [13]**).**

small positive voltage offset is generally present between the theoretical curves and the experimental ones [13], as Figure 33 depicts.

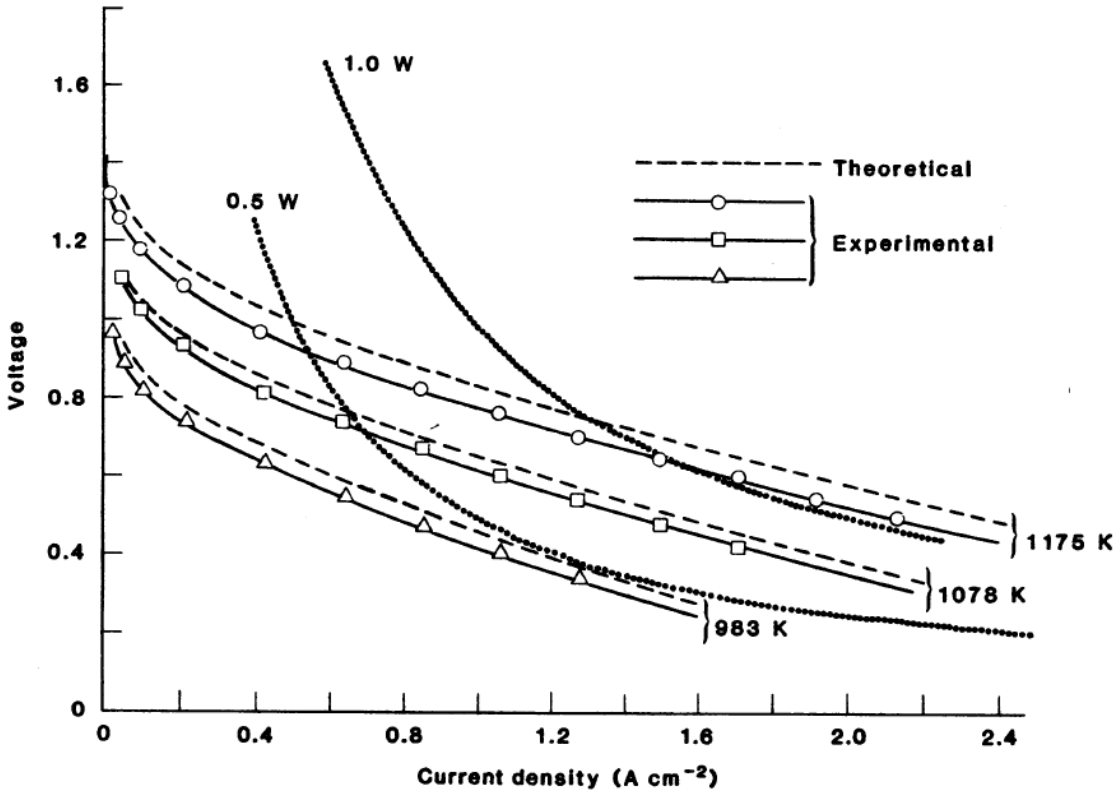

Figure 33. Experimental and predicted AMTEC voltage-current density curves in a liquid-anode vapour-cathode [13]**.**

5.4 Modelling of vapour anode/vapour cathode systems

As stated above, the Langmuir empirical approach applied to a liquid-anode/vapour-cathode system leads to the current-voltage characteristic derived in [13].

Now, considering a vapour-anode/vapour-cathode system like that depicted in Figure 34 and following the same approach as in [13], the two partial contributions (anodic and cathodic) of the evaporating molar flux to the circulating current density are:

$$\overleftarrow{n} = \frac{\alpha_a P_{v,a}}{\sqrt{2\pi P_M R T_a}} = \frac{\overleftarrow{i}}{zF} \tag{73}$$

$$\vec{n} = \frac{\alpha_c P_{v,c}}{\sqrt{2\pi P_M R T_c}} = \frac{\vec{i}}{zF} \tag{74}$$

The net current density of cations $i = \vec{i} - \overleftarrow{i} = zF(\vec{n} - \overleftarrow{n})$, thus the final rearranged expression is:

$$i = \frac{zF\Delta P}{\sqrt{2\pi P_M R T_m}} \left[\frac{P_{v,c}}{\Delta P} \sqrt{\frac{2T_m}{T_c}} \frac{\alpha_c}{\sqrt{2}} - \frac{P_{v,a}}{\Delta P} \sqrt{\frac{2T_m}{T_a}} \frac{\alpha_a}{\sqrt{2}} \right] \tag{75}$$

where $\Delta P = P_{v,a} - P_{v,c}$ and $T_m = (T_a + T_c)/2$ (for a symmetric cell layout and a small BASE thickness, the BASE temperature can be considered equal to T_m), which can be further rewritten as:

$$i = i_0 \left[A \frac{\alpha_c}{\sqrt{2}} - B \frac{\alpha_a}{\sqrt{2}} \right] = i_0 \Phi(\alpha_a, \alpha_c, T_a, T_c) \tag{76}$$

where:

$$i_0 = \frac{zF\Delta P}{\sqrt{2\pi P_M R T_m}}$$

$$A = \frac{P_{v,c}}{\Delta P} \sqrt{\frac{2T_m}{T_c}} \qquad B = \frac{P_{v,a}}{\Delta P} \sqrt{\frac{2T_m}{T_a}}$$

It is worth to note that, in (10) the dependence on the semi-elements pressures does not appear explicitly, as in the modelled cell, semi-elements pressures are the vapour pressures at respective temperatures (they are accounted for in the parameters A and B).

The internal resistance of the cell is constituted by the BASE resistance (the inverse of conductivity, in turn dependent on the electrical mobility and diffusion coefficient) and by the resistance at electrodes, on which over-voltage phenomena may occur. The open-

circuit voltage will instead give us information on the maximum voltage that can be generated by the cell.

As an assumption, overvoltage phenomena due to concentration polarisation have been considered negligible. This assumption is justified if the mass transfer is small, and therefore concentration can be considered uniform in space. Under this hypothesis, the voltage drop measured in a generic closed circuit condition across the external load ΔV is equal to the open circuit voltage of the cell E_{oc} diminished by the product between the circulating current and the internal ohmic resistance r, in accordance to Ohm's law.

Applying the same approach as [13] to a vapour-anode/vapour-cathode AMTEC-like device as represented in Figure 34, one gets to the following expressions for pressures at membrane interfaces, anode-side and cathode-side respectively:

$$P_2(i) = P_2(i=0) - \frac{\sqrt{2\pi P_M RT_a}}{zF\alpha_a} i \tag{77}$$

$$P_4(i) = P_4(i=0) + \frac{\sqrt{2\pi P_M RT_c}}{zF\alpha_c} i \tag{78}$$

being P_2 and P_4 the local pressures at BASE surfaces, anode-side and cathode-side respectively, and being

$$P_2(i=0) = P_{v,a}\left(\frac{T_m}{T_a}\right)^{1/2} \tag{79}$$

$$P_4(i=0) = P_{v,c}\left(\frac{T_m}{T_c}\right)^{1/2} \tag{80}$$

the vapour pressures at anodic and cathodic temperatures, respectively, in condition of open circuit.

After few mathematical arrangements, the final expression for the voltage drop across the external load is:

$$\Delta V = \frac{RT_m}{zF}\ln\left[\frac{\alpha_c}{\alpha_a}\sqrt{\frac{T_a}{T_c}}\right] - \frac{RT_m}{zF}\ln\left[\frac{\delta_c + i}{\delta_a - i}\right] - i\rho \tag{81}$$

which is of the form

$$\Delta V = C_0 - C_1 \ln\left[\frac{\delta_c + i}{\delta_a - i}\right] - i\rho \tag{82}$$

with:

$$C_0 = \frac{RT_m}{zF}\ln\left[\frac{\alpha_c}{\alpha_a}\sqrt{\frac{T_a}{T_c}}\right] \qquad C_1 = \frac{RT_m}{zF}$$

$$\delta_c = \frac{zF\alpha_c P_v(T_c)}{\sqrt{2\pi P_M RT_c}} \qquad \delta_a = \frac{zF\alpha_a P_v(T_a)}{\sqrt{2\pi P_M RT_a}}$$

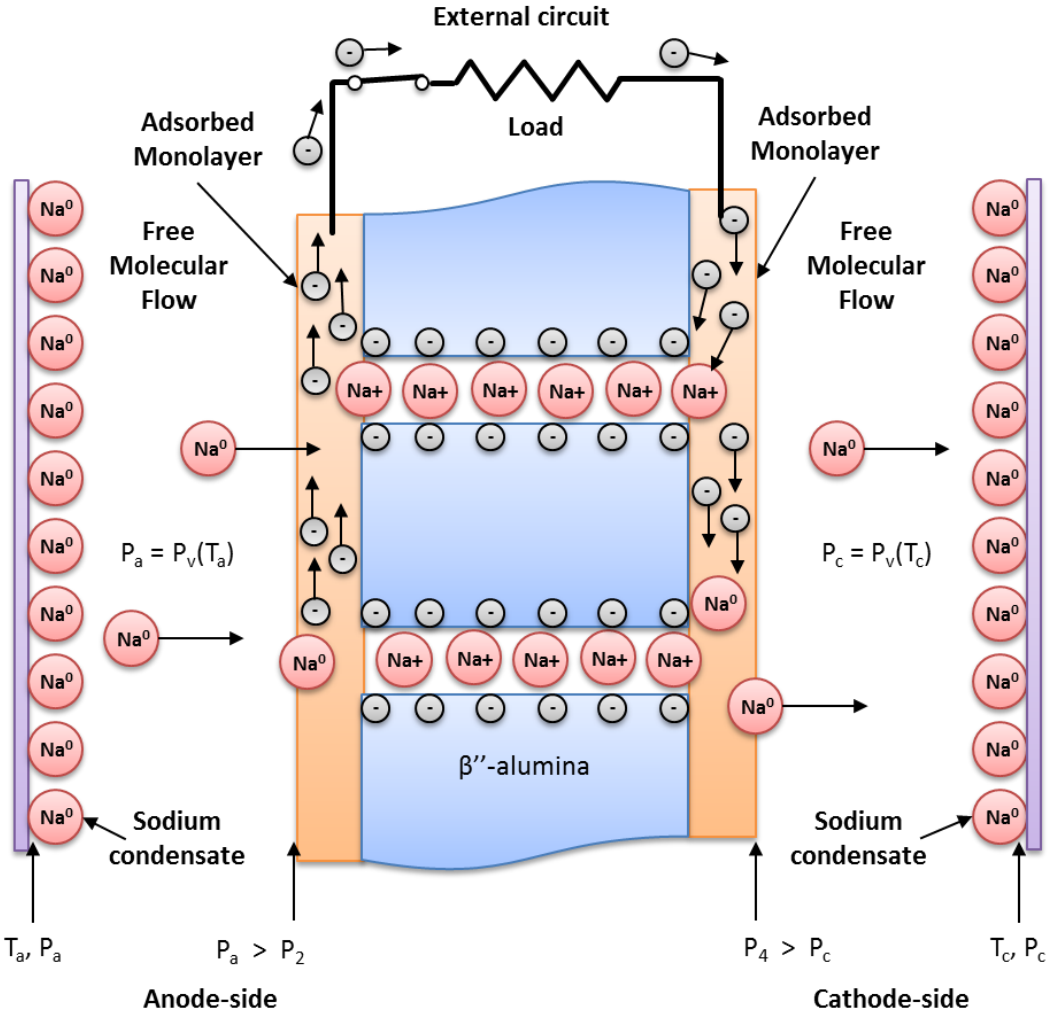

Figure 34. Microscopic processes occurring in the BASE and its interfaces in the vapour-anode/vapour-cathode AMTEC-like cell described and modelled in this work (adapted from [13]**).**

5.5 Novel Statistical Thermodynamics-based Model

The Langmuir approach which allowed to model the electrical characteristics of the cell is confirmed by Cole's experimental data [13], and so it has got empirical bases, as the Hertz-Knudsen law itself. In order to understand how the performances of a second

generation AMTEC-like device are related to the working fluid-membrane pair, some further investigation is needed on the mutual dependence of its characteristic parameters through a theoretical approach.

In the present work, a novel model of the current density has been developed, starting from purely theoretical considerations derived from statistical thermodynamics and kinetic theory of gases.

5.5.1 Preliminary Considerations

It is important to understand the phenomena underlying the operation of the cell, in order to obtain a precise mathematical modelling, aimed at solving any problems about design choices, enhancements and technological developments, and going deeper on cell physics.

As the theoretical cell voltage does not depend on the metal used – if not through the metal valence – the cell current, on the contrary, is strongly influenced by the chemical-physical characteristics of the working fluid.

The electrical current flowing through the circuit is proportional to the number of electrical charges (cations crossing the electrolyte in number equal to the electrons circulating into the outer circuit, for monovalent electrolytes).

For the metal to be ionised at the interface with the electrolyte, releasing one or more electrons, and to cross the membrane, each atom of it must have an amount of energy greater than the energy barrier necessary to cross the membrane.

From the kinetic theory of gases, it is known that pressure is a macroscopic effect that takes place as a direct consequence of the forces exerted - on a molecular scale - by the gas molecules on the walls of the vessel which contains it, whereas the temperature is a measure of the average kinetic energy of molecules. As the temperature rises, the average velocity which the metal molecules move at in the gaseous state increases and, consequently, also their average kinetic energy.

Every single atom of metal in the vapour-like state moves at its own velocity. From a statistical point of view, it makes no sense to speak about the velocity of the single atom or molecule, but rather of the distribution of velocities. This follows Maxwell-Boltzmann's velocity distribution law, expressed as:

$$f(v) = C\, v^2 e^{-\frac{mv^2}{2k_bT}} \tag{83}$$

where m is the molar mass of the particles (that are supposed to be all equal one another) and C is a normalization constant.

The function f(v)dv expresses the probability that a particle has got a velocity between v and v +dv.

In a system that obeys the laws of classical physics, the Maxwell-Boltzmann's distribution therefore assumes the meaning of probability that a particle has got an energy between E and $E + dE$.

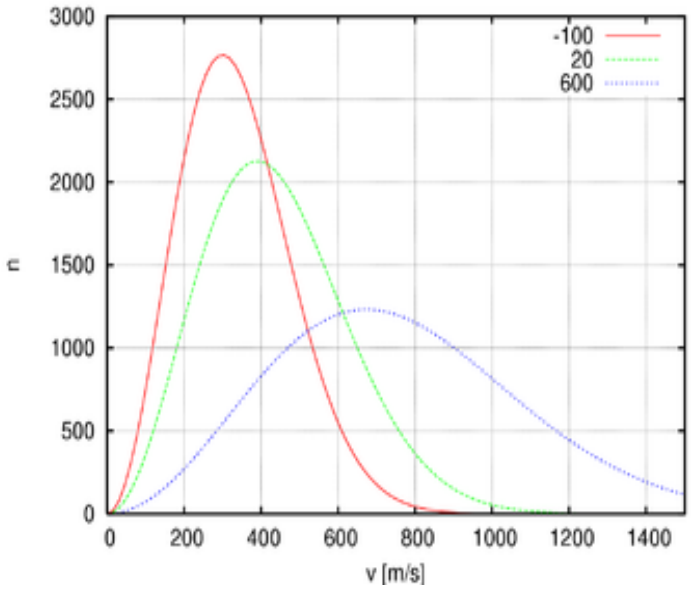

Figure 35. Gaussian distribution of gas velocity at T = -100°C, 20°C and 600°C.

From the normalization condition, according to which the probability that a particle has a velocity between zero and infinite is equal to one, which means that the integral of *f(v)dv* between zero and infinite must be equal to 1, one obtains the value of *C*:

$$C = 4\pi \left(\frac{m}{2\pi k_b T}\right)^{3/2} \tag{84}$$

$$f(v) = 4\pi \left(\frac{m}{2\pi k_b T}\right)^{3/2} v^2 e^{-\frac{mv^2}{2k_b T}} \tag{85}$$

At a given temperature only particles having a kinetic energy greater than the energy barrier needed for the process can cross the electrolyte, thereby contributing to the determination of the cell electrical current and the cell electrical power.

Working with monovalent metals with low energy ionisation (such as sodium) allows to maximize – at the same temperature – the current density (current per unit cell surface) and the ratio between electrical power and cell weight.

Initially, the choice to adopt *as a working fluid*, three other metals that have not been tested to date (zinc, cadmium and mercury) compared with sodium, potassium and lithium, and *as electrolyte* a simple porous β-alumina, will result in a reduction in current density, provided that both zinc and cadmium are bivalent ions and that both of them have a first ionisation energy which is nearly twice with respect to sodium. The latter, therefore, remains the ideal candidate as a working fluid, even with the limits and issues described above.

Of course, I would theoretically expect that, at a given working temperature T, our device supplies a higher power density (potential for current density) with sodium, lithium and potassium (monovalent metals with low ionisation energy) rather than with mercury, cadmium and zinc (bivalent metals and with the highest total energy required between the first and second ionisation).

To date, I expect that the electrochemical device as designed can work with a power density in the range 0.5-1 W/cm^2 with sodium and potassium (used also in traditional AMTEC devices [1] [42]**) and with a power density significantly lower when using zinc and cadmium as working fluid.**

However, it is also worth experiencing the behaviour of zinc and cadmium, taking into account the chemical aggressiveness of alkali metals, which may damage both electrolyte and electrodes, and the fact that over-potential phenomena (mainly dependent on the material used for the anodic and cathodic electrodes and on their porosity as well) or considerations about the cost of materials, might totally reverse the theoretical predictions in favour of zinc and/or cadmium.

In fact, the over-potential phenomena may be reduced by specifically selecting a doped electrolyte thickness that minimizes resistance to the crossing of cations, that is the internal ohmic resistance of the cell and choosing porous electrodes capable to minimize the concentration difference between bulk and electrode interface, known as *concentration polarization*, consisting of a material that can reduce the energy barrier of activation and the overvoltage phenomena associated with the current transfer.

Although the experimentation is the only way that can confirm which is the best working fluid in terms of energy (voltage and current) produced at a given temperature, it is useful to make predictive estimates using a theoretical model, even if simplified, that could lead to other experimental investigations about other "potential candidate" working fluids for use in AMTEC-like devices, in the particular temperature conditions obtainable with the thermal energy source used. What might happen is that – at least theoretically – although at a given temperature it would be convenient to work with a given working fluid (the voltage is directly proportional to the temperature, so the higher the temperature is, the greater the voltage is), at other temperatures this might not be true and a different working fluid might be more effective in terms of density of the maximum power produced.

While I am reasonably confident that the model and theoretical predictions of open circuit voltage values will be close to the experimental ones, I cannot be sure about the

theoretical predictions of the current, which will only give us indicative information useful for understanding the physics of cell and allow us to better focus the aim of the search.

There is, however, a limit condition that is worth to be investigated from a theoretical point of view. It occurs in short-circuit conditions. In such circumstances, the power transferred on the external load is zero as well as the voltage difference across the external load. The cell potential discharges itself to the internal resistance due largely to the conductivity of the membrane, which no longer depends on work against the electric field but exclusively from diffusion phenomena and gaps transfer within the membrane. For each cation that diffuses through the membrane there will be another one that abandons the membrane, leaving a "hole", which in turn will spread within the membrane, mainly influenced by temperature, thus operating the progressive replacement mechanism of cations as charge carriers (which are initially dispersed in the membrane) with new cations diffusing from the bulk interface within the membrane itself.

In other words, if one closes the circuit on a very small resistance (short-circuit), the electrical potential difference between the electrodes drops to zero and, consequently, the difference in chemical potential will determine the cell short-circuit current. The sum of all current inputs stabilizes to a definite value, in steady state, as long as the differential pressure between the two semiconductors is maintained constant. In the absence of "someone" or "something" that keeps the partial pressure difference between the chambers ("driving force" of the process), the circulating electric current will rapidly decrease and consequently decrease the electromotive force until the full discharge of the cell occurs. In this condition, the two semi-cells will have the same pressure and the same temperature and it will be $\Delta G = 0$, $E_{oc} = 0$ and $I_{sc} = 0$.

The short-circuit current will be useful to collect information and therefore to estimate the value of the internal resistance of the cell, by correlating experimental data to theoretical predictions.

5.5.2 Model Development

The device working principle here modelled is depicted in Figure 34.

The number of particles that statistically can ionise at the interface with the BASE and can cross it, in a generic closed circuit condition (i.e. a generic external load), is equal to the number of gas particles that have a kinetic energy k higher than a certain energy barrier E_m, which shall depend on the total impedance of the system (both internal and external contributions).

Since the energy barrier E_m accounts for all possible energetic contributions to be overcome (ionisation of the atoms or molecules, adsorption/desorption energy, diffusion energy) , and that a mole of gas contains an Avogadro number N_A particles, then the kinetic energy that a particle of molecular mass m must have is:

$$k = \frac{1}{2} m v^2 \geq \frac{E_m}{N_A} \tag{86}$$

from which one obtains that the gas particles which can ionise and cross the BASE are those with velocity v greater or equal to v_{lim} , being

$$v_{lim} \geq \sqrt{\frac{2E_m}{mN_A}} \tag{87}$$

In this modelling, therefore, E_m/N_A is the energy barrier that the particle has to overcome at expenses of its kinetic energy, when the electric circuit is closed on an external load.

Such energy requirement, however, is necessary but not sufficient for a particle with velocity v to ionise and cross the membrane. In fact, the ionisation takes place at the interface with the BASE which is located geometrically in a well-defined spatial position of the semi-cell. Only the collisions occurring against the surface of the BASE can generate cations. Therefore, the particles capable to ionise and cross the BASE must have velocities greater than or equal to v_{lim}, with at least one velocity component orthogonal to the membrane surface.

Therefore, considering a particle having the above-mentioned requirements, hitting against the surface of the BASE it loses its kinetic energy, ionises and passes through it. Thus, each ionisation of a particle results in a decrease in the internal energy of the gas vapours of the working fluid metal, therefore, it can be said that over time, if nothing keeps externally the pressure difference between the two BASE-separated chambers, the average quadratic velocity of the particles (microscopic effect) and the temperature of the semi-cell (macroscopic effect) decrease.

However, assuming isothermal condition in each semi-element, the required ionisation energy is provided by an external heat source.

Let's say L the height of the semi-cell, that is the distance between the BASE and the upper surface of the semi-cell parallel to the membrane (which delimits the volume of the semi-cell). Over a time interval of observation Δt, the particle p and/or the other particles that acquire its velocity for the considerations made above on the isothermal hypothesis can only make a definite number of effective collision.

The number of particle collisions that may produce an ionisation depends on the component v_x of the particle velocity and on the size L. In the time interval between two consecutive collisions, the particle runs along the x-axis the distance $2L$ (it moves back and forward between two opposite walls) with velocity v_x.

Hence, the time interval τ between two collisions is:

$$\tau = \frac{2L}{\tilde{v}_x} \tag{88}$$

being $\tilde{v}_x$ the average velocity of the particle along direction x, so the average number of collisions that the particle has got in the observation time Δt is equal to:

$$\tilde{n}_u = \frac{\Delta t}{\tau} = \Delta t \frac{\tilde{v}_x}{2L} \tag{89}$$

Replacing the average velocity of a particle along direction *x* according to the kinetic theory of gases, and introducing the condition of perfect gas[2], one gets to the average number of total collisions in the volume of the cell, in the observation time interval Δt:

$$\tilde{n}_{u,tot} = \frac{PN_A S_m}{2RT}\sqrt{\frac{k_B T}{m}}\Delta t \tag{90}$$

where S_m is the BASE cross sectional area. The number of effective collisions shall therefore be a fraction of total collisions, i.e. equal to total collisions multiplied by the ratio between the number of particles having a velocity greater than or equal to v_{lim} and the total number of particles N_T, which is by definition the integral of the Maxwell-Boltzmann's velocity distribution $f(v)$:

$$\tilde{n}_{u,eff} = \frac{N(v \geq v_i)}{N_T}\tilde{n}_{u,tot} = \tilde{n}_{u,tot}\int_{v_{lim}}^{\infty} f(v)dv \tag{91}$$

where:

$$f(v) = 4\pi\left(\frac{m}{2\pi k_B T}\right)^{3/2} v^2 \exp\left(-\frac{mv^2}{2k_B T}\right) \tag{92}$$

[2] Due to the high operating temperatures and the low operating pressures, we can apply the perfect gas theory to the working fluid vapour, i.e.:

1. Gas is made up of a very high number of molecules, which we will call particles.
2. The particles interact with each other and with the walls of the container only by means of perfectly elastic collisions, in which mechanical energy is retained.
3. Given that during collisions, molecules exercise mutually weak forces, the potential energy of these interactions is totally negligible compared with kinetic energy. This implies that between the collisions, the particles follow straight trajectories.
4. Particles are considered as material points and hence their kinetic energy is only translational.
5. There are no external forces applied on the system. This implies that the particle motion directions are distributed in an isotropic way, i.e. averagely equal in any direction, and that there are no preferential directions of motion.

In the observation time interval Δt all the effective particles transfer to the electrode the total charge Q_{tot} equal to:

$$Q_{tot} = ze\tilde{n}_{u,tot} \int_{v_{lim}}^{\infty} f(v)dv \tag{93}$$

Substituting equation (87) and rearranging, the total current flowing in the semi-cell, related to velocity v_{lim}, is:

$$I(v_{lim})_{semicell} = \frac{Q_{tot}}{\Delta t} = \frac{zFPS_m}{2RT}\sqrt{\frac{RT}{P_M}} \int_{v_{lim}}^{\infty} f(v)dv \tag{94}$$

Equation (91) can be written separately for the anode and the cathode, if different operating (temperature and pressure) or geometrical conditions apply.

At very high threshold velocities, as those of a hot vapour, which correspond to high energy barrier to be overcome, the approximate solution of the integral is:

$$\int_{v_{lim}}^{\infty} f(v)dv \cong \sqrt{\frac{2}{\pi}} \frac{v_{lim} \exp\left(-\frac{v_{lim}^2}{2RT/P_M}\right)}{\sqrt{RT_M}} \tag{95}$$

Introducing the concept of current density i, defined as the circulating current per unit membrane area, substituting (92) in (91) and rearranging, one gets to the expression for the cathodic and anodic current densities, i_c and i_a:

$$i_c = \frac{zF}{RT_c}\frac{P_c}{\sqrt{2\pi}} v_{lim,c} \exp\left(-\frac{v_{lim,c}^2}{2RT_c/P_M}\right) \tag{96}$$

$$i_a = \frac{zF}{RT_a}\frac{P_a}{\sqrt{2\pi}} v_{lim,a} \exp\left(-\frac{v_{lim,a}^2}{2RT_a/P_M}\right) \tag{97}$$

Substituting the anodic and cathodic threshold velocities, the net current density of cations flowing in the cell is $i=i_c-i_a$:

$$i = \frac{zF}{\sqrt{\pi P_M R}}\left[\frac{P_c}{\sqrt{T_c}}\sqrt{\frac{E_{m,c}}{RT_c}}\exp\left(-\frac{E_{m,c}}{RT_c}\right)-\frac{P_a}{\sqrt{T_a}}\sqrt{\frac{E_{m,a}}{RT_a}}\exp\left(-\frac{E_{m,a}}{RT_a}\right)\right] \tag{98}$$

Finally, in analogy with the theory of the barrier symmetry factor β [43], considering a symmetric energy barrier (β=0.5, [44]), rearranging and lumping, in few steps one gets to the form:

$$i = i_0\left[A\frac{\gamma_c}{\sqrt{2}}-B\frac{\gamma_a}{\sqrt{2}}\right] \tag{99}$$

where i_0, A and B have the same expressions as in equation (76), and

$$\gamma_j = \sqrt{\frac{E_m}{RT_j}}\exp\left(-\frac{E_m}{2RT_j}\right) \qquad j = a,c$$

In conclusion, the circulating current density in a vapour-anode/vapour-cathode AMTEC-like device can be written in the compact form:

$$i = i_0\Psi(E_m, T_a, T_c) \tag{100}$$

where the energy barrier E_m changes when external operating conditions change (i.e. when the external load changes), being fixed all other geometrical and physical internal parameters of the cell (BASE thickness, operating temperatures).

It is worth to note that equation (100) has got the same structure as (76).

The new approach presented in this work leads to the same conclusions as in T. Cole's modelling [13], i.e. the cell current density of the form (98) is consistent with (75), and the available voltage is of the form (82).

Comparing the two approaches, further considerations can be made, giving an explanation of the cell physics and the physical meaning of some characteristic variables.

The expression of the current density derived through both the Langmuir and statistic thermodynamic approaches for a saturated vapour-anode/saturated vapour-cathode is actually a general expression, which includes as a particular case the result obtained by Cole et al. in [13]. The sticking coefficient for a gas-solid or liquid-solid interface can be defined

as $\alpha=r_{ads}/Z_W$ where r_{ads} is the adsorption rate per unit area (molecules per m^2 per s) and Z_W is the collision frequency, which for a gas-solid system is

$$Z_{w,gas} = \frac{p}{\sqrt{2\pi m k_B T}} \tag{101}$$

and for a liquid solution-solid system is

$$Z_{w,liq} = C_{sol}\left(\frac{k_B T}{2\pi m}\right)^{1/2} \tag{102}$$

being C_{sol} the concentration of the solution in molecules per m^3 [39]. As the concentration of a pure, liquid-phase metal is much higher than that of metal atoms in a rarefied vapour phase, then the collision frequency in a liquid is in turn much greater than in a gas, and so the sticking coefficient on the liquid-side is negligible with respect to the gas-side. Therefore, equation (76) reduces to

$$i = i_0 A \frac{\alpha_c}{\sqrt{2}} \tag{103}$$

Replacing expressions for i_0 and A, recalling (80) and simplifying one gets back to (68).

In particular, looking at the terms in brackets in (76), one may state that the sticking coefficient depends, as already known in [40], on surface temperature and kinetic energy of impinging particles (in our case related to bulk temperatures T_j) and surface coverage and structural details of BASE (in our case described by the energy barrier E_m, which actually in our model takes also into account the effect of the external load) according to the following expression:

$$\alpha_j = \sqrt{\frac{E_m}{RT_j}} \exp\left(-\frac{E_m}{2RT_j}\right) \qquad j = a, c \tag{104}$$

It follows that $\Psi \equiv \Phi$. It is known from theory that the sticking coefficient α ranges between 0 and 1 (limits included), but if one plots (104) as a function of E_m, he or she would find a global maximum $\alpha_{j,max}=\exp(-0.5)\approx 0.606$ at $E_m=RT_j$, which is lower than 1. This suggests that statistic thermodynamics reasons would exclude the possibility of 100% effective adsorption, i.e. every single impinging particle adsorbs onto the BASE surface, independent of the nature and efficiency of the electrode.

Expression (76), if taken alone, could induce erroneously to the conclusion that the circulating current density depends on two independent variables (anodic and cathodic sticking coefficient). Equation (104) demonstrates instead that, once the external load has been established, the anodic and the cathodic sticking coefficients are not independent, but related one to the other through the energy barrier, E_m.

The sticking coefficient is a characteristic quantity of the pair working fluid-BASE and it is also related to the geometric features (i.e. BASE thickness) [45, 46] and to the ion conductivity of membrane.

Such a conclusion seems to be in contrast with the definition of sticking coefficient as known in literature, which depends only on surface temperature and geometry of the surface. Actually, the BASE thickness influences the total resistance of the circuit as it affects directly the internal resistance, and in turn the BASE temperature T_m due to Joule effect. The BASE temperature, which is a unique, common value between anode and cathode, can be introduced in (104) by use of (79) and (80). By doing so, the known dependence of the sticking coefficient on the BASE surface temperature and the applied local interface pressures is restored.

This means that for each condition of external applied load, a unique total resistance of the equivalent electric circuit is determined, which sets a unique circulating current density, in turn driven by a unique cathodic interface over-pressure (with respect to the cathodic pressure) and a unique anodic interface under-pressure (with respect to the anodic pressure), determining in turn the respective sticking coefficients.

In open circuit conditions, as obvious, both the sticking coefficients do not depend on any current, but only on the BASE temperature and applied local interfacial pressures, being absent any contribution of over-pressure or under-pressure due to the current.

Similarly, it can be said can say that the sticking coefficient, affecting the polarisation curve in the Langmuir approach and being dependent on the external load in our approach, determines the non-ohmic behaviour of the AMTEC-like cell.

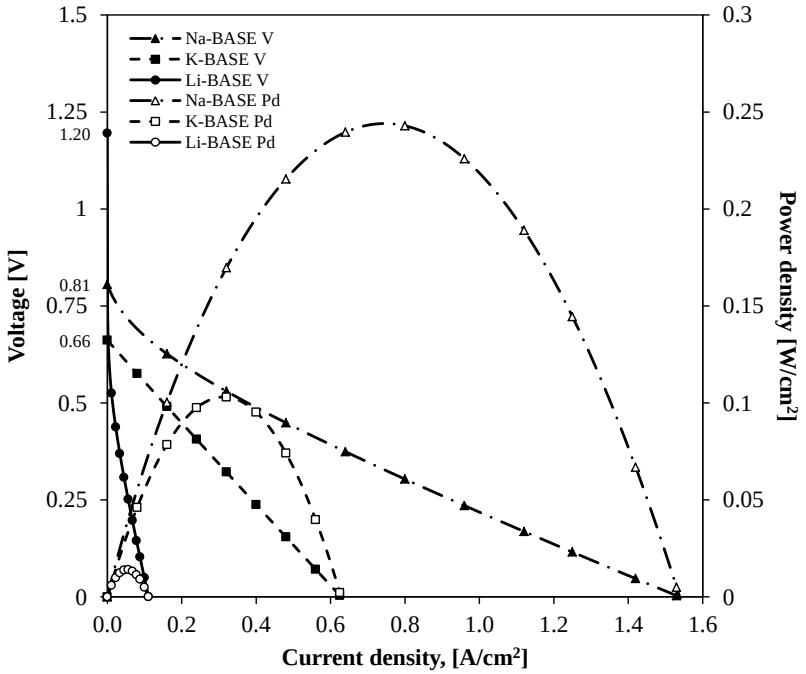

Figure 36. Computed polarisation and power curves for three different vapour-anode/vapour-cathode AMTEC-like devices, operating with sodium, potassium or lithium vapours respectively. Simulation conditions: membrane thickness 1.5 mm, anode temperature 1000 K, cathode temperature 500 K, $\alpha_a=\alpha_c=1$ (effective adsoption), vapour pressure are computed as function of temperature according to [47].

Higher energy barrier, that under the same operating conditions (i.e. anodic and cathodic temperatures and external load) means low BASE conductivity, implies lower performances in terms of output power density.

As equation (98) suggests, when the energy barrier goes to zero or infinite, the current density tends to zero, as well as the power density extractable from the device. This suggests that for each possible anodic and cathodic operating temperature, an optimal combination of BASE and working fluid might exist, which maximises the extractable power density.

As a proof of this, Figure 36 illustrates the polarisation curves and power curves of an AMTEC-like device, computed with the model so far developed, operating at the same conditions (anode temperature 1000 K, cathode temperature 500 K) but with different working fluids and BASEs (sodium vapour/Na-BASE, lithium vapours/Li-BASE and potassium vapours/K-BASE). The choice of the working fluids has been due to the availability of electrical resistivity data of commercial ion conducting membranes (by IONOTEC ltd., 14 Berkeley Court, Manor Park, Runcorn, Cheshire WA7 1TQ, England). Figure 36 reports the voltage-current density curve as well as the corresponding power density, as a function of the circulating current density or – equivalently – as a function of the external load applied.

Provided the same operating conditions and membrane geometry (thickness 1.5 mm), sodium-BASE performs better than potassium-BASE and the latter in turn better than lithium-BASE, in terms of maximum output power density. Such behaviour can be attributed to the higher resistivity of lithium-BASE (approximately one order of magnitude higher with respect to the sodium-BASE), which produces higher ohmic losses in the cell even at low circulating current density. This results in a greater maximum power density extractable from sodium-BASE device.

Sayed Waqar Hasan et al. in [45, 46], Ilia Pavlienko in [48] and William Anderson et al. in [42] have all found experimentally similar voltage vs current density and power density vs current density curves for AMTEC and AMTEC-like cells.

Furthermore, some manipulations of (76) in condition of open circuit ($i=0$), using (79), (80) and (104) and solving for E_m allow to obtain the BASE open circuit energy barrier $E_{m,0}$

$$E_{m,0} = 2R\frac{T_a T_c}{T_c - T_a}\ln\frac{P_{v,a}T_c}{P_{v,c}T_a} \tag{105}$$

Similarly, considering the short-cut condition (*ΔV=0*) applied to (81), introducing (76) and (104) and substituting the expression for α_a, α_c, δ_a and δ_c, then a complex implicit correlation between $E_{m,sc}$ and the areal resistance of BASE can be found.

CHAPTER VI

EXPERIMENTAL RESULTS

6.1 Experimental Tests with Hydrogen

6.1.1 Procedure

This chapter deals with the experimental tests carried out with hydrogen on the simplified home-made device. The experimental procedure followed during hydrogen tests carried out is depicted in Figure 37.

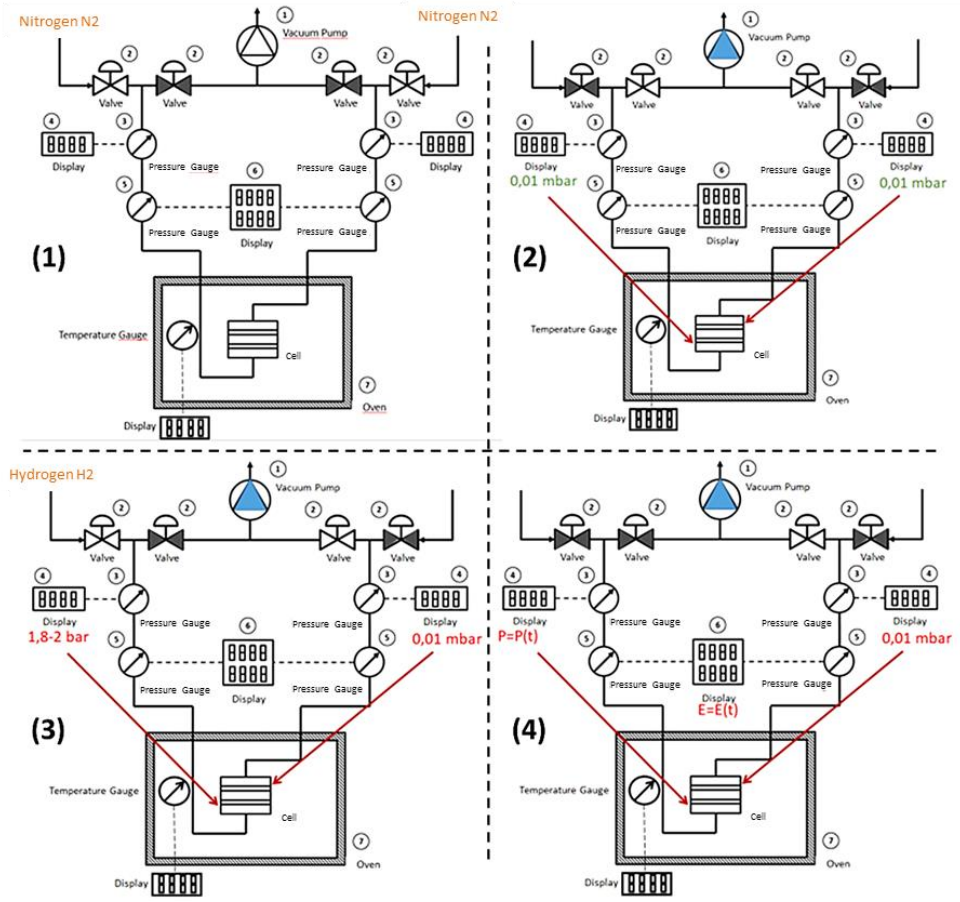

Figure 37. Experimental sequence adopted for tests: (1) washing with nitrogen, (2) creation of vacuum in both chambers, (3) pressurization of a chamber with hydrogen and (4) insulation of pressurized line and starting of measurements.

All the phases of the procedure were carried out at T = 25°C. In the first phase, the Nupro valves (2) of the suction line of the pump were closed and three washes with nitrogen have been made (taken from a vessel installed in line) in both chambers. Then, the

nitrogen feed valves were closed and those of the suction line were open, whilst the two chambers of the device were brought to a pressure of about 10^{-2} mbar.

Then, the Nupro valve of the line connected to the bottom chamber of the device was open and hydrogen was fed inside it (taken from a vessel) up to a pressure of 1.9±0.1 bar. Of course, the introduction of hydrogen modifies initially even the pressure inside the upper chamber, which grows up to 10^{-1} mbar, and then goes back to the initial value (order of magnitude 10^{-2} mbar).

Finally, the feed valve of hydrogen was closed: this time instant represents the actual beginning of the test, so the data logging of the three instruments has been started (high field PTX pressure gauge, low field EDWARDS pressure gauge, digital high precision FLUKE multimeter). So, pressures in the two chambers and the voltage generated at the electrodes have been measured and logged for the whole duration of the test, which is considered completed as soon as the read potential difference becomes zero.

As the system hadn't got perfect sealing, the upper chamber (the vacuum one) was affected by leakages of air from outside. Despite this, the external air flux due to the not-perfect sealing did not lead to an increase of pressure because the leaked air itself was immediately suctioned by the vacuum pump. In the bottom chamber, instead, hydrogen leakages towards outside were likely to occur for a certain period of time, as long as the pressure of the chamber was higher than the atmospheric one. Since this moment, in fact, the systems reached equilibrium (inner pressure equal to outer pressure).

In the experimental test no. 3, different operating conditions were adopted with respect to tests no. 1 and 2. As I am going to discuss onwards, such a choice depended on the results of the first to tests with hydrogen, which have been considered affected by a multitude of the perturbing and dissipative phenomena, that I am going to treat in the following paragraphs and that do not allow to appreciate qualitatively and quantitatively the main study subject, which is the generation of electrical voltage at the interface, promoted by the difference of (partial) pressure of the working fluid into the two chambers of the device.

In test no. 3, I tried to isolate, as much as possible, the perturbing and dissipative phenomena. With regards to that, it was decided to operate in both chambers (after the preliminary washing with nitrogen) with initial hydrogen pressures greater than 1 atm and one different than the other one: by doing so, during the whole test (which is considered terminated as soon as both chambers reach the pressure of 1 bar), there is no possibility of leakages from the external ambient towards the chambers, none chambers being operating under vacuum. The missed contamination of the working environment by other species leaking by diffusion (oxygen and nitrogen), made possible that the pressure inside the chambers was due exclusively to hydrogen only, in every time instant of the test (one-component system).

6.1.2 Results and discussion

During experimental tests, it has been noted that the pressure of the vacuum chamber (P1), measured with the pressure gauge EDWARDS, has remained approximately constant during the whole test.

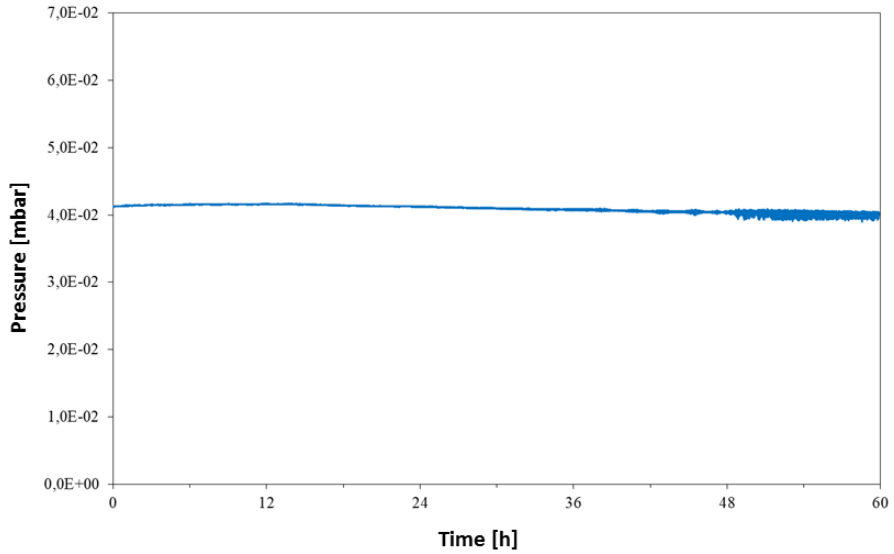

Figure 38. Time trend of vacuum chamber pressure (test no. 1).

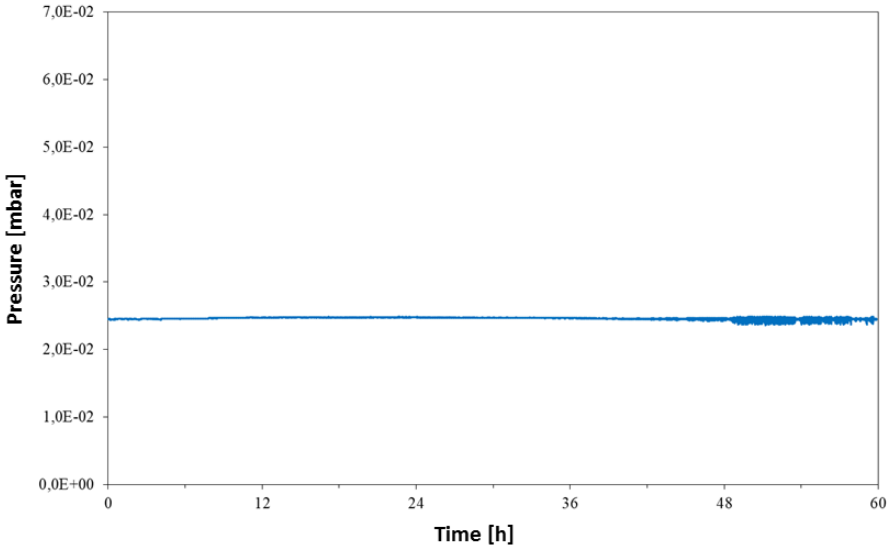

Figure 39. Time trend of vacuum chamber pressure (test no. 2).

The pressure of hydrogen in the bottom chamber (P2), measured with the pressure gauge PTX, which at initial time is 1.9±0.1 bar has exponentially decreased down to the value of 1 bar (due to losses by leakages), and stayed then constant during time, being in equilibrium with the external ambient pressure.

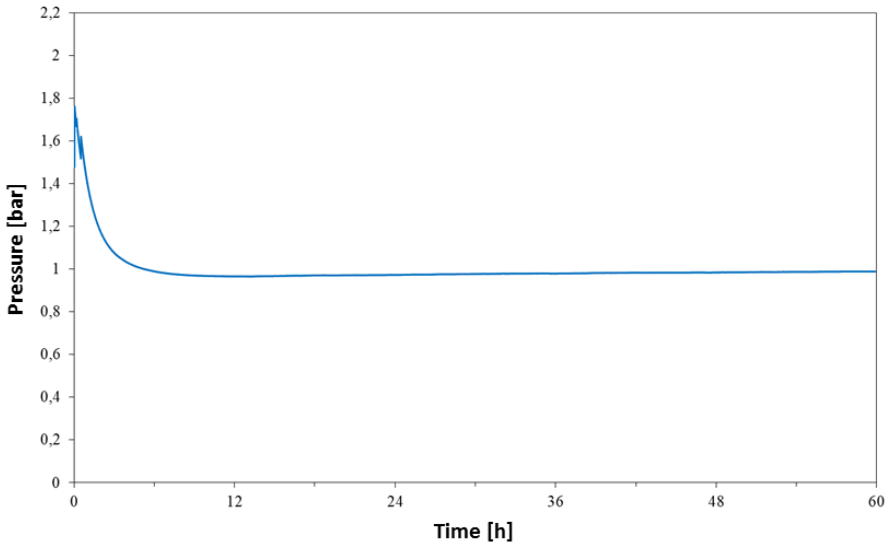

Figure 40. Time trend of pressurized chamber pressure (test no. 1).

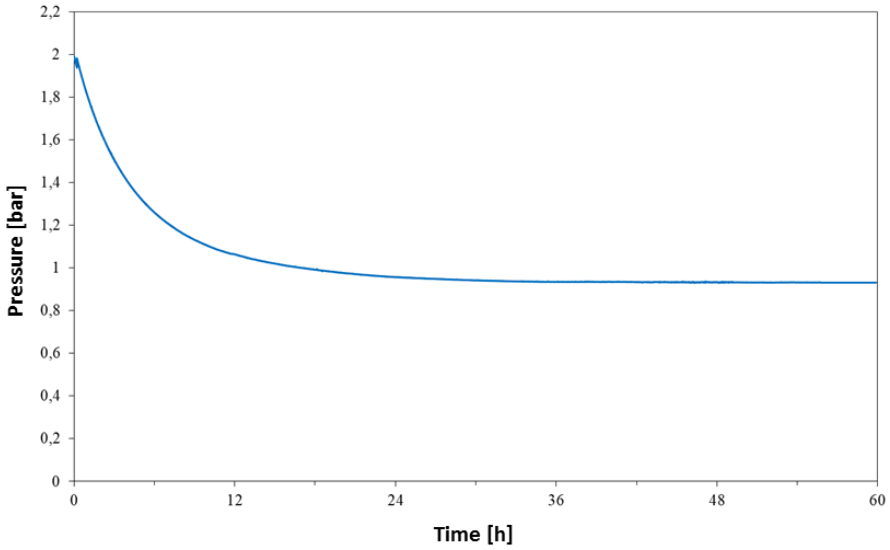

Figure 41. Time trend of pressurized chamber pressure (test no. 2).

The theoretical cell voltage decreased a little, slowly and linearly during both tests, being such a voltage calculated directly from the pressure values read in the two chambers, by applying (32). With regards to that, it is worth to observe that the value of theoretical voltage so calculated could be considered reliable only in the first part of the test, i.e. as long as the pressure in the bottom chamber was still sufficiently higher than the atmospheric pressure and then one could be reasonably sure about the fact that – at least in the bottom chamber – there was only the hydrogen initially introduced (one-component system hypothesis).

The actual cell voltage first increased to a maximum value near to the theoretical value, then decreased down to a limit value, stationary for a long time period (about 22000 seconds, equal to about 6 hours), and finally started to decrease again down to some residual millivolt.

The theoretical voltage calculated with (32) actually did not describe correctly the actual trend of the measured voltage, right because of the presence of perturbing effects inside the vacuum upper chamber, that made invalid the hypothesis of one-component system. The theoretical calculated voltage was not the "actual", or better, the "corrected"

theoretical voltage, which one can obtain by modelling the system taking into account such perturbing phenomena.

As it can be seen from Figures 38 to 41, the first two tests, carried out under the same experimental conditions, gave approximately the same reproducible results.

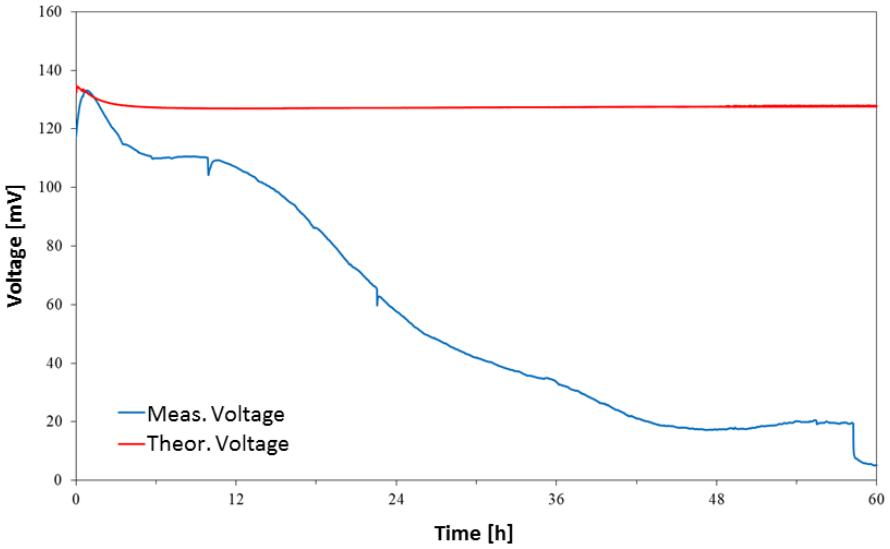

Figure 42. Time trend of measured and theoretical voltage (test no. 1).

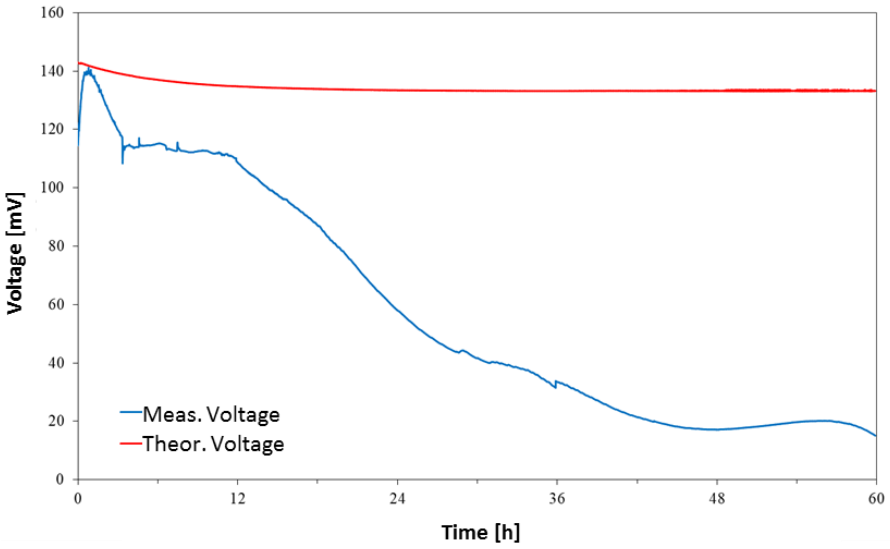

Figure 43. Time trend of measured and theoretical voltage (test no. 2).

In test no.3, the two values of pressure at the beginning of the test in the anodic and cathodic chambers were, respectively, 2,479 bar(a) e 2,313 bar(a): pressures were left free to evolve, as done in the previous tests, monitoring them at a sampling frequency of one minute, together with the measured voltage. The trends of pressures and voltages obtained during the whole test (47 hours) are illustrated in Figure 44.

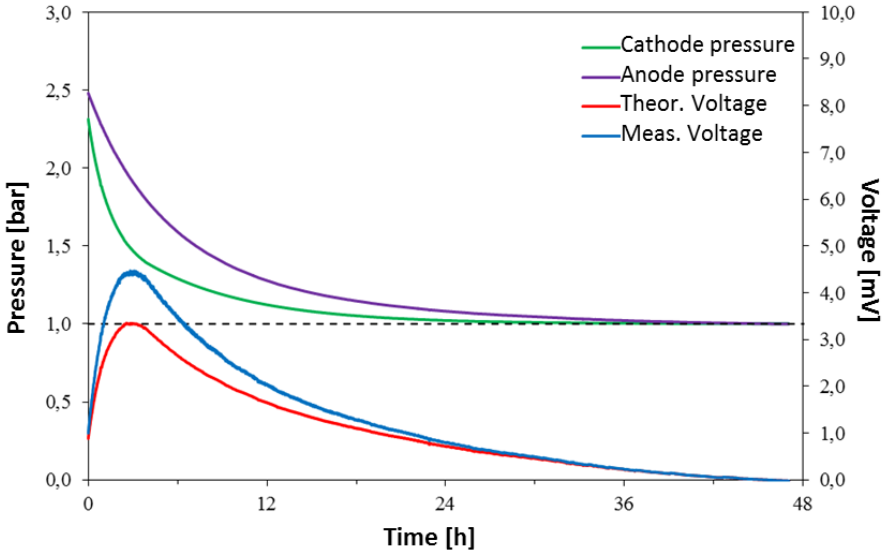

Figure 44. Time trend of anodic pressure, cathodic pressure, measured and theoretical voltage (test no. 3).

From Figure 44 it can be firstly noted that the two pressures in the chambers had different temporal evolutions and in particular it was not observed the maintenance of a constant pressure difference between chambers, but a faster decreasing of pressure in the lower pressure chamber. This is, for sure, a proof of a different quality of sealing of the two chambers, as otherwise it would had been more reasonable to expect more significant leakages from the higher pressure chambers, i.e. a greater pressure loss (greater slope of the curve).

Moreover, it can be noted that the theoretical voltage trend (calculated on the basis of values read by the instrumentation) was different with respect to the previous tests and – contrary to the first – qualitatively very similar to the trend of the measured voltage.

However, it must be considered that in test no. 3, both pressures varied with time (vacuum was no more maintained in one of the two chambers), and then – as could naturally be expected – the theoretical voltage tended to zero both near the initial and the final instant of the test (horizontal slope in the latter case), since pressures tend to equalize.

The measured voltage tended to be equal to the theoretical one, as the ratio between the anodic and cathodic pressure tended to unity. This happened in the initial but also in the final ones, i.e. at infinite time, when the measured voltage tended to zero.

6.1.3 Interpretation of experimental results

In order to interpret the voltage curves vs time detected by the instrumentation, one has to consider that the tests are affected by some disturbing phenomena variable in time, being function of the instant pressure in the two chambers.

Such disturbing phenomena always have as effect, in some way, the alteration of the concentration of the working fluid, intended as the amount of matter per unit volume.

These disturbing phenomena can be attributed basically to:

1) Concentration difference in correspondence of the membrane interface, membrane-side, with respect to the compartment-side. This happens in both chambers and is due to not-modelled phenomena, such as **solution/sorption/"solution-membrane" partitioning** of active species ("solution-diffusion" model).

2) Concentration difference near membrane interface, compartment-side, between the membrane surface and the chamber bulk, due to the not-modelled phenomenon of **concentration polarization**, which is necessary and physiological in order to guarantee the diffusive flux in a stagnant medium.

3) **Not-ionised hydrogen permeation** from a chamber to the other one, through membrane porosity or due to internal leakages, phenomenon not-easily measurable, which contributes to move the equilibria since it causes variations of bulk concentration.

4) Concentration variations in the bulk of the vacuum chamber, caused by the not-modelled phenomena of **air leakage from outside**, moved by the existing pressure difference.

5) Concentration variations in the bulk of the pressurized chamber, caused by the not-modelled phenomena of **hydrogen leakage towards outside**, moved by the existing pressure difference (as long as the chamber is at a pressure higher than the atmosphere).

6) Concentration variations in the bulk of the pressurized chamber, caused by the not-modelled phenomena of **molecular diffusion of between the residual hydrogen of the pressurized chamber towards atmosphere and the external air (nitrogen + oxygen)**, which may occur once reached the atmospheric pressure in the chamber.

In order to assess the influence of the different contributions of various disturbing phenomena, let's try to model them as function of their characteristic variables.

The different concentration at the membrane interface, membrane-side, with respect to the concentration at the membrane interface, compartment-side, due to the sorption on porous support phenomena can be modelled by a simple proportional law, typical of a "solution-membrane" partitioning equilibrium, widely validated for the gas separation process ("gas separation", see [49]):

$$P_{int} = K\, P_{bulk} \tag{106}$$

Therefore, one gets:

$$P_{int}^{anode} = K_a\, P_{bulk}^{anode} = K_a\, P_a \tag{107}$$

$$P_{int}^{catodo} = K_c\, P_{bulk}^{catodo} = K_c\, P_c \tag{108}$$

obviously $K = K(P, T, membrane)$.

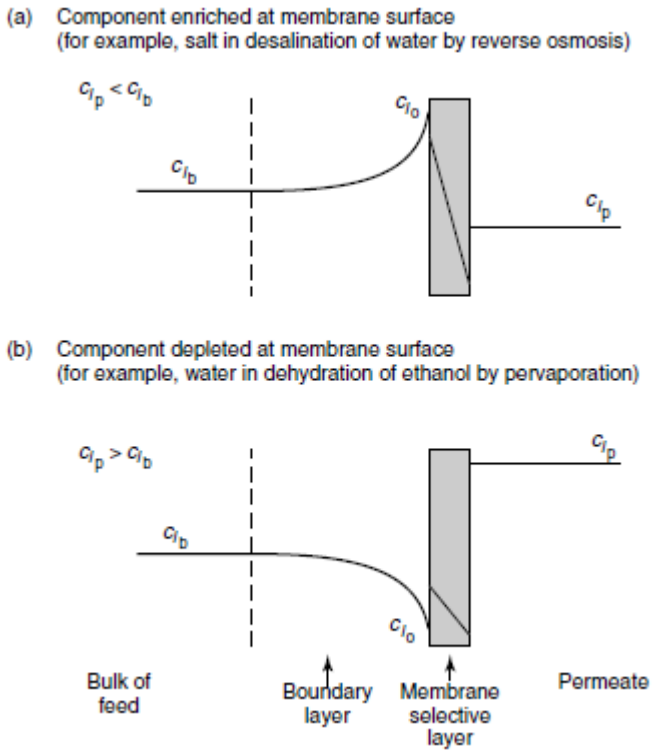

Figure 45. Concentration gradients established after permeation through selective membrane [49]**.**

Now, if substituting such concentrations into the theoretical equation for the estimation of the voltage, one gets:

$$OCV = \frac{RT}{nF} ln\left(\frac{P_{int}^{anode}}{P_{int}^{catode}}\right) = \frac{RT}{nF} ln\left(\frac{K_a}{K_c}\right) + \frac{RT}{nF} ln\left(\frac{P_a}{P_c}\right) \quad (109)$$

OCV being the measured open circuit voltage. But,

$$\frac{RT}{nF} ln\left(\frac{P_a}{P_c}\right) = E_{theoretical} \quad (110)$$

therefore

$$OCV = E_{theoretical} + \frac{RT}{nF} ln\left(\frac{K_a}{K_c}\right) \quad (111)$$

where the term $\frac{RT}{nF} ln\left(\frac{K_a}{K_c}\right)$ has dimension of a voltage and can be treated as an over-potential due to sorption/solution in membrane E_{stm}, caused by the above mentioned sorption/solution phenomena which, as known, typically depends on the applied pressure, and then – in our case – on the pressure existing in the anodic and the cathodic compartments:

$$E_{stm} = E_{stm}(P_a, P_c, T, membrane) \quad (112)$$

$$OCV = E_{theoretical} + E_{stm} \quad (113)$$

By analogy, even the variations of bulk concentration of neutral hydrogen (not ionised) determined by **hydrogen permeation through the membrane**, with respect to those which can be deduced if the phenomenon was (ideally) absent, can be modelled by introducing an over-potential. Even in this case, by doing so one'd get:

$$OCV = E_{theoretical} + E_{perm} \quad (114)$$

where

$$E_{perm} = E_{perm}(P_a, P_c, T, membrane) \quad (115)$$

Concerning, instead, to the different bulk concentration in the pressurized chamber due to hydrogen diffusion phenomena towards atmosphere (leakages) as long as the pressure is higher than 1 atm and, subsequently, air diffusion phenomena from the atmosphere towards the chamber, starting since the equilibrium pressure (1 bar) is reached,

this cannot be modelled easily, unless one introduces (as above stated) molecular diffusion laws (first and second Fick's law) and considers the partial pressure of hydrogen inside the two chambers, instead of the total ones (partial pressures are hardly measurable with the instrumentation available at INAF labs in Palermo).

Hence, the use of the expression of the theoretical cell voltage, as derived from Nernst's law, will lead to the insurgence of errors due to the missed correspondence between the total pressure value measured and the actual hydrogen (partial) pressure in the semi-cell.

In the high pressure chamber (bottom semi-cell), at the initial time of the test, pressure is maximum (1,8-2 bar) and therefore I am reasonably sure the, at least initially, only hydrogen is present in chamber. For this reason, I can state that the total pressure in the chamber (read by the instrumentation) is equal to the partial pressure of hydrogen, being also taken into account that external air has no possibility to diffuse towards an ambient (the chamber itself) which operates at higher pressure. As time elapses, the pressure inside the chamber decreases and the error committed when using the total pressure as a measure of the hydrogen pressure begins to grow.

The error is minimum (or nil) until the pressure in the chamber equals the atmospheric pressure (exactly at this time, the atmosphere inside the chamber is still composed by hydrogen only), and then it becomes more and more significant as time elapses, as air begins to diffuse into the chamber (driven by molecular diffusion, due to a concentration difference with respect to outside). In any case, it must be noted that, being the pressure (whatever partial or total) influencing on the theoretical voltage or on the measured one via logarithmic law, the error would result some way "mitigated".

In the vacuum chamber (upper semi-ell), where initially there was hydrogen as a consequence of the washes performed, only and exclusively at initial instants of the test it would be correct to assume the total pressure read by the instrumentation as equal to the effective partial pressure (or, better, fugacity) of hydrogen. This depends, obviously, on the extent of leaking phenomena, i.e. on the rate of contamination of external air towards the internals of the semi-cell, caused by the not perfect sealing. Surely, after a certain,

presumably very long period of time (but not easily predictable), all residual hydrogen would be entirely suctioned by the vacuum pump and replaced by air. Therefore, the hydrogen partial pressure would be decreasing in time, despite the total pressure in chamber (read by the instrumentation) remains the same, constant at a value of about 10^{-2} mbar.

This determines, presumably, the peak in voltage in OCV vs t curves, which is detected in the initial part of the test, providing that from a certain point onwards, however, permeation and sorption/solution phenomena become predominant on external air leakage towards the low pressure chamber. In the initial part of the test, the error due to the presence of a multi-component system is minimum in the upper vacuum chamber and nil in the bottom pressurized chamber.

As time elapses, however, the hydrogen pressure in the high pressure chamber (1,8-2 bar) decreases, due to hydrogen leakage to atmosphere, caused by bad sealing. So, the hydrogen pressure is decreasing, until reaching the equilibrium pressure (1 bar). At this point, the molecular diffusion of hydrogen towards atmosphere and air towards the chamber begins even in the high pressure compartment. Therefore, even in this case, the hydrogen partial pressure will go decreasing in time, despite the total pressure in the chamber remains constant at about 1 bar. As a consequence, the cell voltage will go decreasing as well, until reaching a value near to zero (terminal part of tests no. 1 and 2 curves). The maximum error due to the presence of a multi-component system in both chambers will occur at long time period (when time tends to infinity) and the theoretical voltage got by (2) would not be in agreement with actual voltage, providing that the hydrogen concentration (partial pressure) in the two chambers differs a lot from the total pressure in the two chambers.

Nevertheless, as first approximation, it is reasonable to consider that such disturbing phenomena (which can be hardly modelled and/or detected with the instrumentation available) are confined only in the terminal regions of the voltage curves. Hence, I can extract from tests no. 1 and 2 a long enough time period (about 22000 seconds, i.e. about 6 hours) during which the difference between theoretical cell voltage and measured voltage

is quite constant. This can be deduced in both tests and it is thought to be essentially due to the first two disturbing phenomena (sorption/diffusion and hydrogen permeation).

In such region, applying the principle of superposition of effects, one can therefore write as follows:

$$OCV = E_{theoretical} + E_{stm} + E_{perm} \tag{116}$$

i.e., provided $E_{stm} + E_{perm} = \Delta E_p$,

$$OCV = E_{theoretical} + \Delta E_p \tag{117}$$

with $\Delta E_p = \Delta E_p(P_a, P_c, T, membrane)$ total membrane over-potential.

Defining the cell efficiency as $\alpha = \frac{OCV}{E_{theoretical}}$, one will get:

$$\Delta E_p = \alpha E_{theoretical} - E_{theoretical} = (\alpha - 1)E_{theoretical} \tag{118}$$

hence ΔE_p is the (positive or negative) voltage which has to be added to the theoretical voltage in order to get the measured voltage, which is an indirect measurement of the cell efficiency.

If one re-writes:

$$E_{theoretical-corrected} = OCV = \alpha E_{theoretical} = \frac{RT}{nF} ln\left(\frac{P_a}{P_c}\right)^{\alpha} \tag{119}$$

If $\alpha = 1$ then ideal operating conditions are considered (so that the full "driving force" is effectively available for the generation of the electrical potential and there are no secondary perturbing or dissipative phenomena) or – more in general – at near-ideal conditions (so that, despite secondary phenomena exist, their perturbing or dissipative effects compensate one another);

if $\alpha < 1$ the measured voltage will be lower than the theoretical one and in absence of such a correction one would overestimate the value of the generated voltage;

if $\alpha > 1$, finally, then the measured voltage will be higher than the theoretical one and in absence of such a correction one would underestimate the value of the generated voltage.

To be noted that $\left(\frac{P_a}{P_c}\right)^{\alpha}$ can be seen as an ideal/isentropic or polytropic expansion depending on the value of α, which can be now thought as function of the operating conditions of the pressure in the two chambers, of the temperature of the system (more correctly, in the two chambers) and of the nature of membrane:

$$\alpha = \alpha(P_a, P_c, T, membrane) \tag{120}$$

The corrective coefficient α is, in the end, an omnicomprehensive cell global efficiency factor, which lumps the effects of the perturbing and dissipative phenomena (leakages, contamination of chambers caused by not-perfect sealing, permeation through membrane due to the non-ideality of membrane itself) and of the secondary phenomena (concentration polarization, partitioning equilibrium of species between membrane and compartment in correspondence of membrane surface). Provided that there is a great uncertainty and difficulty of modelling of several perturbing phenomena operating simultaneously which – in general – can be thought to contribute together to the non-predictability of the generated voltage through (32), it was decided to carry out a new test with hydrogen (test no. 3) trying – as much as possible – to reduce the number of simultaneous potential disturbs, to limit the number of disturbing phenomena to one per time. By doing so, the extent of each of the phenomena can be estimated, and a more reliable model can be produced, capable to predict a theoretical voltage which takes into account the superposition of all perturbing and dissipative effects and has a time trend quite similar to that of the measured voltage (actual voltage).

With reference to tests no. 1 and 2, it would be possible to calibrate the coefficient α according to the following procedure:

- calculate the coefficient for each logged time instant, by using its definition;

- plot the coefficient as a function of a process variable, chosen among those which one thinks it could depend on, or a combination or function of them;

- obtain the calibration curve, which can predict the value of the coefficient starting from the known process conditions.

In such way, it would have been possible to correct the theoretical voltage through (119), to get an estimation probably more reliable of the performance of the cell, with respect to what could be obtained by applying (32).

Nevertheless, in tests no. 1 and 2, among the variables which one thinks the efficiency coefficient α could depend on, only the anode-side pressure is appreciably variable in time (provided the conditions at which tests were carried out). In fact, the system has been maintained isothermal (this leading to exclude the variable temperature) and – as it has been seen – that the level of vacuum realized into the cathodic chamber maintains constant in time (this leading to exclude the variable cathodic pressure). Moreover, few or nothing is known or can be estimated about the effect of the nature of the membrane (porosity and sorption level).

The choice would then have been obliged as one could calibrate the coefficient α only as function of the anodic pressure and/or on the ratio between the anodic and the cathodic pressure (expansion ratio). Nevertheless, it has been observed that, being the theoretical voltage calculated with (119) starting from the total pressures read by instrumentation, the use of (119) would have been considered conceptually correct as long as only hydrogen is present in the two chambers (even if leaking towards outside, from the pressurized chamber). As soon as the pressure in the anodic chamber (the pressurized one) would have decreased to the atmospheric level, provided that in this moment the molecular diffusion of air from outside which progressively replaces the internal hydrogen atmosphere, the pressure read by the pressure gauge could not be referred to the hydrogen only (the total pressure does not coincide with the partial pressure of hydrogen). Hence, in this case, the value of the theoretical voltage calculated with (119) would have been "no more reliable", because calculated from an incorrect value of pressure of hydrogen.

In the light of this, the calibration of α would have been possible, or at least "conceptually correct" only during the period in which the anodic pressure is reasonably higher than the atmosphere, i.e. typically during the first hours from the beginning of the tests no. 1 and 2. During the first phases of the tests, in fact, as anticipated before, it is thought that only leaking phenomena towards outside and neutral hydrogen permeation through membrane can occur in the anodic (pressurized) chamber, and only external air leaking phenomena can occur in the cathodic (vacuum) chamber, leading to a continuous decrease of the hydrogen concentration due to mixing and suction by the vacuum pump. Such aspect is well illustrated in Figure 46.

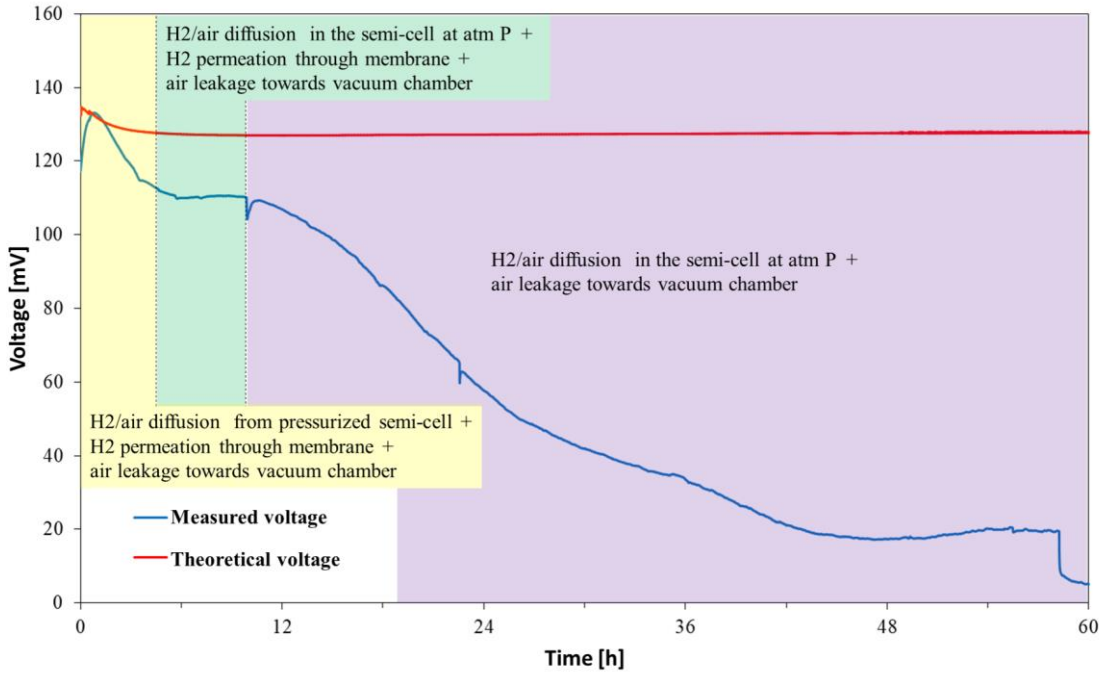

Figure 46. Indication of perturbing and dissipative secondary phenomena on the experimental curve (test no. 1).

Test no. 3 with hydrogen as working fluid as well but different operating conditions aimed to suppress or limit the insurgence of some parasitic phenomena, as anticipated above.

In particular, operating this time with both chambers with a pressure above the atmosphere, I tried to eliminate the phenomenon of air leakage from outside towards the cathodic chamber (which in previous test was maintained under vacuum) and limit the duration of the test to the moment in which the pressure in the two chambers equals and becomes equals to 1 atm, to impede the molecular diffusion of hydrogen towards outside and of air towards inside in both chambers. By doing so, phenomena described in points no. 4 and 6 of the list reported at the beginning of paragraph can be excluded, whilst the other secondary phenomena there described still apply.

Comparing tests no. 1, 2 and 3, analogies and differences can be identified. As an example, it was demonstrated that in the first hours of the tests (yellow region in Figure 46) the trend of the measured voltage is similar in all the tests performed, showing a behaviour initially increasing to a maximum, obtained in correspondence of the maximum pressure ratio detected, and then decreasing to an asymptotic value (different from a test to another due to the different operating condition and affection of perturbing phenomena), resulting in a characteristic "bell" shape.

In particular, this value is maintained for a certain period, equal to the extension of the "bell" of tests no. 1 and 2 (green region of Figure 46), and then it continues to decrease in subsequent hours, while in the test no. 3 the reaching of the asymptotic value is obtained in correspondence of the end of the test (47 hours). In the first case, then, the reaching of the "plateau" occurs in shorter times and this is presumably due to the higher driving force available between chambers and to the fact that one of those is continuously maintained under vacuum: evidently, the continuous suction of the pump connected to the cathodic chamber makes the transitory of depressurization of the anodic chamber terminate in shorter times, caused to molecular not-ionised hydrogen permeation through membrane (point 3 of previous list) and internal leaking between chambers. The "plateau" in of voltage in tests no. 1 and 2 has stayed constant as long as hydrogen was present in the anodic chamber, replaced by molecular diffusion by leaking air. In test no. 3, instead, the two pressures decrease more slowly and with different trends, being the driving force available for leakages lower, and the generated voltage has a "wider" trend, showing a

region characterized by sorption/solution-diffusion and hydrogen permeation (yellow region of Figure 46) which interests the whole test.

By comparing instead the curves of theoretical and measured voltage of test no. 3 only, it can be noted that the experimental trend is qualitatively well reproduced by the theoretical model, apart from a diffused deviation, higher when the pressure ratio is far from unity. Having clarified , above, the motivations about the possibility of introducing a corrective coefficient α taking globally into account the effect of all secondary phenomena not-rigorously modelled, in the following the result of calibration of such a coefficient is shown (for test no. 3).

The coefficient α has been calculated by using its definition, for each point experimentally detected and it had been plotted against the logarithm of the expansion ratio (anodic pressure/cathodic pressure), obtaining the green curve of Figure 47. The choice to correlate, in some way, α to the pressure ratio has been discussed above.

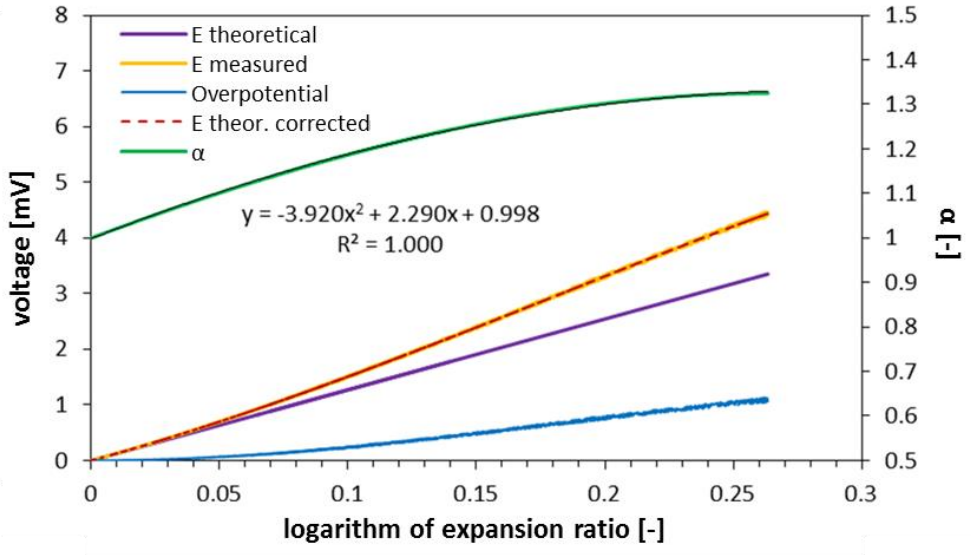

Figure 47. Calibration curve of the coefficient α and trend of theoretical, corrected and measured voltages, as a function of the logarithm of the expansion ratio (test no. 3).

It was found that the trend of α as a function of the expansion ratio, under the experimental operating conditions of test no. 3, is well described by a second order

interpolation curve, and this can be explained by saying that in this test all perturbing effects can be attributed to only two opposite phenomena:

1. as the pressure ratio increases, the probability and the extent of the phenomenon of not-ionised molecular hydrogen permeation through membrane increase, which contributes to the decrease of the generated voltage as the driving force of the process decreases;
2. as the pressure ratio increases, the probability and the extent of the phenomena of hydrogen sorption on porous lattice and subsequent solution-diffusion of ionised hydrogen through membrane increase, which contributes to the increase of the
3. generated voltage as the driving force of the process increases.

Hence, the two contributions move towards opposite directions and, even if it is not possible to better quantify the extent of single phenomena, at least qualitatively and limited to the considered pressure range, such interpretation can be considered as reliable.

At this point, by correcting (32) with coefficient α, calculable "a priori" knowing the instantaneous pressures in the two chambers, one gets the new (121), predictive and validated with regards to the generated voltage by the cell in the form:

$$E^*_{oc} = \alpha(P_a, P_c)\frac{RT}{nF}\ln\frac{p_a}{p_c} = E_{measured} \qquad (121)$$

$$\text{with } \alpha(\mathrm{P_a}, \mathrm{P_c}) = -3.920\left[\ln\left(\frac{\mathrm{P_a}}{\mathrm{P_c}}\right)\right]^2 + 2.290\left[\ln\left(\frac{\mathrm{P_a}}{\mathrm{P_c}}\right)\right] - 0.998 \text{ and } \mathrm{P_a} = 1\sim2{,}5 \text{ bar}$$

By using this correlation, the corrected trend of the theoretical voltage can be obtained, as reported in Figure 48.

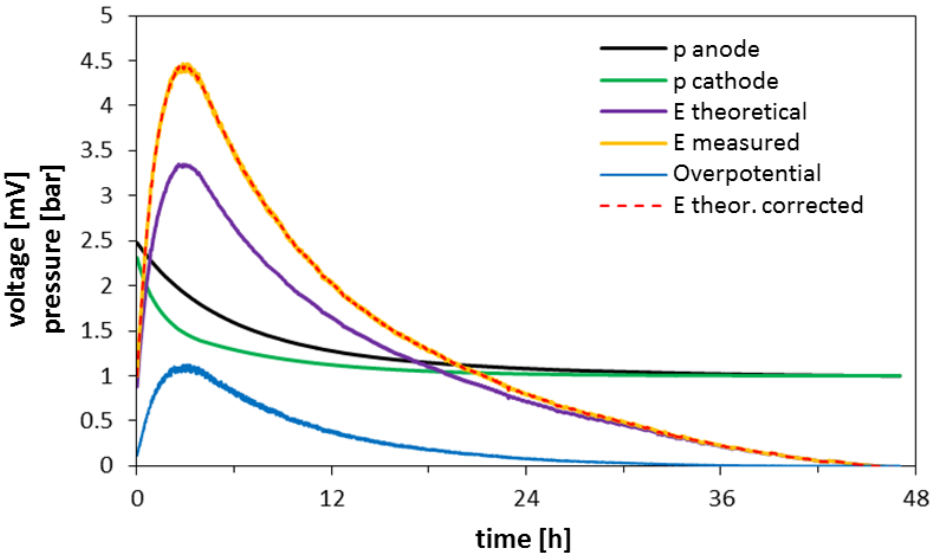

Figure 48. Time trends of anodic pressure, cathodic pressure, over-potential, theoretical, corrected and measured voltages (test no. 3).

Now, in the light of what done for test no. 3, an attempt of calibration of α has been done even for tests no. 1 and 2, limited to the region in correspondence of the top of the "bell", where I think, as explained before, that diffusion phenomena are negligible with respect to those of permeation and sorption. The results of such a *fitting procedure* are shown in Figure 49 and Figure 50.

In such figures the following curves are plotted:

- the portion of curve of measured voltage during the test, in the pressure range considered;

- the portion of the curve of theoretical voltage vs logarithm of the pressure ratio, which, if extrapolated towards the direction of low P_a/P_c, intersects the horizontal axis in the origin;

- the corresponding over-potential curve (difference between the two above listed);

- the curve of corrected theoretical voltage, fixed by the calibrated coefficient α.

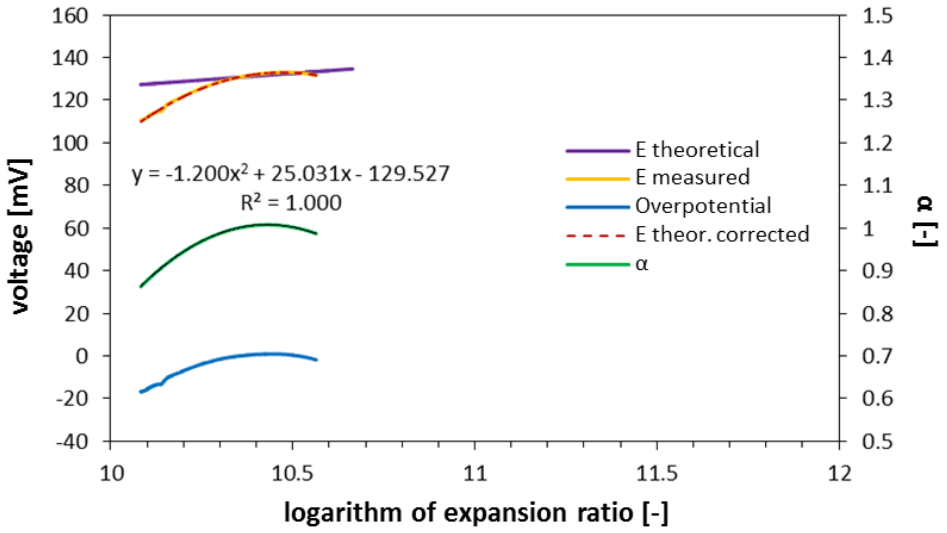

Figure 49. Calibration curve of the coefficient α and trend of theoretical, corrected and measured voltages, as a function of the logarithm of the expansion ratio (test no. 1).

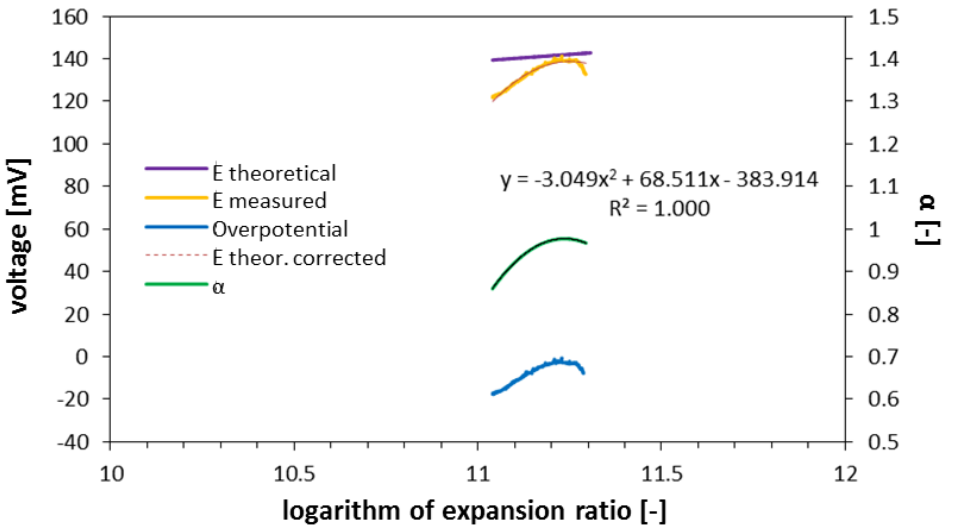

Figure 50. Calibration curve of the coefficient α and trend of theoretical, corrected and measured voltages, as a function of the logarithm of the expansion ratio (test no. 2).

From Figure 49 and Figure 50 it can be appreciated how the quadratic nature of the calibration correlation of α is valid even in tests no. 1 and 2, provided that it is intended applied exclusively to the region near the top of the "bell". Regarding to this, it is noted

that despite all the calibration curve have qualitatively the same trend, their analytical expression is strongly dependent on the range of pressure ratio considered, sign of the fact that the actual dependency of the perturbing/dissipative phenomena on the single pressures in the two chambers is more complex. In other words, α depends not only on the pressure ratio but also on the absolute value of one of the two.

The calibration correlation for α are the following:

$$\alpha(P_a, P_c) = -1.200\left[\ln\left(\frac{P_a}{P_c}\right)\right]^2 + 25.031\left[\ln\left(\frac{P_a}{P_c}\right)\right] - 129.527$$

$$\text{with } P_a = 1\sim2 \text{ bar and } P_c = 4{,}13 \cdot 10^{-2} \text{ mbar}$$

$$\alpha(P_a, P_c) = -3.049\left[\ln\left(\frac{P_a}{P_c}\right)\right]^2 + 68.511\left[\ln\left(\frac{P_a}{P_c}\right)\right] - 383.914$$

$$\text{with } P_a = 1\sim2 \text{ bar and } P_c = 2{,}45 \cdot 10^{-2} \text{ mbar}$$

Using the correlations so obtained, it was possible to get the trends of the theoretical corrected average according to (121) of the tests no. 1 and 2, and reported in Figure 51 and Figure 52) within the time interval ranging from the beginning of the test to the moment in which the anodic pressure reaches 1 bar(a). In the mentioned figures, it is also reported the trend of the anodic pressure, while the cathodic one is not reported, because it was maintained constant thanks to the continuous operation of the vacuum pump, at values $P_c = 4{,}13 \cdot 10^{-2}$ mbar and $P_c = 2{,}45 \cdot 10^{-2}$ mbar, respectively for tests no. 1 and 2 (these values would be over range and not appreciable in the graph).

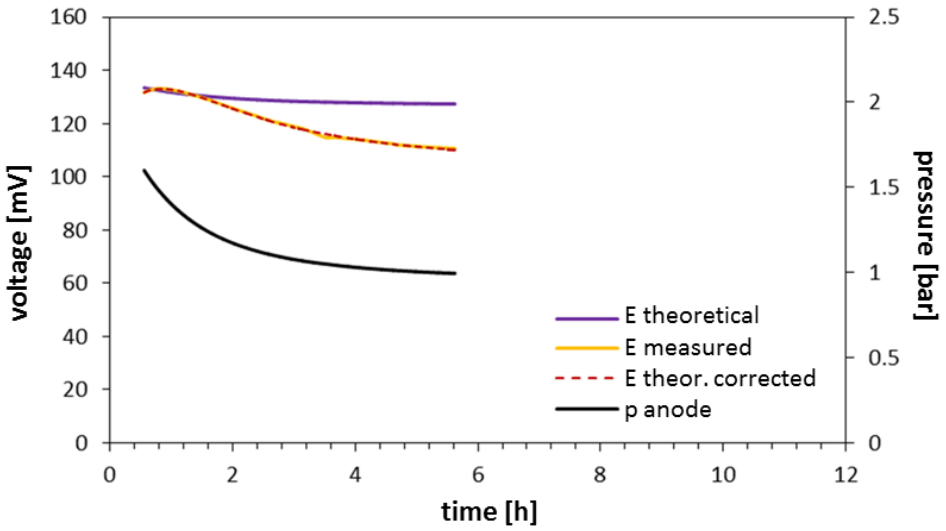

Figure 51. Time trends of anodic pressure, theoretical, corrected and measured voltages (test no. 1).

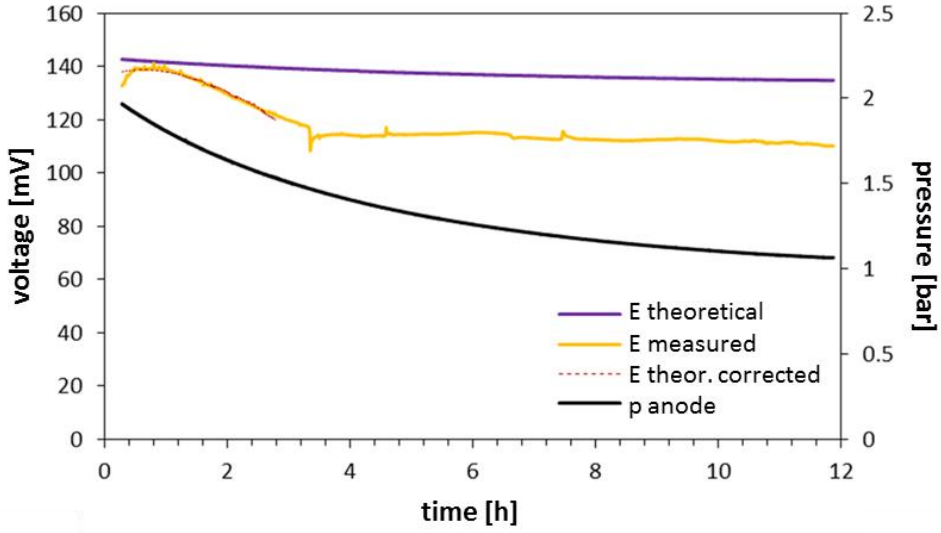

Figure 52. Time trends of anodic pressure, theoretical, corrected and measured voltages (test no. 2).

6.1.4 Conclusions about tests with hydrogen

The law which expresses the theoretical cell voltage, (121) derived by the mathematical modelling of the system called "simplified device" well interprets the results obtained through the tests with hydrogen, provided that a corrective coefficient is used, so

that it takes into account the perturbing effects due to sorption/solution phenomena and permeation phenomena (which are more significant in the first instants of the test, i.e. when the driving forces of convective phenomena are maxima). Moreover, the expression got and corrected by such an adjustable coefficient can be considered valid if and only if the remaining disturbing phenomena discussed in the present document (molecular diffusion between hydrogen and air and various leakages) can be neglected, so it is expected that it loses validity at long times.

Nevertheless, for the future tests to be carried out with other metals as working fluid, it will result very important to isolate such perturbing effects, rectifying as much as possible the experimental apparatus and the measuring instrumentation, in order to make it as more similar as possible to the physical system represented by an AMTEC cell.

6.2 Design and Realisation of a Non-Alkali Metal TEC

Model simulations confirmed that the electrical performance of a cell, even operating with new working fluids, is a trade-off between the voltage generated by the vapour pressure difference occurring when operating within a temperature range compatible with solar energy concentration systems, on one side, and the solid electrolyte electrical and geometrical features, on the other side, which shall be able to grant good electrical and mechanical performances. Lower ionic conductivity and thicker solid electrolytes lead to greater internal areal resistance which in turn produces higher voltage drops inside the cell itself, at expenses of the useful power density available on external load.

In particular, although lithium presents the highest open circuit cell voltage with respect to potassium or sodium, the maximum extractable electric power density is much lower than K-based or Na-based cells, at equal working temperatures, due to the higher ionic resistance of Li-based solid electrolytes with respect to other ones. As authors stated in [50], such behaviour is due to kinetic causes, e.g. to the membrane energy barrier E_m and to the sticking coefficient α, introduced in the model in order to describe the energetic and statistic aspects of the phenomena involved in the process. The membrane energy barrier

actually depends also on the external load, besides on the BASE ionic conductivity and thickness. Such energetic and statistical approach is valid for both the saturated liquid-anode/saturated vapour-cathode systems (as those described in [13]) and the saturated vapour-anode/saturated vapour-cathode ones modelled in [50]. This suggests that optimal high-performing working fluid-BASE pairs may exist and be particularly suitable for the use in solar-driven Metal ThermoElectric Converters. Moreover, in order to achieve higher, significant and usable power density at practical common operation voltages, a number of cells has to be series connected.

Considering the aggressiveness of metal vapours on both steel and alumina parts and the need to operate at milder temperatures (both aspects affecting the durability of the device), low melting point metals belonging to groups IIB (Zn, Cd, Hg), IIIA (Ga, In, Tl) and IVA (Sn, Pb) have been identified as potential promising working fluids, deserving more investigations.

6.2.1 New Working Fluid and Doped Electrolyte Preparation

In order to investigate new potential working fluids, different than alkali metals, new solid electrolytes are needed, properly conditioned or "doped" in compliance with the same diffusing metal ion as the working fluid. Commercially available solid electrolytes can be found, based on sodium, lithium, potassium, barium, strontium, silver and lead (from Ionotec LTD). Unfortunately, no zinc, cadmium, mercury, gallium, indium, thallium, tin based solid electrolytes exist, neither on commercial or laboratory scale, due to lack of market demand, despite some studies on divalent beta"-aluminas can be found in literature [51]. Therefore, the adoption of a system or technology capable to dope already commercially available solid electrolytes is needed.

Beta"-aluminas are excellent conductors for bivalent ions, as demonstrated in [24]. They are prepared starting from a sodium beta"-alumina, by substitution of the sodium cation with cations Ba^{2+}, Sr^{2+}, Cd^{2+}, Hg^{2+}, Pb^{2+}, Mn^{2+}, while the Zn^{2+} beta"-alumina is

prepared starting from a Ag^+ beta”-alumina by substitution of the silver cation with the Zn^{2+} cation.

Table 5. Selected electrical and transport properties of zinc, cadmium and lead based beta”-aluminas.

	Zn β”-alumina	**Cd β”-alumina**	**Pb β”-alumina**
Ion conductivity σ [$\Omega^{-1}m^{-1}$] @ 600°C	0.1221	2.171	51.87
Resistivity ρ [Ω m] @ 600°C	8.1917	4.606e-1	1.928e-2
Areal resistance ρ_{areal} [Ω m^2] @ 600°C 0.5 mm thickness	4.096e-3	2.303e-4	9.638e-6
Diffusion coefficient D [m^2/s]	4.648e-12	1.054e-10	-

The greater propensity of silver ions in Ag^+ beta”-alumina to be substituted by Zn^{2+}, with respect to the sodium or lithium ions in Na^+ and Li^+ beta”-aluminas respectively, does not lie with thermodynamics but primarily with kinetic reasons, i.e. with the fact that silver favours the melt phase while sodium and lithium favours the solid phase. At ambient temperature, the ion conductivity of other-than-sodium beta”-aluminas are two orders of magnitude lower than sodium beta”-alumina, while the differences are less evident at temperatures higher than 750 K. As an example, the Pb^{2+} beta”-alumina shows an ion conductivity close to that one of sodium even at temperatures lower than ambient one [51].

Solid electrolytes doped with divalent cations can be obtained either from beta-alumina or from beta”-alumina. Divalent cation-doped beta”-aluminas are kinetically more stable than beta-aluminas and do not show hysteresis phenomena both in heating and cooling. Moreover, unlike doped beta-alumina that may present a certain number of cracked crystals due to ion substitution, as reported by Yao at al. [52], beta”-alumina are not subject to cracking, provided that the difference in ionic radius of the divalent and the monovalent cation is not too large.

The replacement mechanism of the monovalent cation with a divalent one can be either by the simple high-temperature diffusion of divalent metal vapours or by the lower temperature diffusion of cations of a chloride salt of the divalent metal [51]. In some cases, the high vapour pressure of metal salts (e.g. mercury salts) requires the use of ceramic- or quartz-sealed crucibles and lower temperature process, with consequent lengthening of the diffusion process and, in most cases, a small replacement percentage of the sodium cations.

Dunn et al. [23] demonstrated that beta"-aluminas show very fast diffusion while divalent cations (Ba^{2+}, Sr^{2+}, Cd^{2+}) diffuse more slowly in beta-alumina. Most of divalent cations replace a large percentage of sodium cations in the membrane within the first hour of diffusion and, in some cases, complete substitution can be obtained in few minutes if membranes thinner than 0.2~0.3 mm are used.

6.2.2 Estimation of ion conductivity from diffusion data

De Nuzzio et al. [53] and Dunn et al. [54] obtained replacement percentage vs time curves of cadmium, zinc and strontium cations during substitution in sodium beta"-aluminas via radiochemical techniques based on ^{22}Na. The substitution percentage ε% can be described by an expression like:

$$\varepsilon\% = 100 \cdot \frac{2}{L} \int_0^{\frac{L}{2}} \exp\left(-\frac{x^2}{4Dt}\right) dx \qquad (122)$$

in which L is the solid electrolyte thickness, D is the diffusion coefficient and t is time. Expression (1) can be derived analytically from mass balances based on the first and the second Fick's laws, according to the penetration theory [28].

The diffusion coefficient of doping cations in the beta"-alumina was retrieved by best-fitting of experimental data collected at constant temperature. Hence exchange percentage fitted data allow to determine indirectly the diffusion coefficient D of a certain ionic species in beta"-alumina, and this in turn can be related to the ion conductivity σ through the Nernst-Einstein [43] relationship which applies at constant temperature T:

$$\sigma T = nz^2 e^2 \frac{D}{k_B} \tag{123}$$

where n is the number density (which is a measure of the density of the crystalline lattice), z is the metal ion valence, e is the elementary charge and k_B is the Boltzmann's constant.

The same procedure as reported in [51] has been adopted in the present work, together with experimental data of exchange percentage vs time available from [54], in order to estimate the ion conductivity of zinc, cadmium and lead based beta"-alumina solid electrolytes, which is in turn needed for model simulation of electrical performance of such devices.

Best-fitted values for the diffusion coefficient are $4.648 \cdot 10^{-12}$ m^2/s at T=500 °C for zinc and $1.054 \cdot 10^{-10}$ m^2/s at T=600 °C for cadmium, which lead to ion conductivity of 0.1081 and 2.171 $(\Omega\ m)^{-1}$ respectively. The ion conductivity of lead-doped beta"-aluminas has been derived directly from conductivity vs temperature data from [51], and has been found to be equal to 51.87 $(\Omega\ m)^{-1}$ at T=600 °C. In order to make a comparison between the three different metals at the same temperature, Zn^{2+} β"-alumina conductivity was extrapolated according to equation $\sigma/\sigma_0=T/T_0$, derived from experimental conductivity data reported in [51], resulting in 0.1221 $(\Omega\ m)^{-1}$ at 600°C. Table 1 summarises the adopted electrical and transport properties of Zn, Cd and Pb β"-aluminas.

6.2.3 Cell model simulations

Model simulations of the Zn, Cd and Pb saturated vapour-anode/saturated vapour-cathode systems, based on the mathematical model developed in [50], have been carried out and produced polarisation and power curves reported in Figure 53.

Anode and cathode temperatures in all cases are set to 973 K and 773 K respectively, while BASE thickness is 0.5 mm and metal vapour pressures are calculated with data reported in [47]. For these simulation, the sticking coefficients are set equal to 1 on both sides of the BASE (effective adsorption), following [8].

As it can be seen, the performances obtainable with divalent cations are qualitatively similar (as expected) to those obtained with monovalent alkali metals (sodium, potassium and lithium) and reported in a previous paper [50].

However, power density values (0.125, 1.92 and 1.71 mW/cm^2 for Zn, Cd and Pb respectively) are definitely much lower than those computed in [50] for a sodium cell (240 mW/cm^2) and even one order of magnitude lower than those computed for a lithium cell (14.1 mW/cm^2), although the durability performance could be better than sodium, considering the chemical aggressiveness of such alkali metal on membrane, electrodes and stainless steel enclosure. This behaviour can be related to the much lower ion conductivity of BASE divalent cations with respect to monovalent cations, being equal the operating temperature. In addition to this, it has to be considered that supply cost of zinc, cadmium and lead is lower than sodium.

By observing the characteristic parabolas (Figure 53) describing the power density vs the current density, there is an evident difference in magnitude, with cadmium and lead based systems showing significantly larger values than zinc-based cell. Three different trends have been obtained instead in the polarisation curves of Zn, Cd and Pb systems. Regarding zinc and cadmium systems, the polarisation curve is actually a straight line, the former showing a much higher resistivity with respect to the latter, resulting in a greater slope of the line, which makes zinc system less suitable for practical applications with respect to cadmium and lead. Lead-based systems provide lower resistivity, especially at normal current density regimes, as demonstrated by the change in slope of the polarisation curve. This suggests, together with the higher useful maximum power density obtainable with respect to zinc, that saturated lead vapour-anode/saturated lead vapour-cathode devices deserve more investigation and could have interesting development.

Results from the planned experimental campaign are necessary to confirm the theoretical model predictions here presented.

Among other metal elements not included in model simulations, tin might have advantages compared to lead, due to the much lower boiling temperature, i.e. higher volatility and higher vapour pressure. Indium, gallium, thallium and all other low-melting

point monovalent metals should exhibit higher ionic conductivity and be more suitable for applications in solar concentration systems.

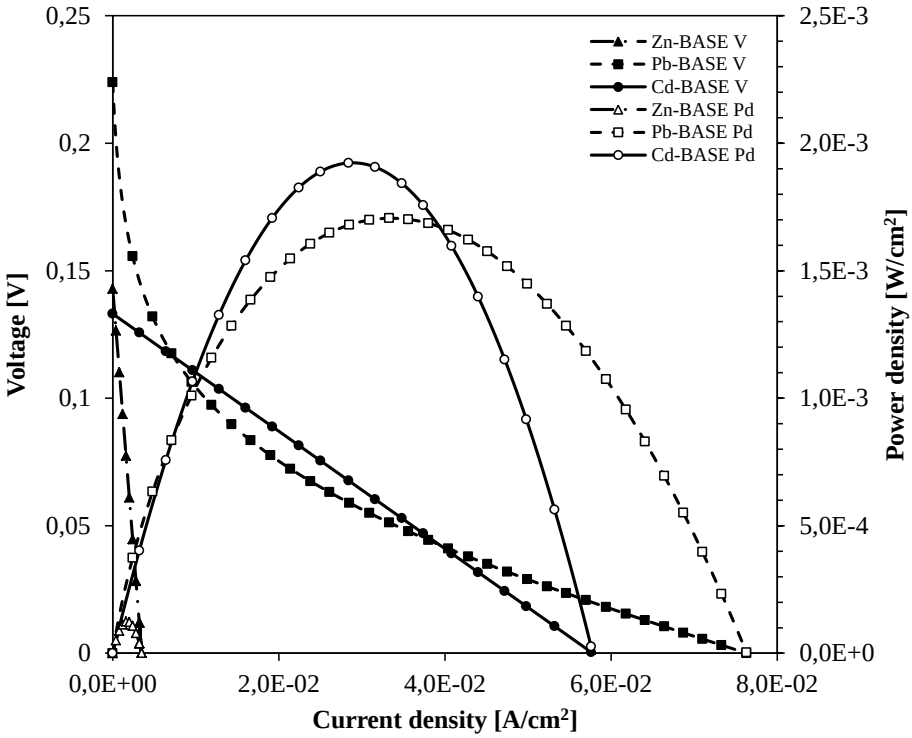

Figure 53. Computed polarisation and power curves for three different vapour-anode/vapour-cathode AMTEC-like devices, operating with zinc, cadmium or lead vapour, respectively. Simulation parameters: membrane thickness 0.5 mm, anode temperature 973 K, cathode temperature 773 K, $\alpha_a=\alpha_c=1$ (effective adsorption); vapour pressures are computed as function of temperature according to [47]**.**

6.2.4 Experimental Apparatus and Procedure

An experimental apparatus has been proprietary developed in order to carry out measurements of electrical performances of an AMTEC-like single-cell device operating with non-alkaline metals working fluids coupled with the proper BASE, suitable for solar

energy applications. The first experimental campaign will be performed using zinc as a working fluid.

With reference to Figure 54, the experimental apparatus is composed of: the cell composed of two symmetric semi-elements (5), designed and manufactured in-house as described in the following; a turbomolecular vacuum pump (1) connected to the vacuum chamber (7) and to the vacuum circuit; four Nupro vacuum valves (2); two Pirani pressure gauges (3) and controller (6); two feedthrough connections for power supply and electrical I-V signals (8); two cell temperature controllers and two K-type thermocouples (4).

It is worth to precise that the vacuum chamber is necessary in such a home-made lab-scale testing device in order to ensure that no air contaminations and leakages occur through the not-perfect seal between the two semi-elements, where the membrane disc is placed. An industrial/commercial version of the device, to be used for power generation only, would not need the extra chamber.

A certain amount of ultrapure solid metal is put inside the two semi-elements of the cell, then the cell is assembled and put inside the vacuum chamber. The chamber is alternatively flushed with gaseous nitrogen and evacuated by the vacuum pump and the operation is repeated 4-5 times in order to remove all traces of air. After the final flush, high vacuum is created inside the chamber by the vacuum pump, and the two semi-cells are heated at two different and constant temperatures by electric band heaters. In this condition, a differential pressure is set across the two semi-elements (i.e. the vapour pressure difference due to the different anodic and cathodic temperatures) which can be fine-tuned and kept constant by regulating the temperature difference.

The external electric circuit is closed either on an I-V tracer during measurement tests, which automatically applies a variable load, ranging from open circuit to short-cut, in order to obtain the polarisation and power curves, or on another electric load, during normal operation.

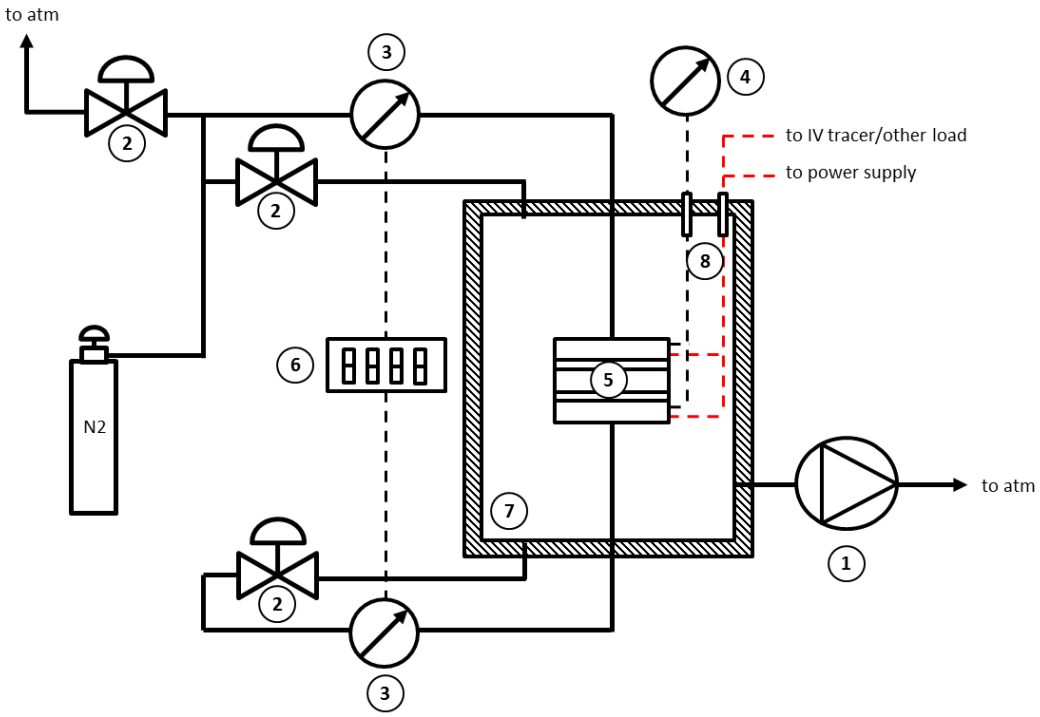

Figure 54. Simplified sketch of the developed experimental apparatus: (1) vacuum pump, (2) Nupro vacuum valve, (3) pressure gauges, (4) temperature gauges, (5) experimental cell, (6) pressure reader, (7) vacuum chamber, (8) feed-through connections for power supply of electric band heaters and control and measurement signals. In particular, the external electric circuit can be closed either on an I-V tracer device (during measurement test) or on another load (during normal operation).

6.2.5 Design and Realisation of the Experimental Cell

Figure 55 shows a picture of the experimental apparatus. Figure 56 depicts different views of the proprietary experimental cell developed in this work, which has been designed in Siemens SolidEdge ST10 software [55]. In the following, the executive details of the manufacturing of the device are presented.

Figure 55. Proprietary developed experimental apparatus with indication of main items: (A) vacuum chamber; (B) experimental cell; (C) vacuum circuit; (D) feed-through system for power, control and signal connections; (E) vacuum pump.

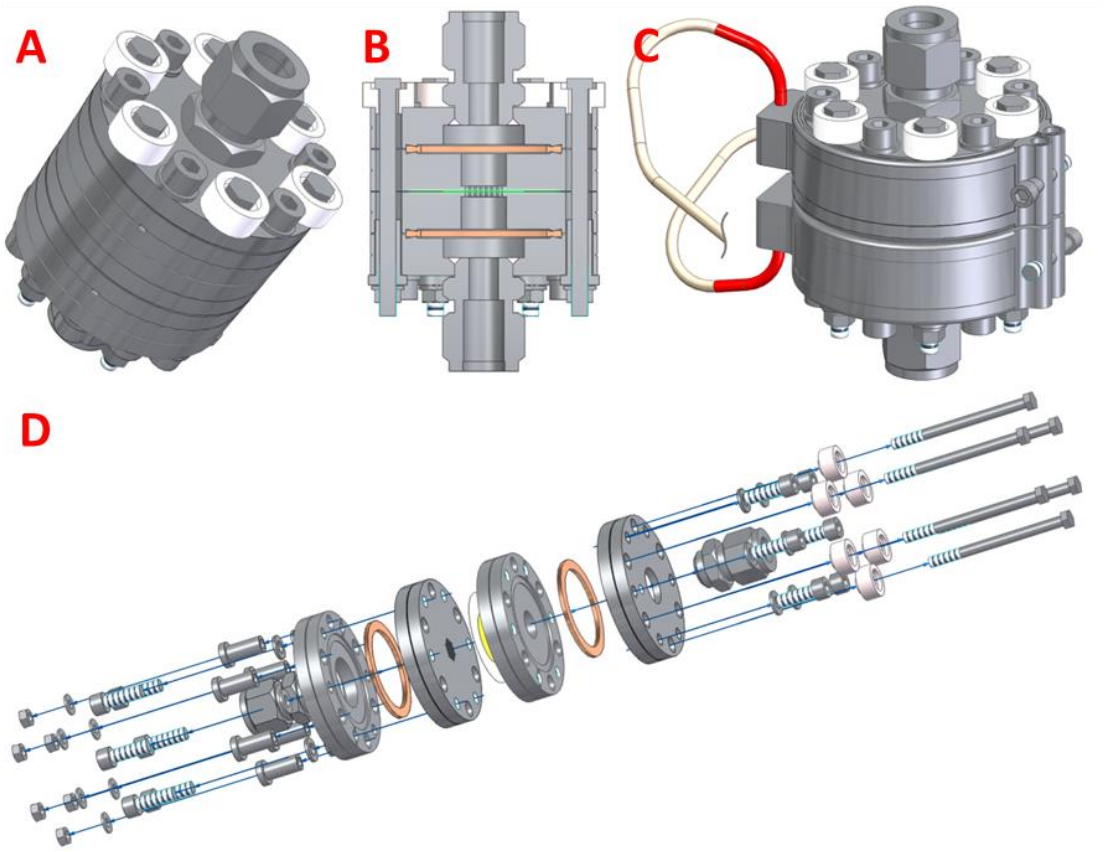

Figure 56. 3D views of the experimental cell: (A) assembled experimental cell; (B) transverse sectional view with indication of the BASE (green) and ring gaskets (copper); (C) assembled cell with electric band heaters installed; (D) exploded view with focus on bolts assembly.

The electrochemical device is made up of two semi-cells which are electrically separated by a ceramic disc. The semi-cells are constituted by four Conflat DN40 AISI 316L stainless steel commercial flanges.

In particular, as I aim to design a system capable to maintain a differential pressure between the two chambers through a β”-alumina disc, a double drilling on each flange has been done, at the same distance from the existing holes: the first set of holes has a diameter of 8.5 mm while the second one has a diameter of 6.6 mm, separated by a 30° pitch along the circumference. The smaller diameter hole set guarantees the closure of the two flanges

which constitute each chamber (semi-cell) while the larger diameter hole set is for clamping the two chambers and maintain the β-alumina disc in position.

The Conflat flanges include a circular slot where proper DN40CF copper ring gaskets are placed, in order to ensure a hermetic sealing towards the external environment.

An additional hole for the installation of an O.D. 1/4" stainless steel tube is realised on the outer flange, for the connection to the external vacuum circuit.

To let the alkali metal be positioned inside the semi-cell, on the two inner flanges of chambers, a circular 10 mm deep compartment has been realised. The chamber wall facing the β"-alumina disc on both chambers has been perforated with an hexagonal pattern grid of circular holes, having a diameter of 1.2 mm each and a pitch of 1.5 mm.

When assembling the two semi-cells 6 cylindrical Macor insulators (o.d. 8 mm, i.d. 4.5 mm) have been used together with 6 hexagonal screws and 6 nuts, in order to ensure electrical insulation and good clamping between the semi-elements. The assembly parts of the semi-cell are reported in Figure 57 together with the assembled experimental cell.

Two 400W band electric heaters are clamped to the two semi-elements in good thermal contact with the lateral surface of the semi-cells. Such heaters provide the thermal energy needed to maintain a constant temperature inside the cell, which in turn determines the vapour pressure of the metal investigated as working fluid. The heating system is completed by two K-type thermocouples directly screwed onto the anodic and cathodic outer flanges, and connected to a temperature controller which switches the heaters on and off to maintain a constant temperature set point.

The mass transfer from the hot, high pressure semi-element to the cold, low pressure one leads to the progressive depletion of the metal mass in the hot semi-element, which passes into the cold one through the membrane until the pressure in the hot semi-element falls below the vapour pressure that the element would have at the anodic temperature. The device does not include a re-circulation system from the cathodic chamber back to the anodic chamber and thus it cannot work as a renewable battery producing electric power over a long time, however, it works as a test device for a sufficient time to perform the material characterizations. Basically, the electrical characteristic of the cell remains

constant as long as the amount of metal is sufficient to ensure a two-phase system (liquid-vapour equilibrium) in both semi-elements.

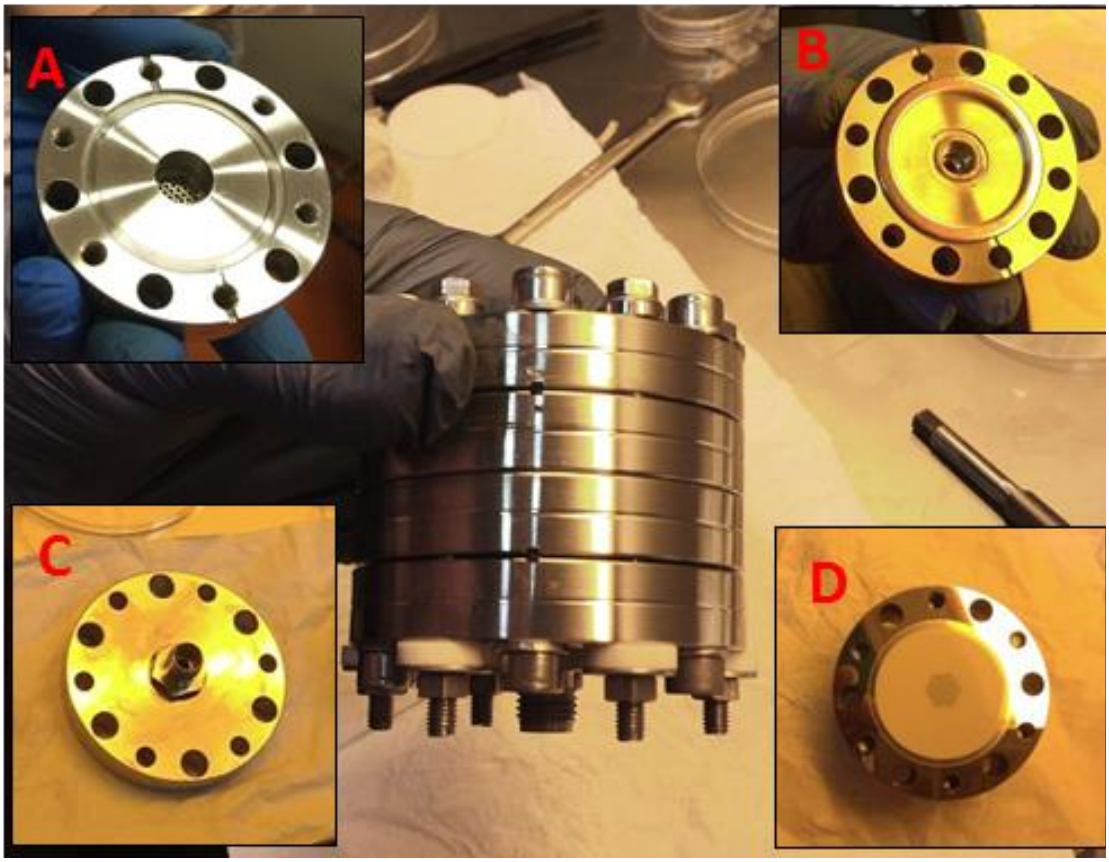

Figure 57. Assembled experimental cell and assembly parts: (A) internals of the inner flange with view of perforated grid and solid zinc slot; (B) installation of the copper ring gasket on the internal face of outer flange; (C) external face of outer flange, (D) placement of the membrane on the external face of inner flange.

UNIVERSITÀ
DEGLI STUDI
DI PALERMO

CHAPTER VII

INDUSTRIAL APPLICATION AND DEVELOPMENT OF A SECOND GENERATION AMTEC-LIKE CELL

7.1 Potential application to solar energy

The simple design proposed in chapter IV would simplify the manufacturing of the cell, reduce costs and make it suitable to combined application with discontinuous heat source, as solar radiation.

In fact, both in parabolic linear and parabolic dish solar collectors, the optical focus has got different positions during the day, as it tracks the relative sun position. Due to the effect of gravity, if one or more cells are installed on the focus, then they could have part of the BASE wetted by the melted metal, both at anode and cathode side, being the remaining part in contact with the vapour metal. In a well-designed cell, instead, the BASE would be in contact with metal vapours only for most of the operation during the day.

In a Fresnel-type solar collector, on the other hand, the optical focus does not change its absolute position during the day, as the maximisation of the solar energy capitation lies with the movable mirrors system.

For these reasons the saturated vapour-anode/saturated vapour-cathode configuration seems more indicated for coupling with parabolic linear or parabolic dish collectors, while the saturated liquid-anode/saturated vapour-cathode configurations are particularly suitable for coupling with Fresnel-type solar collection systems. Moreover, both types of AMTEC-like cells can also be easily coupled to waste heat recovery systems as well as to biomass and biogas heat production.

In any case, when applying such a device to any thermal energy available source, a regeneration or recirculation system, like those already provided in current AMTECs, has to be adopted in order to get a continuous operation. The following sections report discussions about our investigated regeneration/recirculation system.

Figure 58. 3D rendering of a Fresnel type solar collector with second generation NAMTEC devices installed in a rotating array. Construction details and assembly are included on the relative patent request no. 102018000007710, deposited on 2018, July 31st.

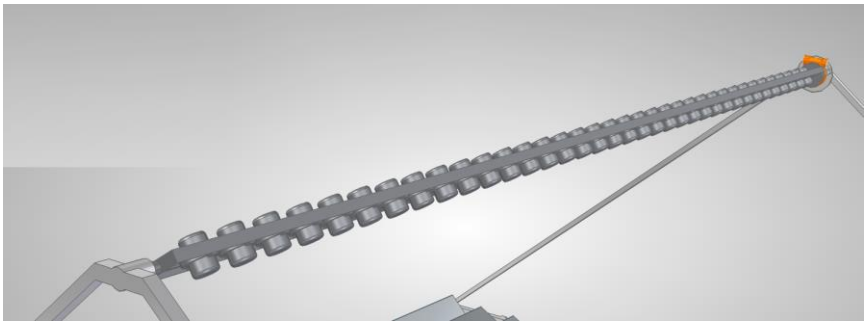

Figure 59. 3D rendering of a particular of the array of second generation NAMTEC devices installed onto a Fresnel type solar collector. Construction details and assembly are included on the relative patent request no. 102018000007710, deposited on 2018, July 31st.

7.2 Novel Cell Regeneration Mechanism

In addition I propose an innovative solution for cyclic operation., characterized by a new, simple, periodic regeneration system, for the renewable heat-to-electrical energy direct conversion, suitable for testing and operation with non-alkali metals as working fluid and properly conditioned beta”-aluminas conducting discs as solid electrolytes, which could have promising applications as second generation electrochemical cells for power generation.

In current AMTEC devices the anodic and the cathodic environments are connected one to the other by a return channel, in which the condensed metal flows by natural or forced circulation. This is enough to ensure, together with the continuous application of a hot source at the evaporator and a cold sink at the condenser, the renewability of the system.

As new mechanism of regeneration of the cell, a simple inversion of the hot and cold semi-element is proposed. When the condensed phase metal content in the hot element is near to total depletion due to evaporation and transfer to the cathode-side through the BASE (i.e. the anode system becomes monophasic), then the cell is literally flipped so that the anodic element takes the place of the cathodic one, and vice versa. In laboratory experiments, the same result is achieved by simply exchange the temperature set-points at anode and cathode on the temperature controller, that would also imply the inversion of polarity of the generated voltage.

The complete cell regeneration mechanism is well described in the patent request no. 102018000007710 titled “Dispositivo per la conversione di energia, sistema di conversione di energia e relativo procedimento di conversione di energia” and deposited by Qohelet Solar Italia S.p.A., Università degli Studi di Palermo (UNIPA) and Istituto Nazionale di Astrofisica (INAF) on 2018, July 31st.

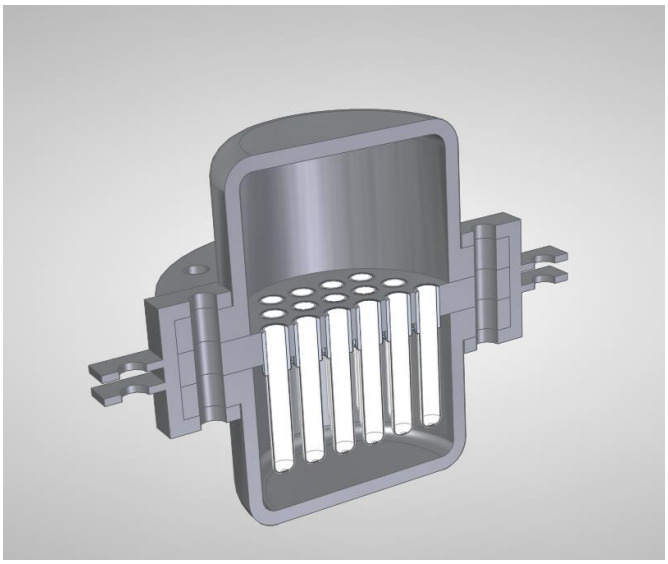

Figure 60. 3D rendering of a second generation multitube NAMTEC device. Construction details and assembly are included on the relative patent request no. 102018000007710, deposited on 2018, July 31st.

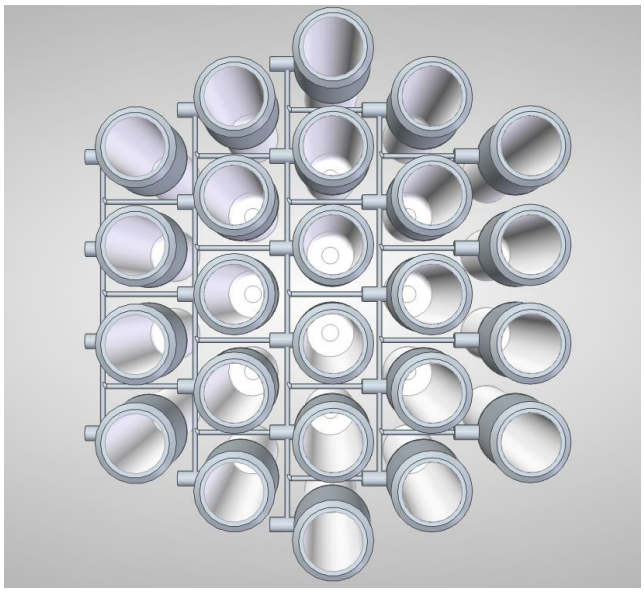

Figure 61. 3D rendering of the tubular beta"-alumina solid electrolytes and their electrical connection into a second generation multitube NAMTEC device. Construction details and assembly are included on the relative patent request no. 102018000007710, deposited on 2018, July 31st.

7.3 BASEs and electrodes in industrial devices

As shown in Figure 62, the beta”-alumina solid electrolyte in the industrial version of the device will be realised in tubular shapes, provided with ceramic-metal joining, in order to increase the electrolyte surface area and then the electrical current density. The adopted BASEs will be chemically doped as discussed in chapter 11, starting from commercial BASEs provided by IONOTEC Ltd.

Figure 62. Beta”-alumina ion conducting ceramic tube with ceramic-metal joining [56]**.**

Furthermore, as known in [1], the electrode is one of the most important components of AMTECs, and it contributes to 15–19% of the overall degradation of the power output. Search for high performance electrode is a feasible approach to improve the power output and efficiency of AMTECs and second generation NAMTECs. This should involve with materials, geometrical optimization (see Figure 63), and a proper vacuum level of AMTECs’ cathode side. Desirable electrode properties include:

(a) Good electrical conductivity;

(b) Good physical bonding with the BASE membrane;

(c) A thermal expansion coefficient that is close to that of BASE;

(d) High permeability to sodium vapour;

(e) High corrosion resistance to sodium vapour;

(f) Low material loss rate by chemical reaction or sublimation; and

(g) Slow grain growth and material migration.

Refractory electrode materials such as TiB_2, LaB_6, TiN, TiC, TiN-TiC, NbN, and NbC offer many of these properties; however, none of them meet all the requirements. Actually, among the properties above, (a)(b)(c)(d)(g) are the most desired parameters in selection of electrode material.

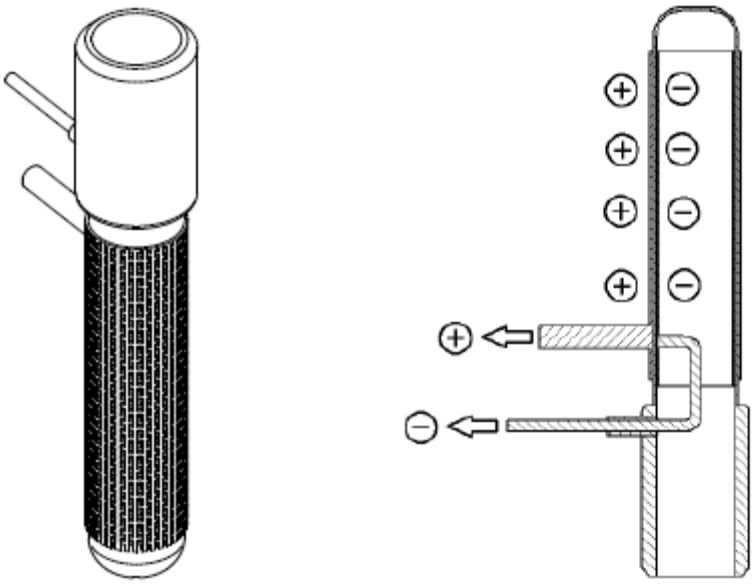

Figure 63. Schematics of installation of porous electrodes onto the outer and the inner surface of a tubular ceramic ion conducting BASE.

The contact between electrode and electrolyte (which is related with the operation lifetime of the electrode through grain size) and the pressure losses (which characterizes the pressure drop due to the diffusion of neutral sodium atoms forming at the BASE–cathode interface through the porous electrode) are two important aspects to be considered during the electrode selection. High performance electrodes should minimise internal

charge-exchange polarization losses, and minimise concentration losses, as well. Additionally, the current collector/electrode contact resistance is also used to evaluate the performance of electrodes.

So, suitable materials for electrode of industrial AMTECs and second generation NAMTECs range from the early metal material (Mo), to the ceramic electrodes (TiN, TiC, TiN-TiC, LaB_6 and TiB_2, etc.), the refractory alloy electrodes (Rh_xW), and the most recent mixed-conducting (ionic and electronic) metal-oxide electrodes (Mo/Na_x-TiO_2 and TiN/Na_x-TiO_2).

CONCLUSION

The present work has focused on heat-to-power generation technologies with special concern in Alkali Metal ThermoElectric Converters (AMTEC).

The state of art of AMTEC as devices capable to directly convert heat to electric energy has been first presented and then the focus has moved to the mathematical modelling of the system. A review of models developed to date has been reported and a novel model of a vapour-anode/vapour-cathode AMTEC-like device has been developed, aiming at the determination of the electrical performances (extractable current and power densities) and based on theoretical considerations form statistical thermodynamics and kinetic theory of perfect gases.

The final expression for the circulating current density derived from the proposed model has been compared to another derived from literature and based on a purely empirical approach. An analogy of terms occurring in the two approaches has been identified, demonstrating the validity of the novel model here proposed, as a tool for prediction of vapour-anode/vapour-cathode devices performances.

In order to overcome criticalities of current AMTEC devices, mainly regarding durability and specific power efficiency, future research should be focused on the development of second generation AMTEC-like devices, able to operate at less critical temperatures, with a regeneration mechanism different than physical condensation at cathode, and with working fluids different than alkali metals, properly coupled with suitable BASEs.

The modelling here presented will be a valuable tool for the optimization parameters of such second generation AMTEC cell.

The final part of the thesis has described the proposed approach to overcome some of the technological limitations of the currently investigated AMTEC cells, focusing in particular on the design of a non-Alkali Metal ThermoElectric cell, based on the same AMTEC operation principle but operating with some other cheaper and more durable and

reliable non-alkali monovalent or divalent low melting point metals belonging to II B group (Zn, Cd, Hg), III A group (Ga, In, Tl) and IV A group (Sn, Pb).

The fabrication of a home-made, lab-scale testing device followed in order to validate the design work and start experimental measurements of cell electric performance, whose results will be necessary to confirm the theoretical model predictions.

Finally, I have briefly discussed about the possible application of such developed device to already existing eco-friendly thermal energy sources, such as solar radiation collection systems, biomass and biogas power systems.

Acknowledgements

The research described in the present work has been developed during the PhD course in Physics, XXX cycle, International Curriculum in Statistical and Interdisciplinary Physics, at Università degli Studi di Palermo.

The research activity has been supported by Istituto Nazionale di Astrofisica (INAF), XACT Laboratory (Palermo, Italy), and has been partially funded by Qohelet Solar Italia S.p.A. (Caltanissetta, Italy).

Special thanks to Ionotec Ltd. (Runcorn, Cheshire, England) for the BASE supply and Archimede S.r.l. (Caltanissetta, Italy) for the technical and scientific support.

References

[1] S.-Y. Wu, L. Xiao and Y.-D. Cao, "A review on advances in alkali metal thermal to electric converters (AMTECs)," *Intern. Journ. of Energy Research*, 2009.

[2] U.S. Department of Energy, Nuclear Energy Research Initiative, "Novel, integrated reactor/power conversion system (LMR-AMTEC)," *Project Number: 99-0198, Research Grant Number: DE-FG03-99SF21987 Final Scientific/Technical Report, Report no. STD-ES-03-04*, 2003.

[3] "Electropedia," [Online]. Available: http://www.mpoweruk.com/amtec.htm.

[4] O. Foust, "Sodium-NaK Engineering Handbook," *Science Publisher Inc: New York*, 1972.

[5] R. Williams, A. Kisor, M. Ryan, B. Jeffries-Nakamura, S. Kikkert and D. O'Connor, "Potassium beta-alumina/potassium ì/molybdenum electrochemical cells," *Proceedings of the 29th Intersociety Energy Concersion Engineering Conference, American insitute of Aeronautics and Astronnautics*, vol. 2, pp. 888-893, 1994.

[6] C. Huang, T. Hendricks and T. Hunt, "Performance analysis of a potassium-BASE AMTEC cell," *Proceedings of the 33rd Intersociety Energy Conversion Engineering Conference, American Nuclear Society*, no. IECEC-98-406, 1998.

[7] A. Barkan, T. Hunt and B. Thomas, "Potassium AMTEC cell performance," *Proceedings of the 34th Intersociety Energy Conversion Engineering Conference, Society of Automotive Engineers*, Vols. 1999-01-2702, 1999.

[8] J.-M. Tournier and M. El-Genk, "An Analytical Model for Liquid-Anode and Vapor-Anode AMTEC Converters," *Proc. Space Technology and Applications International Forum (STAIF-97*, no. 387, pp. 1534-1552, 1997.

[9] M. S. El-Genk and J.-M. Tournier, "Performance comparison of potassium and sodium vapor anode, multi-tube AMTEC converters," *Energy Conversion and Management*, no. 43, pp. 1931-1951, 2002.

[10] K. Onda, T. Masuda, S. Nagata and K. Nozaki, "Cycle analyses of thermoelectric power generation and heat pumps using the beta-alumina electrolyte," *Journal of Power Sources*, no. 55, pp. 231-236, 1995.

[11] M. Lohdi and J. B. Briggs, "Temperature effect on lifetimes of AMTEC electrodes," *Journal of Power Sources*, no. 167, pp. 537-545, 2007.

[12] M. Lodhi, P. Vijayaraghavan and A. Daloglu, "An overview of advanced space/terrestrial power generation device: AMTEC," *Journal of Power Sources*, vol. 103, pp. 25-33, 2001.

[13] T. Cole, "Thermoelectric Energy Conversion with Solid Electrolytes," *Science,* vol. 221, no. 4614, 1983.

[14] N. Weber, "A thermoelectric device based on beta-alumina solid electrolyte," *Energy conversion,* vol. 14, pp. 1-7, 1974.

[15] R. Williams, B. Jeffries-Nakamura, M. Underwood, B. Wheeler, M. Loveland, S. Kikkert, J. Lamb, T. Cole, J. Kummer and C. Bankston, "High power density performance of WPt and WRh electrodes in the alkali metal thermal to electric converter," *Journal of the Electrochemical Society,* no. 135, pp. 893-894, 1989.

[16] F. Rossi, A. Nicolini, M. Filipponi and M. Amantini, "Confronto tecnico economico tra soluzioni per la conversione diretta dell'energia termica in energia elettrica," *63° Congresso nazionale ATI - "Energia per lo sviluppo sostenibile",* 2008.

[17] "Ecoroko," [Online]. Available: http://ecoroko.tistory.com/135.

[18] C. Vining, R. Williams, M. Underwood, M. Ryan, J. Suitor and ., "Reversible Thermodynamic Cycle for AMTEC Power Conversion," *Jour. of electrochemical society,* vol. 140, no. 10, pp. 2760-2763, 1993.

[19] "System Simulation and Transient Analysis," Institute for Space and Nuclear Power Studies, 2006-2016. [Online]. Available: http://isnps.unm.edu/research/transient/#apeam.

[20] R. K. Sievers, T. J. Hendricks and J. C. Giglio, "Evaporation front position control in alkali metal thermal electric conversion (AMTEC) cells". Patent US5939666 A, 1997.

[21] "Power, propulsion and mechanical systems," California Institute of Technology, [Online]. Available: https://sbir.jpl.nasa.gov/powerpropulsionstructure.html.

[22] K.-W. Lee and W.-P. Chun, "AMTEC with heat pipe". Patent US8253008 B2, 2008.

[23] B. Dunn, R. Ostrom, R. Seevers and G. Farrington, "Divalent cation conductivity in beta″ alumina," *Solid State Ionics,* vol. 5, pp. 203-204, 1981.

[24] B. Dunn and G. Farrington, "Fast Divalent Ion Conduction in Ba++, Cd++ and Sr++ Beta"-Aluminas," *Mat. Res. Bull.,* vol. 15, pp. 1773-1777, 1980.

[25] K. Li, Ceramic membranes for separation and reaction, Wiley, 2007.

[26] X. Lu, G. Xia, J. P. Lemmon and Z. Yang, "Advanced materials for sodium-beta alumina batteries: Status, challenges and perspectives," *Journal of Power Sources,* vol. 195, no. 9, pp. 2431-2442, 2010.

[27] "Pila a concentrazione," Wikipedia, [Online]. Available: https://it.wikipedia.org/wiki/Pila_a_concentrazione.

[28] R. H. Perry and D. Green, "Perry's Chemical Engineering's Handbook 8th ed.".

[29] G. Bianchi and T. Mussini, Fondamenti di elettrochimica - Teoria ed applicazioni, Masson, 1993.

[30] "NIST Chemistry WebBook," [Online]. Available: http://webbook.nist.gov/chemistry/.

[31] A. Schock and C. Or, "Coupled thermal,electrical, and fluid flow analyses of AMTEC multi-tube cell with adiabatic cell wall," *Space Technology and Applications International Forum, AIP Conference Proceedings, American Intitute of Physics: New York,* vol. 387, pp. 1381-1394, 1997.

[32] A. Schock, H. Noravian, C. Or and V. Kumar, "Parametric analyses of AMTEC multi-tube cells and recommendation for revised cell design," *Space Technology and Applications International Forum, AIP Conference Proceedings, American Institute of Physics: New York,* vol. 387, pp. 1395-1404, 1997.

[33] T. Hendricks, C. Borkowski and C. Huang, "Development and experimental validation of a Sinda/Fluint thermal/fluid/electrical model of a multi-tube AMTEC cell," *Space Technology and Applications International Forum, AIP conference proceedings, American Insitute of Physics: New York,* vol. 420, pp. 1491-1501, 199.

[34] J. Tournier and M. El-Genk, "Sodium Vapor Flow Regimes and Pressure Losses on Cathode Side of Multitube AMTEC Cell," *Proc. Space Technology and Applications International Forum (STAIF-98),* vol. 420, no. 3, pp. 1595-1606, 1998.

[35] J. Tournier and M. El-Genk, "Sodium Vapor Pressure Losses in a Multitube AMTEC Converter," *Thermophysics and Heat Transfer,* vol. 13, pp. 117-125, 1999.

[36] J. Tournier and M. El-Genk, "Radiation/Conduction Model for Multitube AMTEC Cells," *Proc. Space Technology and Applications International Forum (STAIF-98),* vol. 420, no. 3, pp. 1152-1564, 1998.

[37] J. Tournier and M. El-Genk, "Radiation heat transfer in multitube, alkali metal thermal-to-electric converter," *Transaction of the ASME, Journal of Heat transfer,* vol. 121, pp. 239-245, 1999.

[38] J. Tournier and M. El-Genk, "An electric model of a vapor anode, multitube alkali-metal thermal-to-electric converter," *Journal of applied Electrochemistry,* vol. 29, pp. 1263-1275, 1999.

[39] K. W. Kolasinski, Surface Science: Foundations of Catalysis and Nanoscience, 2012, ISBN: 978-1-119-99035-2.

[40] K.-N. Tu, J. W. Mayer and L. C. Feldman, Electronic Thin Film Science for Electrical Engineers and Materials Scientists, 1992, pp. 101-102.

[41] T. Hunt, N. Weber and T. Cole, "Proc. 13th Intersociety Energy Conversion Engineering Conf, San Diego, CA, USA," vol. 3, p. 2011, 1978.

[42] W. G. Anderson and J. J. Bland, "High efficiency Vapor-Fed AMTEC system for direct conversion,"

Thermacore final report, 1997.

[43] J. O. Bockris, Modern electrochemistry: funndamentals of electrodics, Springer, 2000.

[44] J. Tournier and M. El-Genk, "An Electrical Model of Vapor-Anode, Multitube AMTEC Cell," *Proc. 33rd Intersociety Engineering Conference on Energy Conversion,* 1998.

[45] S. Waqar Hasan, S. Mohd Said, M. F. Mohd Sabri, A. S. Abu Bakar, N. Awanis Hashim, M. M. I. Megat Hasnan, J. M. Pringle and D. R. MacFarlane, "High termal gradient in thermo-electrochemical cells by insertion of a Poly(Vinylidene Fluoride) membrane," *Nature,* 2016.

[46] S. Waqar Hasan, S. Mohd Said, A. S. B. Abu Bakar, M. F. Mohd Sabri, I. Haider Sajid and N. Awanis Hashim, "Optimization of poly(vinylidene fluoride) membranes for enhanced power density of thermally driven electrochemical cells," *J Mater Sci,* 2017.

[47] C. B. Alcock, V. P. Itkin and M. K. Horrigan, "Vapour Pressure Equations for the Metallic Elements: 298-2500 K," *Canadian Metallurgical Quarterly,* p. 309, 1984.

[48] I. V. Pavlienko, "Design, improvement, and testing of a thermal-electrical analysis application of a multiple beta-tube AMTEC converter," *Thesis at Texas A&M University,* 2003.

[49] R. Baker, Membrane technology and applications, Jouh Wiley & Sons, 2004.

[50] G. Tumminelli, R. Candia, A. Collura, U. Lo Cicero, L. Sciortino, S. Ferruggia Bonura, F. Santoro and M. Barbera, "A thermodynamic-statistical model of the electrical characteristics of a 2nd generation AMTEC-type cell for the renewable heat-to-electrical energy direct conversion," *to be submitted,* 2018.

[51] G. Farrington and B. Dunn, "Divalent Beta"-Aluminas: High Conductivity Solid Electrolytes For Divalent Cations," *Soilid State Ionics,* vol. 7, pp. 267-281, 1982.

[52] Y.-F. Y. Yao and J. Kummer, "Ion exchange properties of and rates of ionic diffusion in beta-alumina," *Journal of Inorganic and Nuclear Chemistry,* vol. 29, pp. 2453-2466, 1967.

[53] J. De Nuzzio, R. Seevers, G. Farrington and B. Dunn, "Ion Transport in Ca++, Sr++, Ba++ and Pb++ Beta" Aluminas," *Journal of Solid State Chemistry,* vol. 50, pp. 146-152, 1983.

[54] B. Dunn, B. Karcher and G. Farrington, "Unpublished results".

[55] Siemens Solid Egde ST10, "https://www.plm.automation.siemens.com/it/products/solid-edge/," 2018. [Online].

[56] "Ionotec Ltd," [Online]. Available: http://www.ionotec.com/.

[57] F. Rossi, U. Di Matteo and M. Filipponi, "Opportunità impiantistiche innovative per celle a combustibile ad alta temperatura".

[58] J.-M. Tournier and M. S. El-Genk, "An electrical model for vapor-anode, multitube AMTEC cells," *33rd Intersociety Engineering Conference on Energy Conversion,* 1998.

[59] K. W. Kolasinski, Surface Science: Foundations of Catalysis and Nanoscience, 2012.

[60] J. Coulson and J. Richardson, Chemical Enginering vol. 6 3rd Ed., 1999.

[61] G. Tumminelli, "Tecnologie per la sostenibilità ed il risanamento ambientale - UNIPA," 2013.

[62] K. Tanaka, "Concept design of solar thermal receiver using alkali metal thermal to electric converter (AMTEC)," *Current Applied Physics* , no. 10, pp. 254-256, 2010.

[63] M. S. El-Genk and J. C. King, "Performance analyses of an Nb±1Zr/C-103 vapor anode multitube alkali-metal thermal-to-electric conversion cell," *Energy Conversion and Management,* no. 42, pp. 721-739, 2001.

[64] M. A. Ryan, R. M. Williams, C. Saipetch, A. Kisor, D. O'Connor, M. L. Underwood and B. Jeffries-Nakamura, "Developments in AMTEC devices, components and performance," in *Jet Propulsion Laboratory* , California Institute of Technology.

[65] A. Gil, M. Medrano, I. Martorell, A. La'zaro, P. Dolado, B. Zalba and L. F. Cabeza, "State of the art on high temperature thermal energy storage for power generation. Part 1—Concepts, materials and modellization," *Renewable and Sustainable Energy Reviews* , no. 14, pp. 31-55, 2010.

[66] A. Schock, H. Noravian, V. Kumar and C. Or, "Effect of design variations on AMTEC cell efficiency and of operating parameters on performace of OSC cell design," in *Orbital Sciences Corporation*.

[67] S. P. Badwal, S. S. Giddey, C. Munnings, A. I. Bhatt and A. F. Hollenkamp, "Emerging electrochemical energy conversion and storage technologies," in *Frontier Chemistry*, 2014.

[68] A. Bard and L. Faulkner, Electrochemical methods, 2001.

[69] N. Diez de los Ramos, A. Onea, S. Scherrer, A. Weisenbuger and W. Hering, "Direct Energy Conversion of Heat to Electricity Using AMTEC," *EPJ Web of Conferences,* vol. 79, 2014.

[70] M. Lodhi and N. Ahmad, "Optimization of power of alkali metal thermo electric convertor," *Journal of Power Sources,* vol. 275, pp. 644-649, 2015.

[71] M. Lodhi and V. Malka, "Optimization of the TIEC/AMTEC cascade cell for high efficiency," *Journal of Power Sources,* vol. 156, pp. 685-691, 2006.

[72] M. Lodhi and A. Daloglu, "Performance parameters of material studies for AMTEC cell," *Journal of Power Sources,* vol. 85, pp. 203-211, 2000.

[73] A. Onea, N. Diez de los Ramos, W. Hering, R. Stieglitz and P. Moster, "Direct energy conversion using

liquid metals," *EPJ Web of Conferences 79*, 2014.

[74] S.-Y. Wu, L. Xiao, Y. Cao and Y.-R. Li, "A parabolic dish/AMTEC solar thermal power system and its performance evaluation," *Applied Energy*, no. 87, pp. 452-462, 2010.

[75] M. El-Genk, "Space Nuclear Reactor Power System Concepts with Static and Dynamic Energy Conversion," *J. Energy Conversion and Management Special Issue on Space Nuclear Power and Propulsion*, vol. 49, no. 3, pp. 402-411, 2008.

[76] M. El-Genk and H. Saber, "Modeling and optimization of Segmented Thermoelectric Generators for Terrestrial and Space Applications," *CRC Handbook of Thermoelectrics, CRC Press,* 2005.

[77] M. El-Genk and J. Tournier, "AMTEC/TE Static Converters for High Energy Utilization, Small Nuclear Power Plants," *J. Energy Conversion and Management*, vol. 45, no. 4, pp. 511-535, 2004.

[78] M. El-Genk and J. Tournier, "Conceptual Design of a 100-kWe Space Nuclear Reactor Power System with High-Power AMTEC," *Proc. Space Technology and Applications International Forum (STAIF-2003),* vol. 654, pp. 397-407, 2003.

[79] J. Tournier and M. El-Genk, "Design Optimization of High Power, Liquid Anode AMTEC," *Proc. Space Technology and Applications International Forum (STAIF-2003),* vol. 654, pp. 740-750, 2003.

[80] M. El-Genk and J. Tournier, "High Power AMTEC Converters for Deep-Space Nuclear Reactor Power Systems," *Proc. Space Technology and Applications International Forum (STAIF-2003),* vol. 654, pp. 730-739, 2003.

[81] M. El-Genk and J. Tournier, "Analysis of a Vapor Anode, Multi-tube, Potassium Refractory AMTEC Converter for Space Applications," *Proc. Space Technology and Applications International Forum (STAIF-2001),* vol. 552, pp. 1066-1075, 2001.

[82] J. King and J. El-Genk, "Review of Refractory Materials for Vapor-Anode AMTEC Cells," *J. Propulsion and Power*, vol. 17, no. 3, pp. 547-556, 2001.

[83] J. Tournier and M. El-Genk, "A Model of Electrical Current Collectors in Multitube AMTEC Cells," *Proc. 33rd Intersociety Energy Conversion Engineering Conference*, 1998.

[84] L. Huang and M. El-Genk, "Experimental Uncertainties in AMTEC Vacuum Tests," *Proc. Space Technology and Applications International Forum (STAIF-98),* vol. 420, pp. 1471-1478, 1998.

[85] J. Tournier and M. El-Genk, "Heat Transfer in the Enclosure of a Multitube Alkali-Metal Thermal-to-Electric Converter Cell," *Proc. 7th AIAA/ASME Joint Thermophysics and Heat Transfer Conference*, vol. 357, no. 4, pp. 17-24, 1998.

[86] J. Tournier, M. El-Genk and M. Schuller, "Performance Analysis of a Multitube Vapor-Anode AMTEC Cell," *Proc. 32nd Intersociety Energy Conversion Engineering Conference*, pp. 1184-1189, 1997.

[87] J. Merrill, M. Schuller, P. Hausgen and R. Sievers, "Vacuum Testing of High Efficiency Multi-Base Tube AMTEC Cell," *Proc. 32nd Intersociety Energy Conversion Engineering Conference*, pp. 1184-1189, 1997.

[88] M. Underwood, B. Jeffries-Nakamura, D. O'Connor, M. Ryan, J. Suitor and R. Williams, "A five-volt AMTEC multicell," *American Chemical Society: Washington DC*, vol. 1, pp. 855-859, 1993.

[89] M. Yoichi and M. El-Genk, "Electrical breakdown experiments with application to alkali metal thermal-to-electric converters," *Energy Conversion and Management*, vol. 44, pp. 819-843, 2003.

[90] M. El-Genk, J. Tournier, J. King and Y. Momozaki, "Novel, Integrated Reactor/Power Conversion System (NIR/PCS): Alkali Metal Thermal-To-Electric Energy Conversion Progress Report Performance Period: September 1999–August 2000. Report No. UNM-ISNPS-3-2000," *The University of New Mexico's Institute for Space and Nuclear Studies, Albuquerque, NM,* 2000.

[91] M. El-Genk, J. Tournier and Y. Momozaki, "Novel, Integrated Reactor/Power Conversion System (NIR/PCS): Design and Analyses of Alkali Metal Thermal-To-Electric Conversion Units and Interfacing with Nuclear Reactor, Progress Report II. Report No. UNM-ISNPS-2-2001," *The University of New Mexico's Institute for Space and Nuclear Studies, Albuquerque, NM,* 2001.

[92] M. Lodhi and J. Briggs, "The Grain Size Effect on Thermo-chemical Properties of AMTEC electrodes," *Int. J. Electrochem. Sci.*, vol. 2, pp. 469-477, 2007.